UNIVERSITAT DE BARCELONA

Investigating genetic and mechanistic interactors in familialcardiomyopathy through advanced disease modeling

Rubén Escribá Piera

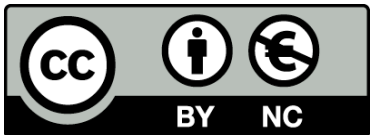

Investigating genetic and mechanistic interactors in familial cardiomyopathy through advanced disease modeling

Tesis Doctoral

Rubén Escribá Piera

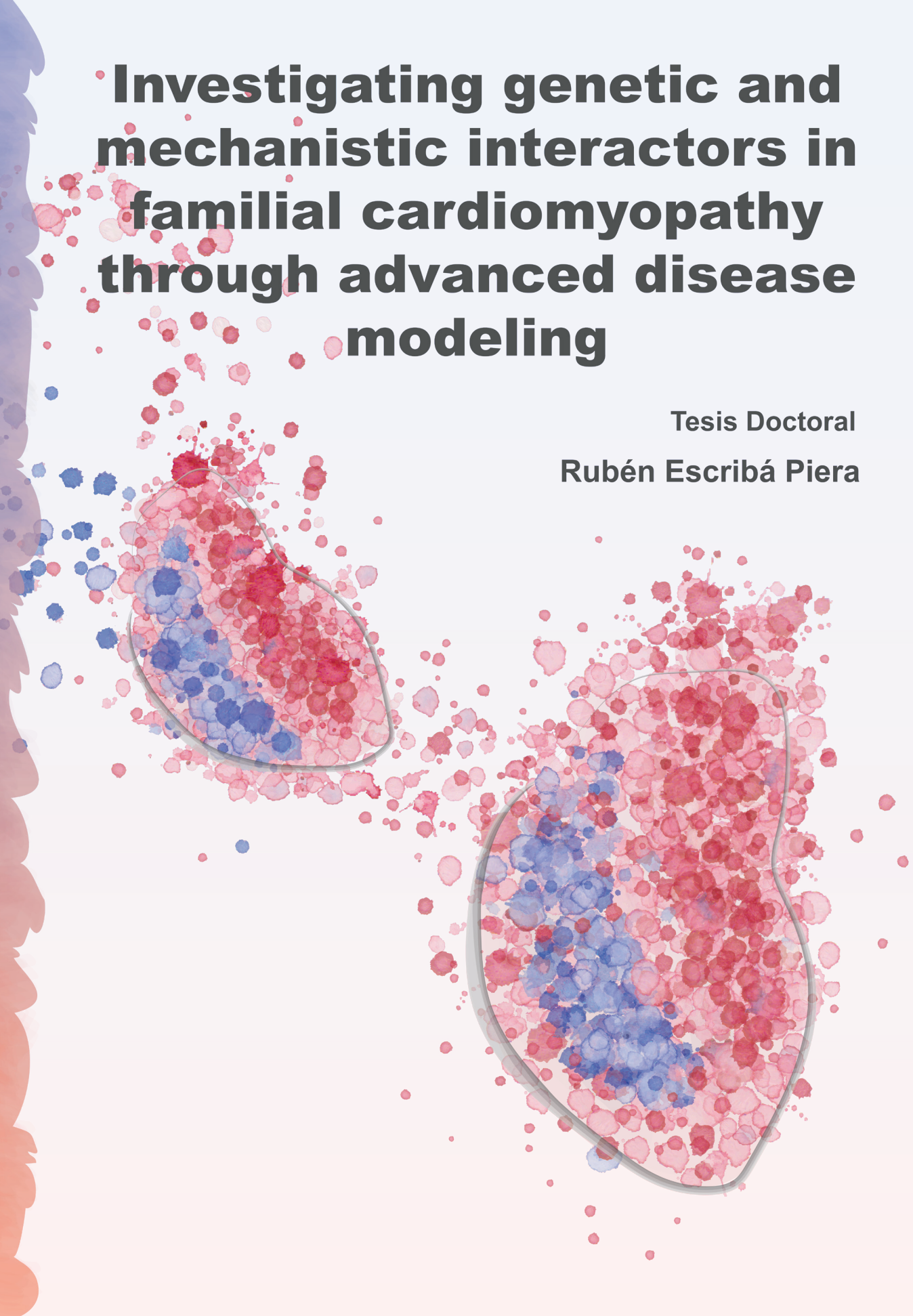

UNIVERSITAT DE BARCELONA

FACULTAT DE BIOLOGIA

PROGRAMA DE DOCTORAT EN BIOMEDICINA

2021

TESIS DOCTORAL

Investigating genetic and mechanistic interactors in familial cardiomyopathy through advanced disease modeling

Memòria presentada per

Rubén Escribá Piera

Per optar al títol de

Doctor

Per la Universitat de Barcelona

Tesi doctoral realitzada sota la dirección del Dr. Ángel Raya Chamorro al Institut d'Investigació Biomèdica de Bellvitge (IDIBELL)

Signat,

El Director:	El tutor:	El Doctorando:
RAYA CHAMORRO ANGEL - 29157851S Digitally signed by RAYA CHAMORRO ANGEL - 29157851S Date: 2021.12.13 14:10:56 +01'00'	DEL RIO FERNANDEZ JOSE ANTONIO - 38552812M Digitally signed by DEL RIO FERNANDEZ JOSE ANTONIO - 38552812M Date: 2021.12.13 12:15:42 +01'00'	ESCRIBA PIERA RUBEN - 74522242B Firmado digitalmente por ESCRIBA PIERA RUBEN - 74522242B Fecha: 2021.12.13 12:18:09 +01'00'
Dr. Ángel Raya Chamorro	Dr. José Antonio del Rio Fernández	Rubén Escribá Piera

CONTENTS

ABSTRACT

Hypertrophic cardiomyopathy (HCM) is the most common inherited cardiac disease and a frequent cause of heart failure and sudden cardiac death. HCM is a highly complex condition defined by clinical and genetic heterogeneity. During last decades, our understanding of the diverse genetic landscape and the pathological molecular mechanisms underlying HCM has increased significantly. However, studying the effect of genetic modifiers of cardiomyopathies is limited by their complex genetic aetiology. A better understanding of the complex genetic mechanisms underlying cardiac diseases is an imperative hallmark for precision medicine. With this aim, we sought to investigate the differing molecular and genetic mechanisms of two siblings with an extensive family history of HCM but divergent clinical manifestations using patient-specific induced pluripotent stem cells (hiPSCs).

For this purpose, we generated patient-specific iPSC from the male, diagnosed with a severe hypertrophic phenotype, and from the female, with mild hypertrophy, whose genetic testing revealed a common pathogenic mutation in the *MYBPC3* gene (K600Nfs*2). Morphological characterization of iPSC-derived cardiomyocytes from mutant carriers revealed that sarcomeric alignment and structure was not compromised. However, *MYBPC3* deficient iPSC-CMs showed reduced contractile force generation without cell shape remodelling. We then took advantage of the CRISPR/Cas9 gene-editing technology to generate *MYBPC3*-corrected isogenic controls in order to better ascribe genotype-phenotype correlations. Functional evaluation of mutant and isogenic iPSC-CMs revealed that cardiomyocytes from the symptomatic patient presented a hypercontractile phenotype as well as faster calcium transients. Further analysis on the mitochondrial bioenergetics indicated an inefficient ATP consumption in sarcomeres from both mutant carriers.

In order to explore whether additional genetic variants were modifying the pathological outcomes in the symptomatic carrier, we performed a whole-exome sequencing of the mutant carriers. We identified a variant of unknown significance (VUS) in the *MYH7* gene (I1927F), the second most common mutated gene in HCM, uniquely present in the severe HCM individual. Although the identified VUS has been previously described in HCM patients, there is not sufficient clinical and functional evidence to ascertain pathogenicity. To precisely evaluate the effect of the VUS, we generated a *MYH7* I1927F corrected isogenic iPSC line using CRISPR/Cas9. Functional evaluation of double and single mutant iPSC-CMs revealed that the additional presence of the *MYH7* variant was responsible for the faster cardiac contraction, strongly supporting a severe pathogenic contribution. Our study provides a unique platform to functionally assess the effect of genetic modifiers.

LIST OF FIGURES

LIST OF TABLES

LIST OF ABBREVIATIONS

α-MHC	alpha-myosin heavy chain
α-TM	alpha-tropomyosin
β-MHC	beta-myosin heavy chain
ADP	adenosine-5’-diphosphate
AGL	amylo-alpha-1, 6-glucosidase, 4-alpha-glucanotransferase
AMP	adenosine monophosphate
ARVC	arrhythmogenic right ventricular cardiomyopathy
ATP	adenosine-5’-triphosphate
bp	base pair
CaMKII	Ca2+/calmodulin-dependent kinase II
cAMP	cyclic adenosine monophosphate
Cas9	CRISPR associated protein-9
CASQ2	calsequestrin-2
CK	creatine kinase
CMRI	cardiac magnetic resonance imaging
cMyBP-C	cardiac myosin-binding protein C
CRISPR	clustered regularly interspaced short palindromic repeats
CSRP3	cysteine and glycine rich protein 3
cTnC	cardiac troponin, Ca^{2+}-binding subunit
cTnI	cardiac troponin, inhibitory subunit
cTnT	cardiac troponin, tropomyosin-binding subunit
DCM	dilated cardiomyopathy
DNA	deoxyribonucleic acid
DRX	disordered relaxed state
DSB	double strand break

E-C	excitation-contraction
ECAR	extracellular acidification rate
ECG	electrocardiogram
ELC	essential light chains
ESC	European Society of Cardiology
ETC	electron transport chain
FCCP	carbonyl cyanide-4 (trifluoromethoxy) phenylhydrazone
FXN	frataxin
GAA	alpha glucosidase
GLA	galactosidase alpha
GSD	glycogen storage diseases
HCM	hypertrophic cardiomyopathy
HDR	homology-directed recombination
hESC	human embryonic stem cell
HF	Heart failure
hPSC	human pluripotent stem cell
Hz	Hertz
Ig	immunoglobulin
iPSC	induced pluripotent stem cell
kb	kilobase-pairs
KDa	kilo dalton
KO	knock-out
LAMP2	lysosomal associated membrane protein 2
LMM	light meromyosin
LVNC	left ventricular non-compaction
LVOT	left ventricular outflow tract
MHC	myosin heavy chain

MLC	myosin light chain
MRPS22	mitochondrial ribosomal protein S22
mtDNA	mitochondrial deoxyribonucleic acid
MTTK	mitochondrially encoded tRNA-lys
MTTL1	mitochondrially encoded tRNA-leu
MYBPC3	myosin-binding protein C3 gene
MYH7	myosin heavy chain 7 gene
mRNA	messenger RNA
NCX	sodium/calcium exchanger
NGS	next-generation sequencing
NHEJ	non-homologous end joining
OCR	oxygen consumption rate
PA	Proline-Alanine
PAM	protospacer adjacent motif
PCr	phosphocreatine
PKA	protein kinase A
PKC	protein kinase C
PKD	protein kinase D
PLB	phospholamban protein
PLN	phospholamban gene
PRKAG2	protein kinase AMP-activated non-catalytic subunit gamma 2
PTPN11	protein tyrosine phosphatase non-receptor type 11
RCM	restrictive cardiomyopathy
RLC	regulatory light chain
RNA	ribonucleic acid
rRNA	ribosomal RNA
RSK	ribosomal S6 kinase

RyRs	ryanodine receptors
SCD	sudden cardiac death
SCO2	synthesis of cytochrome c oxidase 2
SD	standard deviation
SDHA	succinate dehydrogenase complex flavoprotein subunit a
SERCA2a	sarco/endoplasmic reticulum calcium ATPase
sgRNA	single guide RNA
SLC25A3	solute carrier family 25 member 3
SR	sarco/endoplasmic reticulum
SRX	super-relaxed state
t-	transverse
TALEN	transcription activator-like effector nuclease
TAZ	tafazzin
TCAP	titin-cap
TEM	transmission electron microscopy
TMEM70	transmembrane protein 70
TNNI3	troponin I3, cardiac type
TNNT2	troponin T2, cardiac type
TPM1	tropomyosin 1
tRNA	transfer RNA
TTN	titin
TTR	transthyretin
VUS	variant of uncertain significance
WES	whole exome sequencing
WT	wild type
ZFN	zinc finger nuclease

1 INTRODUCTION

1.1 Heart failure and cardiomyopathies

Heart failure (HF) is a continuously rising global health issue with almost 40 million people affected worldwide. The estimated prevalence of HF in developed countries is approximately 1-2% of the adult population (Ziaeian and Fonarow, 2016). However, primarily due to the demographic expansion towards an ageing population, the prevalence of HF is increasing. Data from the Global Burden of Disease Study reported that the number of deaths attributed to cardiovascular diseases increased more than 40% since 1990 (Mortality and Causes of Death, 2015).

According to the European Society of Cardiology (ESC), HF is defined as 'a clinical syndrome caused by a structural and/or functional cardiac abnormality, resulting in a reduced cardiac output' (Ponikowski et al., 2016). Although the cardiac dysfunction is usually caused by myocardial abnormalities, the presence of abnormalities in endocardium, pericardium, valves, hearth rhythm and conduction can cause HF. It is therefore a complex phenotype that represents a final common pathway of diverse natures. It is essential to identify the underlying cardiac problem, as the precise pathology will determine the specific therapeutic approach. However, this effort can be challenging, as the HF term comprises a broad range of underlying aetiologies that are frequently overlapped.

1.1.1 Determinants of heart failure and cardiomyopathies

Genetic and environmental factors are known determinants that influence on the risk and course of HF. Cardiomyopathies, a term reserved for the myocardium disease with known phenotypic or genetic pattern, are a common cause of HF (Czepluch et al., 2018). In 2008, the ESC published the classification of cardiomyopathies, defined as 'myocardial disorder in which the heart muscle is structurally and functionally abnormal, in the absence of

coronary artery disease, hypertension, valvular disease and congenital heart disease sufficient to cause the observed myocardial abnormality' (Elliott et al., 2008). Thus, according to morphological and functional features, cardiomyopathies can be classified into five groups: hypertrophic cardiomyopathy (HCM), dilated cardiomyopathy (DCM), arrhythmogenic right ventricular cardiomyopathy (ARVC), restrictive cardiomyopathy (RCM), and unclassified cardiomyopathies such as left ventricular non-compaction (LVNC) (Elliott et al., 2008). In 2013, the World Heart Federation proposed a standardized classification system that integrates the genetic information as well as the phenotypic description for cardiomyopathies. The so-called MOGE(S) system describes cardiomyopathies according to morphofunctional phenotype (M), organ involvement (O), genetic inheritance pattern (G), aetiological annotation (E) and functional status (S) of the disease. This classification system allows a better flexibility in cataloguing overlapping phenotypic and genetic cardiomyopathies (Arbustini et al., 2013).

1.1.2 Classification of cardiomyopathies

Cardiomyopathies are divided based on both morphological and functional phenotypes. Each phenotype is sub-classified into non-familial and familial forms (Elliott et al., 2008).

Non-familial cardiomyopathies are defined by the presence of a cardiomyopathy in an individual and the absence of the disorder in other members of the family. They are themselves divided into idiopathic, in which there is not and identifiable cause, and acquire cardiomyopathies, in which the cardiac dysfunction is derived as a complication of other disorders.

Familial forms are referred as the existence of the same disease or phenotype that is caused by the same pathogenic mutation in more than one family member. Most of familial cardiomyopathies are caused by single

pathogenic variants that are sufficient to cause the disease. A monogenic cardiomyopathy is sporadic when *the novo* mutations have been produced at the germinal level in one of the parents or occurred for the first time within the family.

1.1.3 Genetic interplay of cardiomyopathies

Although the previous description on the classification of cardiomyopathies may be seen unrefined, it has relevant importance from the clinical diagnosis and management. However, in the practice, there is a wide overlap between the phenotypes, which is mirrored in the genetic architecture (Figure I1A).

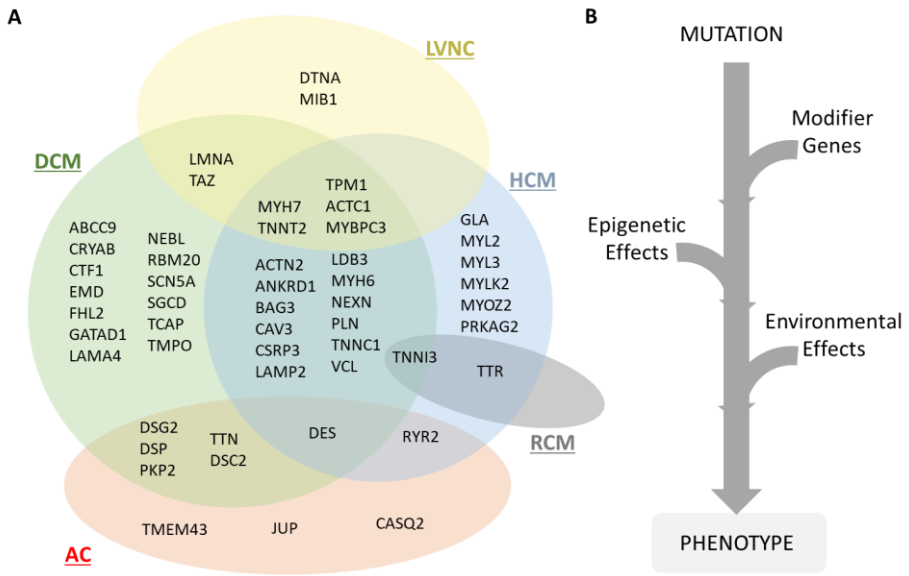

Figure I1. Schematic landscape of genetic cardiomyopathies representing the diverse and complex genetic and phenotypic heterogeneity. **A)** It is shown the most relevant mutated genes that are responsible for cardiomyopathies and **B)** the interplay with genetic, epigenetic and environmental modifiers.

In recent years, next-generation sequencing (NGS) has advance and revolutionized genetic screening, reducing the cost of genetic analysis and

facilitating its application in clinical routine diagnosis. The magnified detection of low frequency or rare variants with NGS is aiding to advance in cardiomyopathy genetics. Yet, it is still challenging differentiating disease-causative mutations from rare polymorphisms (Cahill et al., 2013; Czepluch et al., 2018). Sometimes, detected variants that are not commonly present in the population can only be described as variants of uncertain significance, as the ascribed pathogenicity implication is poorly supported. Thus, robust criteria for pathogenesis needs to be applied to NGS to avoid misinterpretations.

Nevertheless, the presence of multiple genetic low-penetrance variants, epigenetic modifiers or even protective variants that interplay with environmental factors may influence the phenotype and intricate the genetic contribution of cardiomyopathies (Figure I1B).

1.1.4 Common features of cardiomyopathies

Genetic cardiomyopathies are usually early onset and a main contributor to mortality and morbidity in the young population. In addition, the identification of a pathogenic mutation within a family allows the opportunity for an early diagnosis and intervention before the disease status has emerged. Genetic testing of family members has become the standard of care, as it also reduces health system costs (Ingles et al., 2012) and alleviates anxiety and stress of family members who test negative for pathogenic variants.

Several common characteristics of genetic cardiomyopathies has been defined (Cahill et al., 2013; Czepluch et al., 2018). First, mutations within the same gene can produce distinct quantitative variability in the expression of the phenotype, referred to as phenotypic heterogeneity. In addition, mutation in the same disease-associated gene might produce contrasting phenotypes. For example, mutations in the gene codifying for sarcomeric protein cardiac

troponin I (*TNNI3*) may produce DCM, HCM or RCM phenotype (Kimura et al., 1997; Mogensen et al., 2003; Murphy et al., 2004). More interestingly, even the same gene variant can produce a different phenotypic outcome. For example, deletion of arginine 14 in the gene encoding for phospholamban (*PLN*) was described in individuals with late-onset DCM without ventricular arrhythmias and the same mutation was found in a population with early onset 15% of DCM and 12% of ARVC subjects (DeWitt et al., 2006; van der Zwaag et al., 2012).

Second, each cardiomyopathy phenotype can be caused by numerous mutated genes, referred to as genetic heterogeneity (Figure I1A). During the last decades, it has been identified more than 100 genes, whose mutations cause distinct cardiomyopathy phenotypes. Within these genes, a plethora of different variants has been described (allelic heterogeneity). A high proportion of these rare mutations are specific to an individual family and is less common to find hot spot mutations. Given this complex heterogeneity, genetic testing with known gene panels may not be effective and systematic sequencing is therefore needed instead. However, rare variants are highly frequent in the genome and its pathogenicity must be validated. Linkage analysis in large family pedigrees with a clear cosegregation of the mutation with the phenotype is helpful. However, families are frequently small and the proportion of idiopathic cases are considerable.

Third, both penetrance and expressivity are highly variable. That is, the proportion of individuals bearing a pathogenic variant who is phenotypically affected (even within the same family) and the severity of the phenotype, respectively. This means that multiple factors beyond the single pathogenic mutation have an influence on the phenotype (i.e. genetic, epigenetic and environmental modifiers) even in apparently 'monogenic diseases' (Figure I1B). Gender is also a modifier of cardiomyopathy expression. It has been

described that males are frequently more affected in HCM, which has been recapitulated in animal models (Geisterfer-Lowrance et al., 1996). In addition, truncating mutations in the gene coding for titin (*TTN*), are associated with more severe left ventricular dysfunction in males (Herman et al., 2012). These gender differences may be attributable to multiple factors such as hormone levels, gene expression differences or physiological differences, including heart size (McNally et al., 2015).

1.2 Hypertrophic cardiomyopathy

The first report of an HCM phenotype was described in 1958 by Teare, who analysed the clinical and histological characteristics of seven individuals that suffered sudden cardiac death (SCD) (Teare, 1958). During the next decades, the concept of HCM continued evolving in line with the development of new technologies such as the catheterization and echocardiography, which helped to understand the haemodynamic alterations and to define hypertrophic patterns (Santos Mateo et al., 2018).

HCM is the most common inherited cardiac disease and the main cause of SCD in individuals below the age of 35, particularly in young athletes. The prevalence is approximately at 1 in 500 in the general population (Maron et al., 1995). This estimate derives from a young population-based survey that rely on older methods of detection. Given the broad age range of HCM and the late onset for some mutations, HCM prevalence is more likely to be underestimated (Semsarian et al., 2015).

HCM is defined by an increase in ventricular wall thickness or mass in the absence of other loading conditions, such as hypertension or valve disease, that is sufficient to produce the observed phenotype (Elliott et al., 2008). The majority of HCM patients have an asymmetrical pattern of hypertrophy,

affecting mostly the interventricular septum (Figure I2), although other patterns of hypertrophy are observed (concentric, apical or segmented).

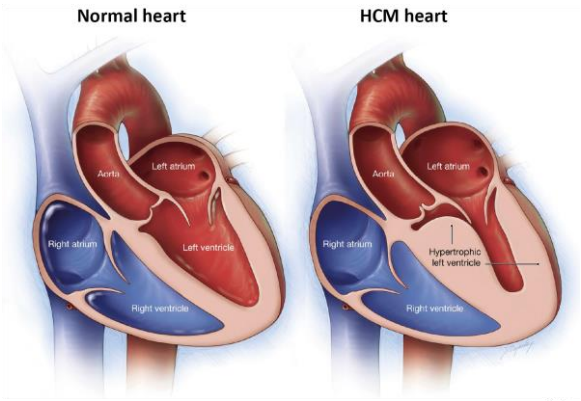

Figure I2. Illustration of the main phenotype observed in HCM patients as compared to a normal heart. Thickening of the ventricular heart and a reduced left ventricular cavity describe the clinical phenotype in HCM. Adapted from Mayo Foundation for medical education and research with their permission.

1.2.1 Genetics of hypertrophic cardiomyopathy

The first HCM mutation was identified in the sarcomeric gene that codifies for the β-myosin heavy chain (*MYH7*) in 1990, becoming the first inherited cardiac disease with a genotype-phenotype relationship (Geisterfer-Lowrance et al., 1990). During subsequent years, mutations in other sarcomere genes were identified, specifically in the genes coding for cardiac troponin T (*TNNT2*) and α-tropomyosin (*TPM1*). These discoveries led to the concept that HCM was a disease of the sarcomere (Thierfelder et al., 1994). The most common genes are described in Table I1.

1.2.1.1. Sarcomere gene mutations

The pattern of inheritance is most frequently autosomal dominant, with locus and allelic heterogeneity. More than 1400 mutations have been described to be associated with HCM.

Table I1. Most common genes associated with hypertrophic cardiomyopathy.

Protein	Gene	Frequency (%)	Location
Sarcomeric			
Thick filament			
β-Myosin heavy chain	*MYH7*	30-40	14q11.2
Regulatory myosin light chain	*MYL2*	2-4	12q23-q24
Essential myosin light chain	*MYL3*	1-2	3p21.3
α-Myosin heavy chain	*MYH6*	<1	14q11.2
Cardiac myosin-binding protein C	*MYBPC3*	30-40	11p11.2
Thin filament			
Cardiac troponin T	*TNNT2*	10	1q32.1
Cardiac troponin I	*TNNI3*	7	19q13.4
α-Tropomyosin	*TPM1*	<5	15q22.1
Cardiac troponin C	*TNNC1*	<1	3p21.1
α-Cardiac actin	*ACTC1*	<1	15q11q14
α-Actinin 2	*ACTN2*	<1	1q43
Z-disc			
Desmin	*DES*	<1	2q35
Cardiac LIM protein	*CSRP3*	<1	11p15.1
Telethonin	*TCAP*	<1	17q12
Calcium handling and regulators			
Phospholamban	*PLN*	<1	6q22.3
Calsequestrin	*CASQ2*	<1	1p13.1
Junctophilin 2	*JPH2*	<1	20q13.12
Other genetic causes			
Danon disease	*LAMP2*	<1/X-linked dominant	Xq24
Fabry disease	*GLA*	0.5-1/X-linked	Xq22.1
Forbes disease	*AGL*	<1/Recessive	1p21.2
Pompe disease	*GAA*	<1/Recessive	17q25.3
Wolff-Parkinson-White syndrome	*PRKAG2*	<1/Dominant	7q36.1
FHL1-related diseases	*FHL1*	<1/X-linked	Xq26.3
Transthyretin amyloidosis	*TTR*	<1/Dominant	18q12.1
Noonan and LEOPARD syndrome	*PTPN11*	<1/Dominant	12q24.13
CFC syndrome	*BRAF*	<1/Dominant	7q34
Friedreich's ataxia	*FXN*	<1/Recessive	9q21.11
MELAS/MERF	mtDNA	Matrilinear	mtDNA

MELAS indicates mitochondrial encephalomyopathy, lactic acidosis and stroke-like episodes; and MERF indicates myoclonic epilepsy with ragged red fibbers. Adapted from (Ho et al., 2015).

MYH7 (coding for β-myosin heavy chain, β-MHC) and *MYBPC3* (coding for cardiac myosin-binding protein C, cMyBP-C), account for 70-80% of all cases of the disease. In approximately 60-70% of familial cases and in 30-40% of apparently sporadic cases, it is possible to detect a mutation in almost all of the sarcomere genes (Alfares et al., 2015; Richard et al., 2003; Sabater-Molina et al., 2018).

Though mutations in *MYH7* and *MYBPC3* are highly associated with HCM, the mechanisms of the disease-causing mutations in these genes may differ. Most of the pathogenic variants in *MYH7* that produce HCM are amino acid substitutions in functional domains and key residues that alter its function. Alternatively, and particularly in the *MYBPC3* gene, approximately 90% of the identified HCM-causing mutations produce a truncated version of the protein.

Mutations in the thin filament proteins account for a small proportion of HCM patients. Remarkably, mutations in the troponin complex proteins, *TNNT2* and *TPM1*, demonstrate a high degree of phenotypic heterogeneity and can give rise to other cardiomyopathy phenotypes (Thierfelder et al., 1994).

Most pathogenic variants associated with HCM are specific to a family or few families (private mutations). However, it has been recognized singular mutational 'hot spots', such as *MYH7* Arg403Gln and Arg453Cys; and *MYBPC3* Arg502Trp, c.1928-2A>G and IVS23+1G (Ho et al., 2015; Oliva-Sandoval et al., 2010), reflecting likely a founder mutational effect.

1.2.1.2. Non-sarcomere gene mutations

About 40% of HCM cases test negative for sarcomeric gene panels, indicating that further loci beyond the sarcomere are responsible for the development of the disease. It is likely, in fact, that several contributing

variants or nonmendelian genetic susceptibility are the underlying cause of HCM. Gene screening has led to reports of mutations in Z-disk and calcium handling proteins, such as muscle LIM protein (*CSRP3*)(Geier et al., 2008), telethonin (*TCAP*)(Hayashi et al., 2004) or calsequestrin (*CASQ2*)(Landstrom and Ackerman, 2012).

In the young, at approximately 5-10% of cases, HCM is frequently associated with congenital syndromes, inherited metabolic disorders or neuromuscular diseases, in which the ventricular hypertrophy is mimicked. These non sarcomeric-based phenocopies represent distinct disorders with different inheritance, pathophysiology and disease management (Lopes and Elliott, 2013; Rapezzi et al., 2013). They include a variety of disorders such as lysosomal and glycogen storage diseases (GSD), disorders of fatty acid metabolism or mitochondrial cytopathies.

Inborn errors of metabolism are more commonly diagnosed in paediatric population with HCM (Colan et al., 2007). They include GSD such as Pompe's disease (glycogen deposition due to *GAA* gene deficiency), Forbes's disease (*AGL* gene deficiency) or Danon's disease (*LAMP2* gene deficiency). Excess of glycogen deposition is also observed in adolescents and young adults due to mutations in the *PRKAG2* gene (Wolff-Parkinson-White syndrome) (Sankaranarayanan et al., 2013). Although the proportion of HCM at the infant population is lower than in adults, it associates frequently as a feature of multisystem disorders such as Noonan and LEOPARD syndromes (Lentigines, Electrocardiographic abnormalities, Ocular hypertelorism, Pulmonary stenosis, Abnormal genitalia, Retardation of growth and Deafness). These examples of RASopathies can be caused by germline mutations that alter the RAS-MAPK cascade or related to mutations in the *PTPN11* gene (Pandit et al., 2007; Sabater-Molina et al., 2018). In adults, non-sarcomeric aetiology is less frequent but includes metabolic storage diseases such as Fabry disease

(mutations in *GLA* gene lead to multisystem accumulation of glycosphingolipids) and familial amyloidosis (amyloid deposition in the myocardium due to mutations in the *TTR* gene) (Sankaranarayanan et al., 2013).

1.2.1.3. Mitochondrial-related causes

Cardiomyopathy commonly appears as a consequence of mitochondrial genetic defects (Holmgren et al., 2003). Mitochondrial disease phenotypes are highly heterogeneous and typically involve multiple organ systems, especially those with high adenosine-5'-triphosphate (ATP) requirements such as the heart, skeletal muscle and the nervous system. Thus, metabolically active tissues would have greater susceptibility to alterations in mtDNA than less metabolically active tissues, with early and more severe pathological manifestations (Hirano et al., 2001). Mitochondria are under dual genome control in which only a minor fraction is encoded by the mitochondrial DNA. Specifically, mtDNA encodes only for 13 subunits of the electron transport chain (ETC) complexes, 2 rRNA and 22 tRNAs (Taanman, 1999). Mutations in either the mitochondrial DNA or, more commonly, in the nuclear genome, can result in mitochondrial dysfunctions (Duran et al., 2019). Nevertheless, mitochondrial mutations are rare and the genotype-phenotype correlation is often limited, since the phenotypes can present in a wide number of pathologies that may vary over time (van der Bliek et al., 2017).

Mitochondrial cardiomyopathies have been associated to mutations in genes that codified for proteins involved in the respiratory chain components (e.g. *SDHA*, *SCO2*, *TMEM70*), mtDNA translation (*MRPS22*), ATP synthesis (*SLC25A3*), phospholipid remodelling (*TAZ*) or mitochondrial rRNA (Duran et al., 2019; Li et al., 2018). Cardiomyopathies caused by mtDNA-related mutations are rare. However, in nearly 40% of patients with mitochondrial

disease, the dominant phenotype is HCM (Limongelli et al., 2017). A well-known example is Friedreich's ataxia. It is a multisystem disease caused by DNA triplet intron repeats of GAA in the frataxin gene (*FXN*), leading to decreased ATP production, mitochondrial iron accumulation, oxidative stress and dysfunction. These patients frequently develop HCM and almost two thirds die from cardiac causes (Jensen and Bundgaard, 2012).

Within the 16.6 kb mitochondrial genome, more than 250 pathogenic mutations has been reported, with many multisystem disorders causing cardiomyopathies (Duran et al., 2019). The most common are MELAS (Mitochondrial Encephalomyopathy, Lactic Acidosis and Stroke-like episodes) syndrome, caused by mutations in the *MTTL1* gene, and MERRF (Myoclonic Epilepsy with Ragged Red Fibres) syndrome, caused by mutations in the *MTTK* gene.

1.2.1.4. Multiple genetic variants in hypertrophic cardiomyopathy

Rapid advancements in high-throughput DNA sequencing have revolutionized genetic screening and the ability to analyse genetic variation of Mendelian disorders, both in healthy and diseased individuals (Lek et al., 2016). Therefore, a vast increase of novel genetic variants has been associated to HCM, often with insufficient evidence (Ingles et al., 2019). This ever-increasing collection of sequence changes has raised important challenges in variant interpretation. For numerous rare novel variants, there is not sufficient information to ascertain pathogenicity and they are thus classified as variants of unknown significance (VUS) (Manrai et al., 2016; Mazzarotto et al., 2020).

A relevant proportion of patients with HCM (2.5-7%) has been reported to carry more than one sequence variants within the sarcomeric genes (Alfares et al., 2015). These complex genotypes include compound heterozygosity (heterozygous mutations in both alleles of the same gene) and double

heterozygous patients (heterozygous mutations in two different genes). Most of the probands with multiple variants carry at least one VUS, which generates uncertainty and adverse consequences for the patients and their relatives, as multiple variants have, in general, a gene-dose effect with a more severe phenotype and an early-onset disease (Alpert et al., 2005; Girolami et al., 2010).

More than one-third of individuals who are clinically diagnosed with HCM test negative for the core sarcomere genes, indicating that the genetic aetiology of these patients is unknown (Maron, 2018). Of note, identifying highly penetrant pathogenic variants in genes not previously associated with HCM is very unlikely. Consequently, most of these individuals may represent non-Mendelian HCM in which subtle effects of multiple variants can cause HCM (Mazzarotto et al., 2020). A recent study of a familial cardiomyopathy has started providing functional effects on the epistatic interactions of rare, inherited heterozygous mutations (Gifford et al., 2019). Gifford et al. observed that when three missense variants were inherited, a severe childhood-onset LVNC was developed. However, these variants were not harmful when observed in isolation (Gifford et al., 2019). Investigations into the complex genetic models of HCM are still largely unexplored and limited mainly by the lack of large sequenced population cohorts for genome wide association studies and by the lack of functional evidences to support genotype-phenotype correlations.

1.2.2 Histological and clinical phenotypes

The histological, morphological and clinical phenotypes of HCM are influenced by several genetic, epigenetic and environmental determinants. Therefore, such multiplicity limits the effect of each modifier to accurately predict the severity and the phenotypic outcome. Nevertheless, the

penetrance of HCM phenotypes is highly variable, ranging from asymptomatic to lethal cardiac dysfunction (Sedaghat-Hamedani et al., 2018).

The main clinical hallmark for diagnosis is the thickened left ventricular wall in the absence of any hemodynamic reason (hypertension, aortic stenosis). The right ventricle is infrequently involved by hypertrophy. The cardiac myocytes are enlarged and have a disarrayed pattern, with loss of normal parallel alignment because of disorganized orientation. Another key histological feature is the interstitial fibrosis (Marian and Braunwald, 2017). Its extent is associated with cardiac adverse clinical outcomes, including SCD and arrhythmias (Briasoulis et al., 2015). In addition, intramural coronary vessels may exhibit wall thickening, conditioning the appearance of myocardial ischemia. HCM is generally associated with normal or small left ventricular cavity and preserved systolic contractile function. In addition, approximately 70% of HCM patients present left ventricular outflow tract (LVOT) obstruction, which is a predictor of adverse clinical consequences when is present under resting conditions (Maron et al., 2006).

Diastolic dysfunction (impaired myocardial relaxation) can also be described as a hallmark of HCM and is characterized by elevated cardiac activation at low calcium concentrations (Fraysse et al., 2012; Michels et al., 2009). It can be influenced directly by HCM mutations and indirectly by the increased interstitial fibrosis (Marian and Braunwald, 2017; Sewanan et al., 2019). Ventricular arrhythmias can be found in a quarter of HCM patients, with a prevalence increasing with age and the extent of fibrosis (Santos Mateo et al., 2018). The electrocardiogram (ECG) is abnormal is most HCM patients and usually precedes the development of hypertrophy (Santos Mateo et al., 2018).

1.3 The cardiac contractile machinery

Cardiac contraction is a complex and precise process that includes sarcomeric myofilament proteins and multiple associated regulatory elements. Within the cardiomyocyte, contraction takes places through a process known as excitation-contraction coupling, in which an electrical stimulus initiates the mechanical sarcomere contraction via the release of calcium to the cytosol.

1.3.1 The sarcomere

The sarcomere is the basic unit of contraction in both striated skeletal and cardiac muscle cells. Among its primary components are myofilament proteins, consisting of thin and thick filaments that extend parallel across the sarcomere where they partially overlap, occupying I- and A-bands, respectively (Figure I3) (Henderson et al., 2017; Huxley, 1957).

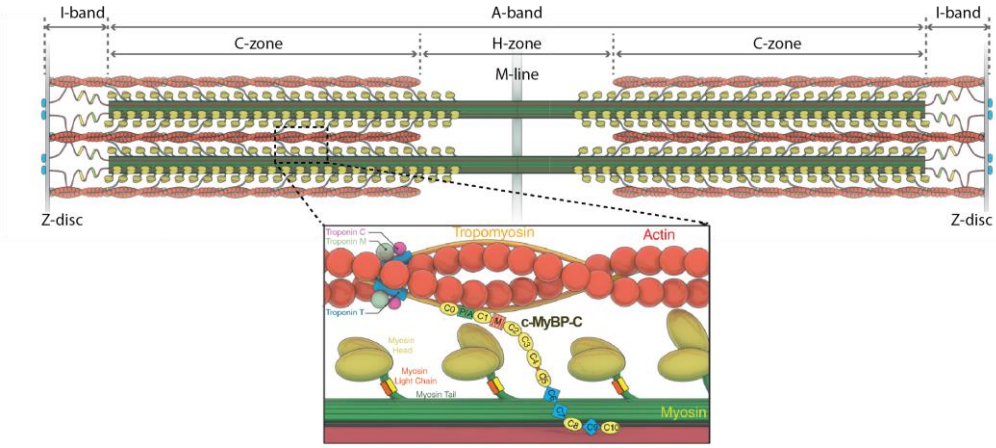

Figure I3. Organization of the sarcomere and the myofilament proteins. (Top) Thin filaments of actin overlaps the myosin thick filaments at the C-zone, where 7 to 9 cMyBP-C proteins are located. (Bottom) The N-terminus of cMyBP-C interacts with actin and myosin heads, while the C-terminus associates with thick filaments. Adapted from (Lin et al., 2017).

1.3.2 Thin filaments

The principal component of the thin filament is actin, which forms a helical structure attached at the Z-disks and stabilized by the structural protein nebulette. Helical structures of tropomyosin also spans along the length of actin, periodically interacting with the troponin complex (Lehman, 2016).

- Actin is a globular protein that polymerizes into filamentous actin (F-actin), forming a coiled-coil within the sarcomere. Functionally, it serves as an anchor to tropomyosin and troponin proteins (Yamada et al., 2020). Specific actin subdomains can interact with other myofilament proteins, such as with the myosin catalytic head region to transduce force generation, or with cMyBP-C to regulate contraction kinetics.

- The intracellular influx of Ca^{2+} produced by different calcium channels is detected and transduced by the troponin complex. This complex is composed of three subunits: cardiac troponin C (cTnC: the Ca^{2+}-binding regulatory subunit), cardiac troponin I (cTnI: the inhibitory subunit) and cardiac troponin T (cTnT: the Tropomyosin-binding subunit). At low Ca^{2+} concentrations, at resting state, tropomyosin is positioned to block the myosin interaction with actin. Following Ca^{2+} release to the cytosol, Ca^{2+} binds to cTnC and triggers conformational changes that expose the actin-binding sites to myosin.

1.3.3 Thick filaments

The major component of the thick filaments is myosin, the molecular motor that drives the sliding of actin and mediates force generation. Along the length of the thick filament and bound to myosin there is titin, the largest known protein that serves as a scaffold to the thick filament. Associated to it, there is also obscurin and cMyBP-C (Wang et al., 2018).

- Cardiac myosin is codified as two major isoforms, the fast α-myosin and the slow β-myosin, expressed by the *MYH6* and *MYH7* genes, respectively. In humans, β-myosin is predominantly express in ventricles, whereas the α-myosin isoform is primarily express in rodents (Gupta, 2007). Myosin serves as a cross-bridge on actin, sliding the thin filaments across the thick filament. Each myosin is a hexameric protein, consisting on two myosin heavy chains (MHCs), two essential light chains (ELCs) and two regulatory light chains (RLCs). The two MHCs produce a long coiled-coil tail structure separated by two globular heads, connected by a converter domain and by a lever arm that binds ELC and RLC. The catalytic head region is projected outward from the thick filament and is the responsible for the physical interaction with actin to form cross-bridges (Rayment et al., 1993). At the myosin C-terminus, the coiled-coil tail binds myosin to the thick filament, where it interacts further with cMyBP-C and with titin.

- Titin is considered the third myofilament and it spans the length of half sarcomere. It provides a structural scaffold for the thick filament proteins as well as a stability. The elastic regions of titin also contribute to passive tension during diastole (Linke, 2018). It interacts with many myofilament proteins, such as actin, nebulette or obscurin (Wang et al., 2018).

1.4 Cardiac cross-bridge cycling and force production

Power stroke generation is a highly regulated process in which thin and thick filament accessory proteins greatly mediate cross-bridges between actin and myosin. During the actomyosin contractile cycle, the chemical energy of ATP is transformed into a mechanical force (Kiani and Fischer, 2016; Wang et al., 2018). The major events are described below and are illustrated in Figure I4.

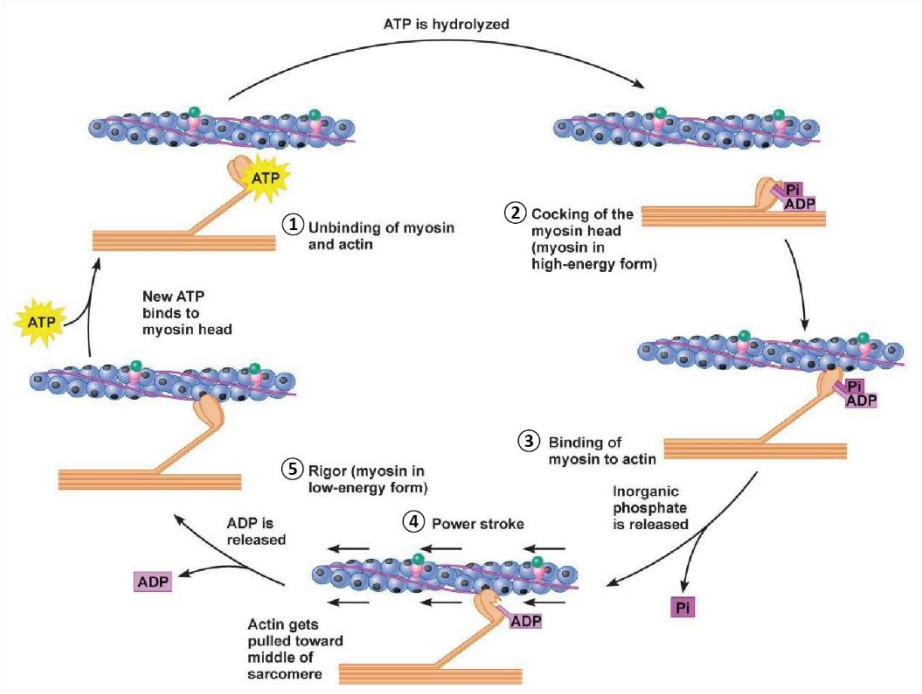

Figure I4. The actomyosin cross-bridge cycle. 1) Upon ATP binding to the myosin head, myosin dissociates from actin. 2) Myosin head recuperates its power stroke and ATP is hydrolysed into ADP-Pi complex. 3) Myosin head binds actin 4) Conformational changes upon binding to actin triggers Pi release and the sliding through actin. 5) The nucleotide-binding pocket opens and ADP is released. Rapidly, a new ATP molecule is then bound to the myosin head for a new cross-bridge cycle (Adapted from Stanfield, 2013).

1) During actomyosin contraction, the cycle begins when an ATP molecule rapidly binds into the opened nucleotide pocket within the globular myosin head. This ATP binding is coupled with the dissociation of myosin from actin.
2) The repositioning into the pre-power conformation follows, in which it is produced the rotation of the converter domain by 65^{o} and the recovery of the power stroke (that is, relaxation). The conformational change imposed by the rotation allows ATP hydrolysis, resulting in the stable adenosine-5'-diphosphate (ADP)·Pi complex.

3) After hydrolysis, a weak interaction between actin and myosin is enabled. The altered conformation triggers the release of inorganic phosphate Pi resulting in an enhanced actomyosin interaction, mediated by electrostatic interaction between the two filaments, and the generation of power stroke.

The generated myosin force produces a sliding movement through actin, cell shortening, and muscle contraction. After ADP release (limited until the cross-bridge is completed), another cross-bridge cycle is ready to take place following binding of a new ATP molecule and muscle relaxation (Geeves, 2016). Overall, cardiac contraction is a complex mechanism that involves several levels of regulation and multiple protein-protein interactions, including actin, myosin, troponin complex, tropomyosin, titin, cMyBP-C and many other proteins and post-translational modifications, mainly phosphorylation, that fine-tune force production.

1.4.1 Hyperdynamic state as a common feature of hypertrophic cardiomyopathy

At the organ level, is generally accepted that hypertrophic heart is characterized by hypercontractility, as evidenced by an increased power output (Spudich, 2014, 2019), and by a poor relaxation. In support to this view, chronic activation of heart contractility produces ventricular hypertrophy (Osadchii, 2007). At the sarcomere level, the biochemical and physical effects of the HCM mutations have been studied in order to understand the observed clinical phenotypes. In many biomechanical assays, the molecular phenotypes can partially explain the hyperdynamic contraction seen in HCM patients: accelerated actin sliding velocities, increased ATPase activity and increased tension development (Moore et al., 2012). However, there is considerable variability in the literature regarding the effects on contractility. Regarding

MYH7 mutations, force generation has been shown to be either reduced (Kawana et al., 2017; Nag et al., 2015) or increased (Adhikari et al., 2016; Sommese et al., 2013), actomyosin sliding velocities either accelerated (Adhikari et al., 2016; Kawana et al., 2017) or reduced (Sommese et al., 2013) and ATPase activity to be increased (Adhikari et al., 2016; Nag et al., 2015). Such discrepancies can be explained by the limitations of the biomechanical assays, which mainly consist of *in vitro* expressed recombinant mutant myosin, myosin purified from animal cardiac tissues or myofibrillar preparations (Moore et al., 2012). In recent years, structural studies are clearing the path for a better understanding of hypercontractility at the molecular scale. They state that most *MYH7* mutations can weaken the super-relaxed state of myosin and increase both the number of accessible globular heads that interact with actin and the catalytic activity of myosin heads (Adhikari et al., 2019; Nag et al., 2017).

The effect of *MYBPC3* mutations on cardiac contractility has also been studied thoroughly, since its protein product cMyBP-C is closely associated with myosin and both genes account for the majority of mutations found in HCM patients. Functional studies indicate that reductions in cMyBP-C content lead to higher cross-bridge kinetics and fewer maximal force of contraction (Hoskins et al., 2010). Supporting the observations that cMyBP-C acts as a 'molecular break' of cardiac contraction (Previs et al., 2012), recent findings showed that *MYBPC3* mutations disrupt myosin conformations, leading to an increase in the number of globular heads accessible for interacting with actin. Hence, increasing the probability of cross-bridge and hypercontractility (O'Leary et al., 2019; Toepfer et al., 2020; Toepfer et al., 2019).

1.5 The excitation-contraction coupling

The process in which an electrical stimulus in the surface membrane (action potential) is linked to the cardiac contraction is known as excitation-contraction (E-C) coupling (Bers, 2002). The main factor that regulates cardiac contraction is the level of intracellular calcium (Allen and Kurihara, 1980), although it can be further controlled by genetic or epigenetic factors, mainly phosphorylation. Proper cardiac function requires that intracellular calcium concentration ($[Ca^{2+}]_i$) increase during contraction (systole) and decrease quickly to low levels for relaxation (diastole) (Figure I5). Both the magnitude and duration of $[Ca^{2+}]_i$ will determine force development (Bers, 2002).

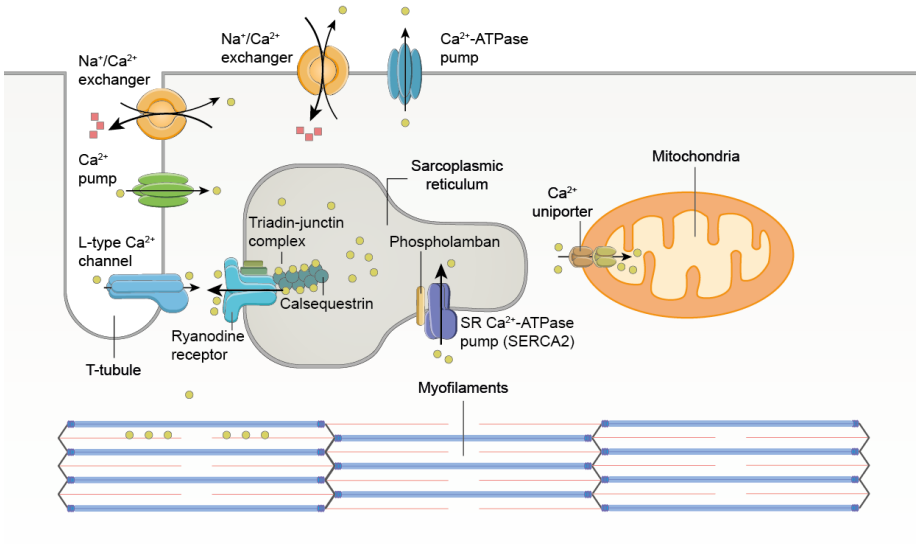

Figure I5. Calcium cycling in ventricular cardiomyocytes. Following an action potential, L-type Ca^{2+} opens and Ca^{2+} enters into the T-tubule-SR junction. The small Ca^{2+} entry is detected by Ryanodine receptors, which release larger amounts of Ca^{2+} from the SR. Then, Ca^{2+} diffuses into the cytoplasm, where it binds to the myofilaments activating the cardiac contraction. For relaxation, Ca^{2+} is removed from the cytoplasm back to the SR mainly by SERCA2 pumps and out of the cell by the Na+/ Ca^{2+} exchanger. Yellow circles represent Ca^{2+}, red squares represent Na^+.

In mammalian cardiac myocytes, the synchronous rise of Ca^{2+} concentration and rapid contraction throughout the entire cell is due by the presence of transverse (t-) tubules. T-tubules are deep invaginations of the surface sarcolemma occurring at the z-line of each sarcomere, forming a complex network in adult cardiomyocytes (Salle and Brette, 2007). E-C coupling depends on the close proximity between the t-tubules network and the sarco/endoplasmic reticulum (SR), the major Ca^{2+} storage organelle within the myocyte.

1.5.1 Calcium release and myofilament activation

During an action potential, clusters of L-type Ca^{2+} channels, located primarily on the t-tubules, open and local $[Ca^{2+}]_i$ rises within sarcolemmal-SR junctions. The local $[Ca^{2+}]_i$ rises up to 10-20 μM and activates ryanodine receptors (RyRs) clusters located at the SR membrane, triggering the release of higher amounts of Ca^{2+}. This process is known as Ca-induced Ca release, and raises the local t-tubule-SR junction $[Ca^{2+}]_i$ to 200-400 μM (Bers, 2008). Ca^{2+} diffuses then to the cytoplasm, where it binds to cTnC to activate the myofilaments.

Although the main trigger of Ca current for E-C coupling is the L- type Ca^{2+} channels, it has been proposed that the Sodium/Calcium Exchanger (NCX) could slightly modulate as well the Ca^{2+} release in cardiomyocytes (Aronsen et al., 2013). However, the influence of NCX is limited because the influx Ca^{2+} rate is several orders of magnitude smaller than for L- type Ca^{2+} channels, and NCX do not colocalize with RyRs (Scriven et al., 2000).

RyRs activity can be regulated by intra-SR Ca, mainly by the Ca-binding protein calsequestrin (CASQ2) via junctin and triadin (Gyorke et al., 2004). As Ca^{2+} is released by RyRs, the gating properties favour their closure. In addition, RyRs and L-type Ca^{2+} channels can also be regulated in a phosphorylation-

dependent manner, by both cAMP-dependent protein kinase A (PKA) and Ca^{2+}/calmodulin-dependent kinase II (CaMKII) (Ginsburg and Bers, 2004), essentially by enhancing their activities.

Upon Ca^{2+} release from the sarcoplasmic reticulum to the cytosol, Ca^{2+} binding to cTnC produces the binding of the N-terminus cTnI to cTnC. This causes cTnT to move together with tropomyosin around on the actin surface, exposing some myosin head binding sites and allowing myosin-actin interactions (Lehman, 2016; Lehman et al., 1994). When myosin head binds to actin, a further movement of tropomyosin away from the myosin-binding sites facilitates the formation of neighbouring actomyosin crossbridges, favouring an increase in cTnC affinity for Ca^{2+} and a contractile force generation via myofilament cooperativity (Lehman, 2016; Yamada et al., 2020).

1.5.2 Calcium decline and relaxation

Termination of calcium release is essential for relaxation of the cardiac muscle and diastolic refilling of the heart. It is important to consider that, in a steady state, calcium fluxes across membranes must be balanced, such that the amount of Ca^{2+} that enters by L-type Ca channels must equal the amount extruded, and the amount that is released by the SR must equal the amount of Ca^{2+} loaded (Eisner et al., 2017). Calcium decline can be modulated by several Ca^{2+} transporter systems. The major contributors to Ca^{2+} removal from the cytosol are both the SR Ca^{2+}-ATPase (SERCA2a) and the sarcolemmal NCX. Minimal contributors are also the plasma membrane Ca^{2+}-ATPase and the Ca^{2+} uniporter in the mitochondria, both accounting for approximately 1% of Ca^{2+} decline (Biesiadecki et al., 2014).

The majority of the Ca^{2+} efflux towards the SR is due to SERCA2a. In fact, in large mammals, the fraction of Ca^{2+} that cycles through the SR is closer to 70%, whereas in rat and mouse is 90-95% (Bers, 2002). SERCA2a pumps two

Ca^{2+} ions per ATP molecule and its activity is mainly regulated by phospholamban (PLB). PLB binding decreases Ca^{2+} affinity of SERCA2a and reduces the rate of Ca^{2+} uptake to the SR, whereas PLB phosphorylation enhance SR Ca^{2+} uptake (Kranias and Hajjar, 2012).

The NCX transporter is the main responsible for the sarcolemmal extrusion of Ca^{2+}, with a minor contribution of the membrane Ca^{2+}-ATPase. In larger mammals, 25-28% of Ca^{2+} decline is due to NCX, while in rat and mouse is less than 4% (Bers, 2002). NCX extrusion of one Ca^{2+} ion is coupled with the entry of three Na^{+} ions, although the transporter is bi-directional and can contribute to Ca^{2+} influx (Kang and Hilgemann, 2004).

Acceleration of calcium decline from the cytosol by the aforementioned channels accelerates relaxation proportionally. However, relaxation (and contraction) is also influenced by cTnC Ca^{2+} affinity and by the intrinsic properties of actomyosin crossbridge cycling rates (Bers, 2008; Biesiadecki et al., 2014).

Cardiac relaxation is initiated by Ca^{2+} decline and following $[Ca^{2+}]_i$ dropping below cTnC-Ca^{2+} binding threshold, it dissociates from cTnC. Subsequent conformational changes contribute then to the inactivation of the thin filament and the blocking of myosin binding sites with actin. The rate of cTnC-Ca^{2+} association/dissociation can be regulated by different thin filament isoforms, mutations and post-translational modifications. For example, it is well established that an increase in cTnI phosphorylation at Ser-23/24 decrease cTnC-Ca^{2+} affinity and accelerates the rate of cTnC-Ca^{2+} dissociation (Wijnker et al., 2013; Zhang et al., 1995).

Actomyosin cross-bridges must release from actin prior to thin filament deactivation. On one side, the rate of cross-bridge release contributes to the rate of relaxation. Secondly, its detachment indirectly contributes to a faster

thin filament deactivation by decreasing cTnC- Ca^{2+} affinity. Of note, the ATPase cycling kinetics within the myosin head has been proposed as the rate-limiting step for cardiac relaxation, as alterations in this rate highly influences muscle contraction and relaxation (Gordon et al., 2000). For example, the cardiac isoform α-myosin has a two-five times faster ADP dissociation rate than the β-myosin isoform (Suzuki et al., 2009). Additionally, cross-bridge kinetics can be regulated by myosin light chains, titin and cMyBP-C.

1.5.3 Abnormal myofilament calcium sensitivity in hypertrophic cardiomyopathy

Calcium mishandling is a central cause of arrhythmias and contractile dysfunction in pathological conditions, such as genetic cardiomyopathies and heart failure. The relation between the concentrations of intracellular Ca^{2+} and force development is a highly regulated process. Numerous reports indicate an increased Ca^{2+} sensitivity in mouse and cellular models of HCM (Baudenbacher et al., 2008; Cazorla et al., 2006; Davis et al., 2016; Fraysse et al., 2012; Frey et al., 2011; Michele et al., 1999), indicating more force development at lower Ca^{2+} concentrations. This increased Ca^{2+} sensitivity predicts cardiac hypercontractility and a delayed intracellular calcium reuptake (prolonging mechanical relaxation). Both consequences are compatible with the preserved systolic function and diastolic dysfunction frequently observed in HCM patients (Ho et al., 2002).

Increased myofibrillar Ca^{2+} sensitivity is not a conclusive hallmark of HCM, as other studies have reported no change (Harris et al., 2002), or even decreased Ca^{2+} sensitivity (Sweeney et al., 1998), indicating that such differences may also depend on the specific mutations and the genetic modifiers.

1.6 Cardiac energy metabolism

The myocardium is constantly supplying blood and energy substrate to the whole organism and, as the brain tissue or skeletal muscle, is one of the tissues with higher aerobic metabolic demand. Structural and functional integrity of mitochondria is fundamental for the proper physiological function of the heart, as mitochondria are essential for the production of energy in form of ATP. The cardiac muscle has low levels of energy reserve, as the total amount of ATP within a myocyte is consumed in 10-15 seconds. Moreover, the cardiac turnover of ATP is 6 kg per day (Neubauer, 2007). The high energetic requirements make the cardiac muscle sensitive to genetic or acquire alterations in energy supply and to an inefficient energy utilization.

Each cardiomyocyte contains hundreds of mitochondria in which their morphological integrity is important for cardiac development, cardiac remodelling during hypertrophy and heart failure. Indeed, pathological changes in cardiomyocytes are reflected in the morphology of mitochondria, which are tightly regulated by quality control pathways including fusion and fission proteins or post-translational modifications (Fan et al., 2020; Ong et al., 2010).

1.6.1 Energy substrate utilization and oxidative phosphorylation

Most of the ATP needed for proper cellular function is produced by the mitochondrial electron transport chain (ETC) complexes in a process called oxidative phosphorylation (Figure I6). It involves two simultaneous processes: (1) the transport of electrons through the ETC complexes (I, III and IV complexes) in the inner mitochondrial membrane, transporting hydrogen ions to the intermembrane space, and (2) the resulting electrochemical proton gradient is harnessed by the ATP synthase (complex V) to produced ATP. The

released electrons and protons come together again in the mitochondrial matrix, generating water and consuming oxygen (Stanfield, 2013 pp. 77-80).

Mitochondrial oxidative metabolism provides over 95% of the energy demands in the healthy mature adult heart with the remainder originating from glycolysis in the cytosol (Stanley et al., 2005). The healthy heart is characterized by its wide substrate versatility, as it is able to metabolize fatty acids, lactate, carbohydrates, ketone bodies and certain amino acids (Heggermont et al., 2016). The major carbon sources that fuel oxidative phosphorylation in mature cardiomyocytes are produced in the fatty acid β-oxidation pathway (more than two-thirds), whereas glucose and lactate are oxidized to a lesser extent (approximately one-third) (Stanley et al., 2005).

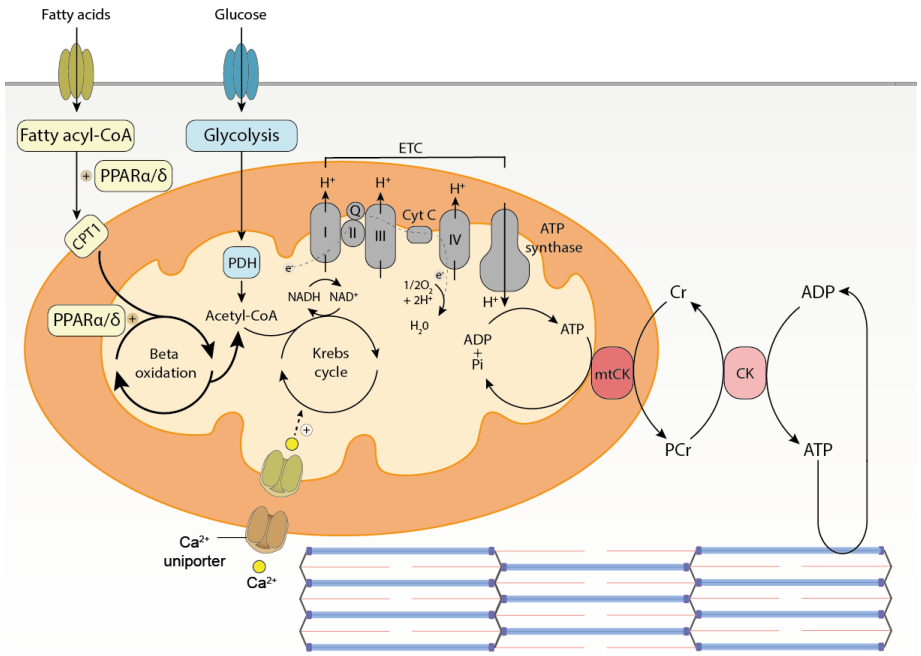

Figure I6. Main substrate sources and mitochondrial energy production in cardiomyocytes. The β-oxidation and the Krebs cycle pathways produce reduced carriers molecules (NADH and $FADH_2$) that donate electrons to the electron transport chain (ETC), generating a membrane potential in the mitochondrial intermembrane space that will drive the synthesis of ATP. The mitochondrial creatine kinase (mtCK)

generates phosphocreatine (PCr) from creatine (Cr). In the myofilaments and in the cytosol, the creatine kinase (CK) maintains constant levels of ATP. PPAR are fatty acid sensors that can modulate lipid and glucose metabolism. PPARα/δ, peroxisome proliferator-activated receptor α/δ; CPT1, carnitine O-palmitoyltransferase 1; Q, coenzime Q; Cyt C, cytochrome C; PDH, pyruvate dehydrogenase.

In contrast, energy metabolism of cardiac precursors during early embryonic development is more dependent on glycolysis, as mitochondrial oxidative metabolism is not fully developed (Chung et al., 2010). Higher activities in the glycolytic pathway enzymes contribute to higher rates of basal glucose uptake and glycolysis in the fetal heart (Lopaschuk and Jaswal, 2010). Moreover, circulating levels of lactate in the fetus are very high. As such, the fetal heart has the capacity to oxidize lactate, accounting for the majority of myocardial oxygen consumption (Werner and Sicard, 1987). Similarly, in the immediate newborn period, approximately half of total ATP produced relies on glycolysis. Later on, in the neonatal heart, less than 10% of total ATP is produced by glycolysis (similar values as in adults). Furthermore, circulating blood levels of lactate drop and lactate oxidation also decreases. In parallel, it is produced a shift towards an increase in fatty acid uptake and β-oxidation, regulated mainly by an increase on the PGC-1α/PPARα pathway and by several metabolic changes (Lopaschuk and Jaswal, 2010).

When the cardiac load increases, a rapid supply of ATP can be accomplished by the metabolic shift from fatty acid oxidation to glucose oxidation, as the glucose oxidation is more energy efficient than that of fatty acids. This homeostatic mechanism controls substrate selection to adapt supply and demands in normal tissues (van der Velden et al., 2018). During heart failure, cardiac energy metabolism can be compromised and is common that the heart can revert to a ‘fetal’ program of energy substrate metabolism (Lopaschuk and Jaswal, 2010), with an initial increase of glucose metabolism and a decrease in fatty acid utilization (Lionetti et al., 2011; Neubauer, 2007;

van Bilsen et al., 2009). Mitochondrial structural abnormalities and altered activities within the respiratory chain complexes also result in a decrease oxidative phosphorylation and energy production during heart failure.

1.6.2 High-energy phosphate metabolism

Despite the high ATP requirements of cardiomyocytes, yet in rest conditions, there is a highly regulated balance between energy production and consumption, thus, maintaining static cellular ATP levels. This cellular energy homeostasis is accomplished mainly by the creatine kinase (CK) energy shuttle system, which is essential to transfer the high-energy phosphate bonds from the mitochondria to the myofibrils and to maintain low ADP levels (Wallimann et al., 2011). The mitochondrial CK catalyses the transfer of the phosphate from ATP to creatine to form phosphocreatine (PCr) and ADP. PCr diffuses more rapidly than ATP from the mitochondria to the myofibrils, where the cytosolic CK catalyses the restoration of ATP and creatine from PCr and ADP (Bessman and Geiger, 1981). The CK system can store up to 10 times the amount of the ATP pool, acting as a fast energy buffer (Wallimann et al., 2011).

The forward reaction takes place in the mitochondrial intermembrane space and the reverse reaction is primarily localized at sites of ATP consumption, such as myosin and SERCA2 ATPases (Cao et al., 2018). CK system compartmentalisation is essential to maximize the availability of energy from ATP, since it maintains low ATP/ADP levels at the mitochondria and high ATP/ADP levels at sites of consumption.

Impaired energy metabolism has been shown in numerous studies of HCM. Mouse model bearing the heterozygous R403Q mutation in the α-myosin heavy chain (αMHC), with abnormal diastolic function and absence of hypertrophy, presented a decrease in PCr and creatine pools with preserved ATP levels (Spindler et al., 1998). A reduction in myocardial PCr/ATP ratio (a

parameter of myocardial energy reserve) was also observed in asymptomatic patients with HCM (Jung et al., 1998). In 2003, Crilley *et al*., showed an altered energy metabolism with a reduction in PCr/ATP ratio even in non-manifesting carriers irrespective of the HCM mutation (Crilley et al., 2003). More recently, the energetic cost of contraction of HCM patients was observed to be highest in myosin mutants, intermediate for cMyBP-C mutants and lowest for idiopathic patients (Witjas-Paalberends et al., 2014). These studies support the hypothesis that a higher tension cost (lower efficiency of contraction) underlie a common property of HCM (Ingwall, 2014).

1.6.3 Inefficient sarcomere contraction and metabolic changes in hypertrophic cardiomyopathy

The inefficient contraction of the sarcomeres as a common pathological phenotype of HCM can be attributed to distinct changes in sarcomere properties: 1) an increase in myofilament Ca^{2+} sensitivity indicating an increase utilization of ATP at the sarcomeres, 2) an enhanced activation/relaxation kinetics, which increase the tension cost for force development, and 3) reduced super-relaxed state of myosin heads (structural conformation of globular heads that prevents interactions with actin and preserves energy consumption), which increase the ATP utilization at low Ca^{2+} levels (van der Velden et al., 2018). Inefficient cardiac contractility also precedes the development of hypertrophy, as seen in asymptomatic mutational carriers of the disease (Timmer et al., 2011). Hence, impaired myocardial energetics could represent the primary cause of HCM, supporting the paradigm proposed by Ashrafian *et al*. almost twenty years ago (Ashrafian et al., 2003). Since then, increasing evidence has suggested that energy depletion has a crucial role in the development and in the broader pathophysiology of HCM (Crilley et al., 2003; Neubauer, 2007; Ormerod et al., 2016; Witjas-Paalberends et al., 2014).

Energy depletion generated by increased ATP consumption may affect other ATP-consuming processes that regulates metabolism and Ca^{2+} homeostasis, such as SERCA2a activity. Hence, leading to increased diastolic calcium levels. In addition, reducing PCr levels or inhibiting CK activity has been linked to heart failure, as it impaired diastolic function and reduced contractility (Hamman et al., 1995; Horn et al., 2001). The consequence of reducing CK activity or the levels of PCr is that ADP levels increase. Indeed, it has been reported increased ADP levels in mouse models of HCM (He et al., 2007; Spindler et al., 1998). Moreover, increasing ADP has been reported to impair relaxation of healthy rat hearts and to increase myofilament Ca^{2+} sensitivity in human HCM samples (Sequeira et al., 2015a; Sequeira et al., 2015b). It has been proposed that diastolic dysfunction can be accounted by energetic deficits that elevate ADP levels and that this mechanism may underlie a dominant role in the progression of HCM (Sequeira et al., 2019).

1.6.4 Seahorse flux analyser as a method to study bioenergetics

Classical methods to characterize the mitochondrial bioenergetics profiles have mostly relied on the use of oxygen electrodes in isolated mitochondria or permeabilized cells (Brand and Nicholls, 2011). The implementation of techniques to analyse mitochondrial function in intact cells has been crucial in the field, since it avoids many of the disadvantages related to previous samples, such as the lack of a complex cellular context or mitochondrial damage during preparation. Several fluorescent-based methods for interrogating mitochondrial respiration have been developed to monitor oxygen consumption or membrane potential (Brand and Nicholls, 2011). However, these methods are incapable to make real-time measurements and adding respiratory chain modulators is intricate. The Seahorse extracellular flux analyser overcomes these issues, becoming the gold-standard technique

for sophisticated respiration assays in a multiwell plated-based format (Ferrick et al., 2008).

The Seahorse flux analyser simultaneously measures extracellular changes of oxygen and proton concentrations, allowing for real-time detection of cellular aerobic respiration and glycolysis rates, respectively. A typical bioenergetic profile experiment to interrogate mitochondrial function is based on the sequential addition of electron transport chain inhibitors (Figure I7).

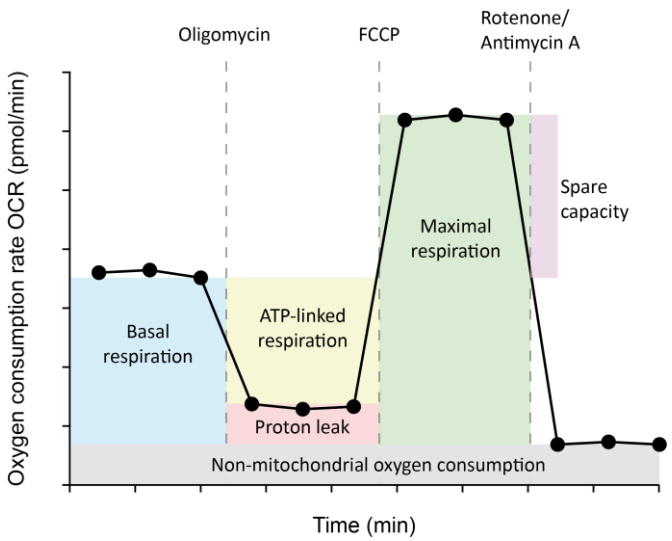

Figure I7. Schematic profile of a mitochondrial respiration assay using the Seahorse Analyzer. Mitochondrial bioenergetics profile is determined by measuring oxygen consumption and H^+ protons during the sequential addition of respiratory chain inhibitors, oligomycin, FCCP and rotenone/antimicyn A.

After measurements of basal oxygen consumption rates (OCR), which represent all the oxygen-consuming processes, oligomycin is then added. Oligomycin is an inhibitor of the F_1F_0-ATP synthase (complex V). As this protein complex converts the electrochemical gradient into ATP synthesis, the reduction in OCR in response to oligomycin is linked to the proportion of ATP generated by the mitochondrial oxidative phosphorylation to meet the cellular energetic demands.

At the second injection, FCCP (carbonyl cyanide-4 (trifluoromethoxy) phenylhydrazone) is used. FCCP is an uncoupler agent that disrupts the mitochondrial inner membrane and dissipates the proton gradient. Consequently, electron flow is no longer regulated by the electrochemical gradient, which causes the ETC to work at maximum capacity and a rapid oxidation of metabolic substrates. Thus, FCCP is used to estimate the maximal potential rate of respiration. An important characteristic that arise upon FCCP exposure is the reserve or spare respiratory capacity. It is a qualitative indicator of the flexibility of the cells to respond to an energetic demand.

Finally, complete inhibition of the mitochondrial ETC takes place after the combined addition of the potent inhibitors rotenone and antimycin A, which inhibits complex I and complex III, respectively. The inhibition of most oxygen-consuming processes enables to determine the contribution of non-mitochondrial oxidases within the cell.

1.7 Cardiac myosin-binding protein C and hypertrophic cardiomyopathy

One of the primary steps in understanding the structure and function of cardiac myosin-binding protein C (cMyBP-C), encoded by the *MYBPC3* gene, was the identification of novel *MYBPC3* mutations in unrelated HCM families (Bonne et al., 1995; Watkins et al., 1995). *MYBPC3* was the fourth sarcomeric gene to be associated with HCM and, together with mutations in *MYH7*, it has become the most common genetic cause of the disease (Behrens-Gawlik et al., 2014).

In 1997, the organization and sequence of the human *MYBPC3* was determined (Carrier et al., 1997). It contains 35 exons spanning more than 21 kb (Figure I8), localized on chromosome 11p11.2. Since then, more than 720 individual *MYBPC3* pathogenic/likely pathogenic mutations have been

identified causing cardiomyopathies (ClinVar variant repository: http://www.ncbi.nlm.nih.gov/clinvar/). The vast majority of known *MYBPC3* mutations are heterozygous truncating mutations including: frameshift mutations (insertion or deletion ≥ 1 nucleotide in the coding region), mutations that affect the normal splicing of mRNA (Frank-Hansen et al., 2008), or non-sense mutations leading to premature stop codons (McNally et al., 2015; Santos Mateo et al., 2018). The fact that truncating mutations in *MYBPC3* result in a reduction of its total mRNA and protein levels and that the truncating protein cannot be found in cardiac tissues from affected HCM patients or HCM mouse models indicates that the disease mechanism is primarily due to haploinsufficiency (Marston et al., 2009; van Dijk et al., 2009).

Cohort studies have shown that mutations in *MYBPC3* have frequently lower penetrance with a delayed disease onset and benign progression as compared to mutations in *MYH7* (Lakdawala et al., 2021; Velicki et al., 2020). However, compound variants or double-truncating mutations have also been described, in which the bi-allelic mutations are associated with neonatal cardiomyopathy and heart failure within the first months of life (Wessels et al., 2015).

1.7.1 cMyBP-C structure and function

In the adult human muscle, there exist three homologous isoforms of MyBP-C: the slow skeletal (*MYBPC1* gene), the fast skeletal (*MYBPC2*) and the cardiac-specific isoform, expressed uniquely in the heart muscle in mammals (*MYBPC3*). cMyBP-C is a large (140 kDa) multidomain protein containing eight immunoglobulin-like (Ig) and three fibronectin (Fn3) domains, numbered from C1 to C10. The cardiac isoform, as compared to the slow and fast skeletal, contains characteristic structural additions: it includes and additional immunoglobulin-like domain in the N-terminus (C0), a 28 amino acids

insertion in the C5 domain, and five phosphorylation sites (four in the M domain and one in the Proline-Alanine (PA) rich region)(Schlossarek et al., 2011)(Figure I8).

In the sarcomere, cMyBP-C is localized in the C-zone within the A-band, forming a characteristic doublet appearance arranged in 9 transverse stripes at 43 nm intervals (Figure I3) (Luther et al., 2008). cMyBP-C is a thick-associated protein that localizes central between thin and thick filaments within the sarcomere. The NH_2-terminal of cMyBP-C interacts with F-actin (C0 to M domains) and with the myosin S2 domain (C1-M-C2), which is regulated by the phosphorylation of the M domain. At its COOH-terminus, cMyPB-C serves as an anchor to the thick filament, interacting with proteins containing four-and-a-half-LIM domains (C6 to C10), with titin (C8 to C10) and light meromyosin (C10).

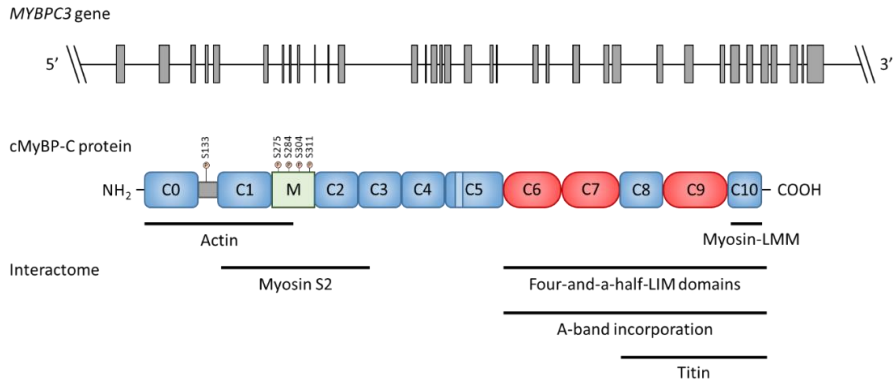

Figure I8. Schematic representation of the *MYBPC3* gene, protein and the domain interaction with other sarcomere proteins. *MYBPC3* contains 35 exons comprising more than 21 kb, which is transcribed into a 3824 bp transcript and translated into a 140-kDa protein. cMyBP-C protein contains eight immunoglobulin-like domains (C0, C1, C2, C3, C4, C5, C8 and C10) and three fibronectin-type III domains (C6, C7 and C9). Main phosphorylation sites within the N-terminal (PA linker between C0 and C1, and in the M motif) and the specific human serine residues are shown.

Although cMyBP-C connects thin and thick filaments across the sarcomere, it is not essential for the assembly and structure of the sarcomere, as cMyBP-C Knock-Out (KO) mouse models are viable and show regular sarcomeres (Harris et al., 2002). cMyBP-C is primarily a regulatory protein and the target of multiple kinases, phosphatases and proteases. Essentially, it regulates cross-bridge cycling kinetics, myofilament Ca^{2+} sensitivity and the contraction-relaxation of the sarcomere (Sadayappan and de Tombe, 2012).

1.7.2 Regulation of cMyBP-C

Cardiac contractility is additionally regulated by post-translational modifications. Post-translational modifications, mainly phosphorylation, have been identified in several sarcomeric and non-sarcomeric proteins, including cardiac troponin I (cTnI), cardiac troponin T (cTnT), α-tropomyosin (α-TM), myosin light chain (MLC) or cMyPB-C (Solaro, 2008). Cardiovascular diseases and myocardial dysfunction have been frequently associated with alterations in the phosphorylation levels on sarcomeric components (Barefield and Sadayappan, 2010).

cMyPB-C function is regulated by multiple phosphorylation sites, localized mainly in the M domain, and targeted in a hierarchical order of events by several protein kinases, such as PKA, protein kinase C (PKC), protein kinase D (PKD), CaMKII and 90 KDa ribosomal S6 kinase (RSK) (Sadayappan and de Tombe, 2012). Phosphorylation of cMyBP-C plays a critical role in the regulation of force generation and contraction kinetics by modulating thin and thick filament activation (Ponnam et al., 2019; Tong et al., 2008). Specifically, cMyBP-C phosphorylation disrupts its interaction with myosin, leading to an enhance myosin-actin interaction and greater force production (Kulikovskaya et al., 2003). cMyBP-C is a highly phosphorylated protein in vivo and has been shown that its overall phosphorylation levels are diminished in both end-stage

heart failure and hypertrophic cardiomyopathy (Jacques et al., 2008). Moreover, in multiple mouse models cMyBP-C phosphorylation is necessary for a normal cardiac function and it is considered cardioprotective after ischemic-reperfusion injury (Barefield and Sadayappan, 2010). In addition, dephosphorylation of cMyBP-C is associated with an increased degradation of the protein, a reduction in actin-myosin cross-bridge cycling and contractile dysfunction (Decker et al., 2005).

1.8 Myosin heavy chain 7 and hypertrophic cardiomyopathy

Pioneering discoveries on the genetic basis of HCM more than thirty years ago by the group of Seidman led to the identification of the first missense mutation in the *MYH7* gene (R403Q) in a familial case of HCM (Geisterfer-Lowrance et al., 1990). Since then, more than 370 pathogenic/likely pathogenic variants have been reported in ClinVar (http://www.ncbi.nlm.nih.gov/clinvar/) as disease causing. The majority of them are missense mutations (Colegrave and Peckham, 2014), implying that mutant proteins are incorporated into the thick filaments, and that such alterations can compromise myosin structure and/or function. As the number of DNA-sequenced individuals or HCM patients increases, it is expected that the amount of detected variants will rise over the years. However, assessing whether the mutation is disease-causing or whether it increases disease susceptibility is challenging. Thus, more than 1400 genetic variants within the *MYH7* gene are classified as uncertain significance in the ClinVar database.

1.8.1 β-Myosin heavy chain structure and mutational landscape

The *MYH7* gene encodes for the cardiac β-myosin heavy chain (β-MHC), the predominant isoform found in human ventricles. As previously described in the section 1.3.3., β-myosin is a multimeric protein comprising two heavy

chains, two regulatory light chains (RLC) and two essential light chains (ELC). The N-terminal part of the β-MHC contains the motor domain, which includes the ATPase and the actin-binding domains. It follows an α-helix region where the ELC and RLC proteins bind. This lever arm domain is responsible for amplifying the motor domain movement (both domains form the region called Subfragment 1) (Figure I9). Following Subfragment 1 is the α–helical tail of β-MHC, composed of Subfragment 2 and light meromyosin (LMM). When the two heavy chains dimerize, a parallel coiled-coil is formed in the myosin tail for filament assembly, and the two globular motor heads are displayed outwards for actin binding (Figure I9). A key domain for filament assembly and formation is localized at the proximal C-terminus (assembly competent domain), which is formed by an heptad repeated sequence.

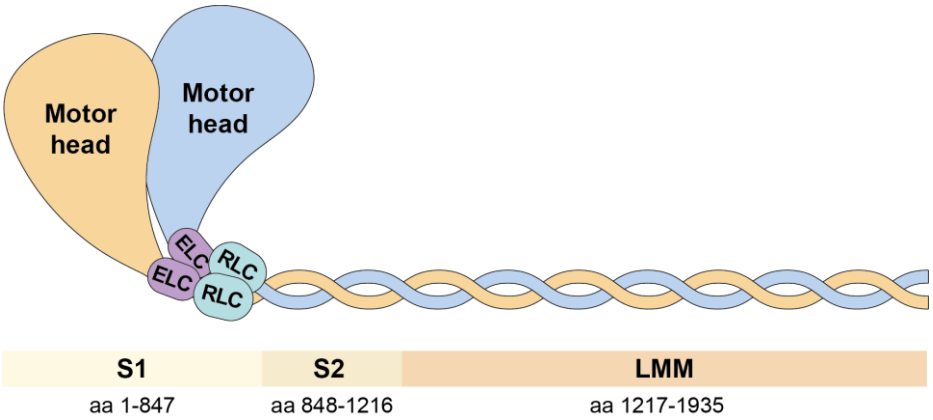

Figure I9. Illustration of the β-myosin structure. β-cardiac myosin is characterized by two globular heads that contain the actin and ATPase binding domains, followed by the lever arm containing ELC and RLC. The tail of the protein is formed by a coiled-coil domain.

Mutations within the *MYH7* gene have been described all along the sequence, affecting all functional subdomains of the protein. However, a significant proportion of these mutations affect the motor head and the lever domain (Colegrave and Peckham, 2014). Specifically, these variants are enriched in the kinetic domain and in a flat surface domain called myosin

mesa, which have been associated with an earlier disease onset (Homburger et al., 2016). About 20% and 17% of mutations are localized in the Subfragment 2 and LMM region, respectively. The molecular consequences of the genetic variants within the tail region may differ from those occurring at the head domain, as a higher penetrance of dilated cardiomyopathy or skeletal myopathy is observed for mutations occurring at the S2 and LMM regions (Colegrave and Peckham, 2014). Thus, missense mutations in the β-MHC can alter several different mechanisms of cardiac contraction such as cross-bridge cycling, ATPase kinetics, force development, sliding velocity, protein-binding affinity or stability (Kraft and Montag, 2019).

1.8.2 Conformational states of β-Myosin heavy chain

Early studies based on X-ray diffraction in skeletal muscle provided evidence for the coexistence of ordered and disordered myosin heads with different dynamic conformations: disordered myosin heads weakly bound to actin, disordered heads not attached to actin, and ordered myosins on the thick filament helix (Malinchik et al., 1997). Currently, it is well known that multiple actin-bound states occur during the myosin chemomechanical cycle (Houdusse and Sweeney, 2016). Because these active myosins are more available to bind actin and exist in multitude of structures and proximities to actin filaments, they appear disordered by X-ray diffraction. Recently, these conformations have been defined as disordered relaxed state (DRX) (Wilson et al., 2014).

Myosin ATP turnover experiments in relaxed permeable rabbit ventricular bundles revealed two subpopulations of relaxed myosins: a normal relaxed state (not attached to actin and not generating force) and a new relaxed state called super-relaxed state (SRX) with a much slower ATP hydrolysis rate, which might contribute to the ordered myosins in the thick filament helix (Hooijman

et al., 2011; Stewart et al., 2010). Thus, the metabolic rate in the three different functional states of myosin is different. In the active actin-bound state the ATP turnover rate is fast (<1 s), in the DRX state with no actin binding the nucleotide rate is slow (<30 s). In the SRX state the ATP turnover is more than 100 s (Nag and Trivedi, 2021).

The SXR is a dormant conformation state in which these myosins are not available for binding to actin. It is estimated that approximately 50-60% of the myosins are in the reserve SRX state (Hooijman et al., 2011; Stewart et al., 2010). In the cardiac muscle, it is suggested that a subpopulation of myosins remains in the SRX state even during sarcomere contraction. Although there is no direct evidence whether these myosins in the SRX are recruited or activated for force generation during increased cardiac load or stress, it has been suggested that SRX myosins may reduce the cardiac metabolic rate and may provide a rapid mechanism to adjust cardiac force generation (Kraft and Montag, 2019).

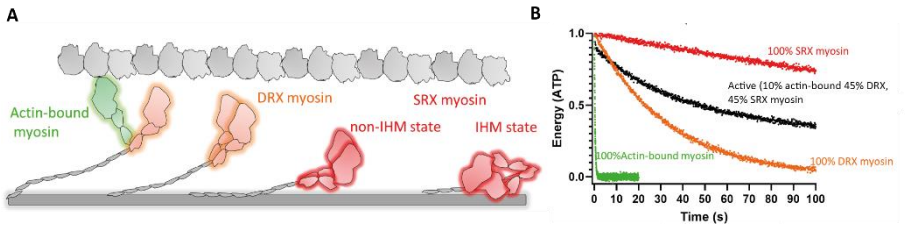

Figure I10. Schematic illustration of the conformational and functional states of β-myosin heads. **A)** Myosin heads that bind actin (green) show the highest ATP utilization and are in balance with the DRX myosin states (orange), which are less active (100-fold). DXR and SXR (in red) are in equilibrium and are also subjected to regulation. SRX myosin states have 10-fold less ATP turnover activity than DRX. The off-state of SRX are proposed to be in an-IHM and non-IHM conformational states. **B)** Simulated ATP consumption of the different myosin states. DRX, disordered relaxed

state; SRX, super-relaxed state; IHM, interacting-heads motif. (Adapted from Nag and Trivedi, 2021).

1.8.3 cMyBP-C regulates the population of super-relaxed state of myosins

Several factors are known to modulate the population of myosin SRX, including the phosphorylation of the RLC, hormones, calcium, ADP or cMyBP-C (Nag and Trivedi, 2021). During recent years, several reports have suggested that cMyBP-C plays an important role in stabilizing the *off*-state of myosin heads close to the thick filament (McNamara et al., 2016; Trivedi et al., 2018). Experiments with cMyBP-C knockout mice showed that the population of SRX myosins was reduced as compared to WT (McNamara et al., 2016). In another study, the same author demonstrated that the phosphorylation on key residues within the M-domain of cMyBP-C were essential for modulating the fraction of SRX myosins from an *off* to an *on*-state (McNamara et al., 2019). More recently, the hydrolysis of ATP was specifically measured on different regions within the sarcomere. The authors showed that in the C-zone, where the cMyBP-C localizes, the ATPase rate was increased as compared to the flanking regions lacking cMyBP-C. Additionally, both SRX and DRX myosin states were primarily observed in the cMyBP-C-containing C-zone region, while in the flanking regions the myosins were mostly DRX (Nelson et al., 2020). These observations are in line with the role of cMyBP-C in regulating contractile output and energetic demand.

1.9 CRISPR/Cas9-based genome editing

The term 'genome editing' was implemented by Urnov *et al*., in which they developed an engineered zing finger nucleases (ZFNs) approach to correct a disease-relevant mutation (Urnov et al., 2005). Based on these pioneering

experiments, the same technology was applied in hPSCs using ZFNs, or the more user-friendly transcription activator-like effector nucleases (TALENs) (Hockemeyer et al., 2011). They provided proof of principle for gene knockouts, insertions of transgenes, repair or introduction of disease-relevant mutations. However, the engineering of these designer nucleases was labour intensive and costly.

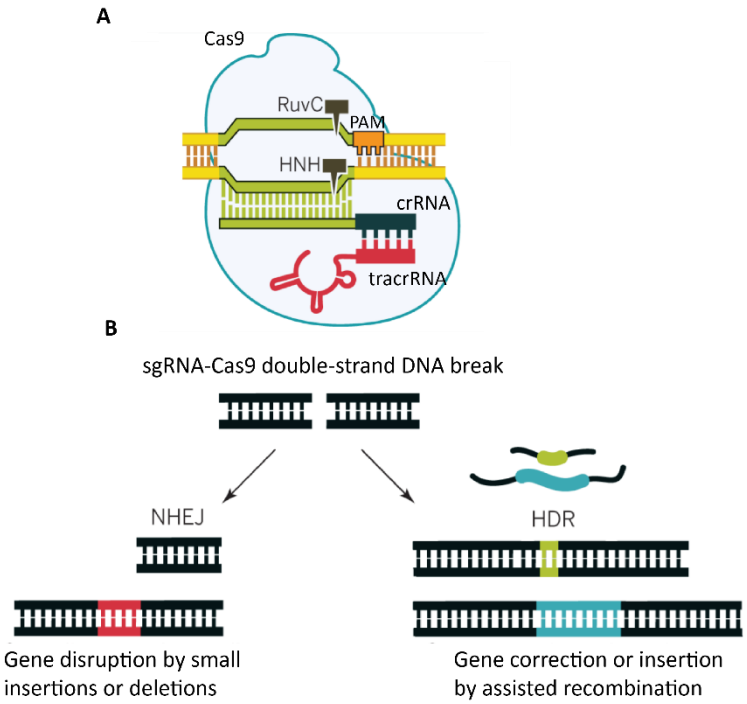

Figure I11. Genome engineering mediated by CRISPR/Cas9 system. **A)** Site-specific DNA recognition is mediated by the chimeric tracrRNA:crRNA, which harbours complementarity to the target sequence (protospacer). The presence of a protospacer associated motif (PAM) 5'-NGG-3' is required for Cas9 endonuclease activity. Double-strand DNA break (DSB) is produced by the HNH and RuvC nuclease domains. **B)** DSB can be repaired by non-homologous end joining (NHEJ) of by homology-directed repair mechanisms. (Adapted from Doudna and Charpentier, 2014).

The need for a simpler and cheaper genome-editing platform was met through the Clustered Regularly Interspaced Short Palindromic Repeats

(CRISPR)/CRISPR-associated protein-9 (Cas9) (Cong et al., 2013; Jinek et al., 2012). The emerged CRISPR/Cas9 system has dramatically improved the efficiency of genetic engineering in several cell types and organisms (Rojas-Fernandez et al., 2015). The CRISPR/Cas9 type II system is part of the bacterial adaptive immune response, found in most bacteria and archaea, which recognizes and cleaves foreign genetic elements. It consists of two components: a) an engineered single-chimeric guide RNA (sgRNA) that bears homology to a genetic locus and provides target specificity b) a Cas9 that acts as a nuclease to make a blunt double strand break (DSB) at the target DNA with complementarity to the 20-nucleotide-long sequence in the sgRNA (Jinek et al., 2012; Mali et al., 2013).

The generated DSB at a defined site can be repaired either by the endogenous precise homology-directed repair (HDR) mechanism or more frequently by the error-prone non-homologous end joining (NHEJ), which can cause small insertions or deletions. The increase of the frequency of DSB at predetermined sites allows for a greater opportunity of the occurrence of non-homologues end joining (NHEJ), or if exogenous targeting vectors or DNA repair templates are present, introduction of transgene sequences (e.g., fluorescence tags or precise genetic modifications) via HDR.

1.10 Induced pluripotent stem cells (iPSC)

The first derivation of human pluripotent stem cells (hPSC) was performed in 1998 when Thomson et al., were able to culture the inner cell mass from pre-implantation embryos (Thomson et al., 1998). These cells, termed human embryonic stem cells (hESCs), reshape the regenerative medicine and development fields as they have the potential to differentiate into any somatic cell, as the *in vivo* equivalent pluripotent cells from the blastocyst. However, hESCs raised ethical concerns due to the destruction of human embryos for

research, as well as technical challenges such as immune rejection of non-autologous cells for clinical applications.

In 2006, Takahashi and Yamanaka published the major technological breakthrough in the field of stem cells, describing a method for reprogramming terminally differentiated adult dermal mouse fibroblasts into cells with a gene expression profile and developmental potential similar to embryonic stem cells by using a cocktail of four transcription factors (Takahashi and Yamanaka, 2006). These cells were termed induced pluripotent stem cells (iPSCs), and the four factors (Sox2, Oct4, KLF4 and c-Myc) were named "Yamanaka factors". One year later, the generation of iPSCs was reported from human cells (Takahashi et al., 2007; Yu et al., 2007). Although initial protocols used dermal fibroblasts, easily obtained from patient's skin, other accessible cellular sources (keratinocytes, cord blood CD133+ cells or peripheral blood mononuclear cells) have been used to generate iPSCs (Aasen et al., 2008; Giorgetti et al., 2009; Su et al., 2016). The resolved limitations associated with hESCs and the highly similar transcriptional and epigenetic profiles of hESCs and hiPSC (Guenther et al., 2010), provides the opportunity for cell transplantation therapies using autologous hiPSCs and to establish disease cellular models (Figure I12).

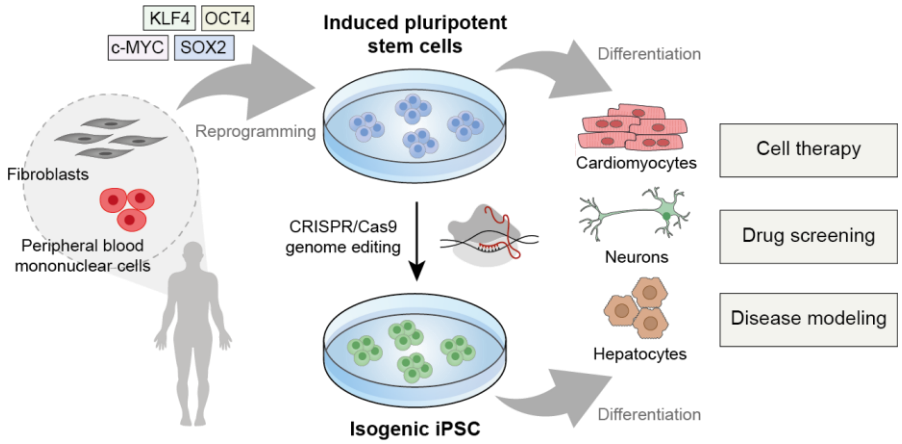

Figure I12. Schematic illustration showing the generation, genome editing and applications of hiPSCs. Somatic cells such as fibroblasts or peripheral blood mononuclear cells are reprogrammed into hiPSC by the transient expression of the 'Yamanaka factors' OCT4, KLF4, SOX2 and c-MYC. Genetic mutations in patient's iPSC can be corrected by CRISPR/Cas9 gene editing approach, creating an isogenic control with identical genetic background. iPSC can be differentiated into the cell type of interest for disease modelling, cell therapy or drug screening.

iPSC technology offers the possibility to generate patient-specific stem cells for modelling human diseases. Identifying the pathological mechanisms underlying human diseases is key in discovering novel therapeutic strategies. While animal-based models have provided valuable insights into the pathogenic mechanisms of numerous human diseases, substantial species-specific differences prevent the recapitulation of key characteristic features of many human conditions (McGonigle and Ruggeri, 2014). Similarly, the use of primary cultures of patient-derived cells, while helpful for studying disease aetiology, is limited by the lack of expandable sources of patients' cells, particularly for hard-to-access cells such as neurons and cardiomyocytes. Therefore, iPSC-based disease modelling appears as an attractive alternative. First, because of their intrinsic properties of indefinitely self-renewal and, secondly, because of their potential to differentiate into almost any cell type of the body.

Only fifteen years after the original description of induced reprogramming to pluripotency, enormous progress has been made in stem cell biology and regenerative medicine using iPSC technology (Lee and Studer, 2010; Omole and Fakoya, 2018; Shi et al., 2017). Furthermore, iPSCs derived from healthy individuals and patients have accelerated advances in developing genuinely human experimental models of disease, novel pathogenic mechanisms have been elucidated (Burkhardt et al., 2013; di Domenico et al., 2019; Wen et al., 2014), new drugs initiated from iPSC-based screenings are in the pipeline (Elitt et al., 2018; Lee et al., 2012; Shcheglovitov et al., 2013) and the first clinical

trials using human iPSC-derived products have been initiated (Kletzl et al., 2019; Mullard, 2015; Naryshkin et al., 2014).

1.10.1 Variability among iPSC

A defining characteristic of pluripotent stem cells is their potential to differentiate into cells of all three germ layers. However, a limiting factor regarding the use of iPSCs is, precisely, the variability in their differentiation potential. Not only the inter-individual differences among iPSCs may have a strong impact in the differentiation capacity toward a specific cell type, but also between iPSC clones from the same individual (Hu et al., 2010; Kajiwara et al., 2012). There have been several attempts to characterize the sources of such variability. Prolonged culture and maintenance of pluripotent stem cells has been shown to promote genomic alterations, most frequently on chromosomes 12 and 17, likely reflecting the selective pressure processes taking place in culture (Baker et al., 2007). More recently, a comprehensive examination of the major sources of genetic and phenotypic variations in iPSC lines was undertaken by genome-wide characterization of 711 iPSC lines derived from 301 healthy individuals, established by the Human Induced Pluripotent Stem Cells Initiative (HipSci). The authors were able to identify consistent inter-individual effects that explained more than 46% of the phenotypic variation among iPSC lines (Kilpinen et al., 2017).

Irrespective of the origin, phenotypic interline variability of iPSCs complicates assigning specific genotypes to disease-related cellular phenotypes. In this sense, the use of targeted nucleases as gene-editing tools is increasingly being used to counteract such variability, enabling the generation of isogenic controls that only differ in the presence/absence of the genetic variants under study. The versatility of targeting almost any locus in the genome to generate the desired targeted genetic modification becomes

essential for the interpretation of the results and to strengthen the relationship between the genotype and phenotype. CRISPR/Cas9 has emerged as the leading genome-editing technique in the context of iPSC-based disease modeling. The advent of CRISPR/Cas9 technology has opened unprecedented opportunities for this purpose, especially due to its simplicity and wide democratization (Jinek et al., 2012).

1.10.2 iPSC-derived cardiomyocytes

Research on cardiac disease is becoming more important as the prevalence of cardiac disorders is increasing, in part due to an improved detection and survival. Animal models have contribute notably to our understanding of cardiovascular diseases. However, genetic and physiological interspecies differences have limited the translation of treatments to the clinic. For example, HCM mutations in the *MYBPC3* or *MYH7* genes introduced in the heterozygous state in mouse models do not develop the pathological septal hypertrophy seen in patients (Fraysse et al., 2012; Geisterfer-Lowrance et al., 1996). Additionally, as mentioned in previous sections, myosin isoforms and calcium channel fluxes also differ between mouse and humans.

Over the last decade, *in vitro* differentiation protocols to derive cardiomyocytes from hPSC have improved drastically. Initial differentiation protocols were based on the formation of spontaneous beating cells from embryoid bodies, which was labour-intensive and inefficient (Kehat et al., 2001). Most recent protocols used chemically defined medium and small molecule compounds to derived cardiomyocytes with relatively high efficiency (Burridge et al., 2014; Lian et al., 2012). Despite this progress, cardiomyocytes generated by current methodologies exhibit a high degree of phenotypic heterogeneity. Reasons include the reprogrammed cell types and the reprogramming protocol itself, different methodologies to derived

cardiomyocytes and the efficiency from such protocols or the level of maturity in culture (Eschenhagen and Carrier, 2019).

Importantly, the main challenge to be addressed is the cellular maturation status (Yang et al., 2014). iPSC-derived cardiomyocytes display characteristics of fetal cardiomyocytes in size, morphology, sarcomeric organization, contraction kinetics, calcium handling, electrophysiology or metabolic function (Jiang et al., 2018). Hence, immaturity of iPSC-derived cardiomyocytes may limit the recapitulation of pathological phenotypes for late-onset genetic cardiomyopathies and their potential for clinical applications.

Several distinct approaches have been developed to address cell immaturity: culturing for extended periods (Kamakura et al., 2013; Lundy et al., 2013), modifying substrate stiffness (Khan et al., 2015; Rao et al., 2013), 3D tissue engineering strategies (Weinberger et al., 2017; Zhang et al., 2013), co-culturing with non-cardiac cells (Giacomelli et al., 2017; Shadrin et al., 2017), applying electrical stimulation (Ronaldson-Bouchard et al., 2018; Valls-Margarit et al., 2019), adding chemicals or smalls compounds (Birket et al., 2015; Iglesias-Garcia et al., 2015) and using neonatal hearts as *in vivo* bioincubators (Cho et al., 2017).

1.10.3 iPSC models of hypertrophic cardiomyopathy

Soon after the generation of hiPSC, the first publications reporting phenotypic abnormalities in the function of patient-specific iPSC-derived cardiomyocytes appeared for congenital long QT syndrome (Itzhaki et al., 2011; Moretti et al., 2010) and for LEOPARD syndrome, in which the first hypertrophic phenotypes were observed (Carvajal-Vergara et al., 2010). Since then, numerous studies have investigated the pathological mechanisms

triggering HCM. A list of iPSC HCM models with mutations in *MYH7* and *MYBPC3* genes are listed in Supplementary Table S1.

Despite the reported recapitulation of disease-associated abnormalities, absolute values for many parameters, such as cell surface area, action potentials, contraction kinetics or peak force varied largely (Eschenhagen and Carrier, 2019). It is likely that many factors, including biological differences, culture conditions, maturity and technical issues may explain that variation (Eschenhagen and Carrier, 2019).

2 OBJECTIVES

The general objectives of the present thesis were to:

1. Determine the functional differences between two siblings with divergent HCM pathological phenotypes using patient-specific induced pluripotent stem cells (iPSC).
2. Investigate the genetic drivers that could modify disease progression in the present HCM family.

To pursue the mentioned objectives, the specific objectives were the following:

Objective 1:

1.1. Generate and characterize patient-specific iPSC from two individuals in a large HCM family.
1.2. Characterize the morphological aspects of HCM iPSC-derived cardiomyocytes.
1.3. Generate the corrected isogenic controls using CRISPR/Cas9 technology.
1.4. Characterize the functional aspects of HCM iPSC-derived cardiomyocytes.

Objective 2:

2.1. Investigate the potential genetic modifiers that are affecting HCM disease progression.
2.2. Generate the isogenic control for the specific genetic modifiers using CRISPR/Cas9 gene editing approach.
2.3. Determine the functional contribution of the genetic modifiers.

3 MATERIALS AND METHODS

3.1 Generation and culture of iPSC

Patients's fibroblasts were converted into transgene-free iPSCs using CytoTune iPSC Sendai reprogramming protocol. Briefly, explant cultures were obtained from skin punch biopsies. Primary cultures of fibroblast were expanded and 100,000 cells were transduced with the Sendai vectors. Medium was then changed to human ESC (hESC) medium, consisting of KO-DMEM (Invitrogen) supplemented with 20% KO-Serum Replacement (Invitrogen), 2mM Glutamax (Invitrogen), 50 µM 2-mercaptoethanol (Invitrogen), non-essential amino acids (Lonza) and 10 ng/ml bFGF (Peprotech). Cultures were maintained at 37°C, 5% CO_2, with media changes every other day. Colonies were picked based on morphology 20-30 days after initial infection and plated onto fresh feeders. Patients-specific iPSC were cultured on Matrigel (Corning) coated dishes with mTeSR1 medium (Stem Cell Technologies). Medium was changed daily, excluding the day right after passaging. Cells were splitted 1:6 – 1:10 by dissociation with 0.5 mM EDTA (Invitrogen) for 2 min at 37°C and plated on Matrigel-coated plates. For this study, two patients' iPSC lines from the same family, each with a pathogenic frameshift (K600Nfs*2) mutation in *MYBPC3*, (MYB1#4 and MYB2#2) have been generated. A control human iPSC line generated from a healthy individual (codename FiPS Ctrl2 SV4F1, registered in the National Stem Cell Bank, Carlos III Spanish National Institute of Health) was used.

3.2 Characterization of iPSC

Expression of Sendai vector transgenes and endogenous pluripotency-associated transcription factors by quantitative Polymerase Chain Reaction (after reverse transcription) (RT-PCR) were assessed as previously described (Sanchez-Danes et al., 2012) and explained in section 3.3. *In vitro* differentiation towards endoderm, mesoderm and neuroectoderm was

carried out as described (Raya et al., 2008) and the immunofluorescence was performed as explained in section 3.4. List of oligonucleotides and primary and secondary antibodies used for iPSC characterization are listed in Table MM1 and Table MM2, respectively.

3.2.1 iPSC karyotyping

Cultures of iPSC were maintained in mTeSR1 medium until 80-90% confluence and karyotyped as described by (Campos et al., 2009). In brief, iPSC cultures were treated with 1 µg/ml KaryoMAX™ Colcemid solution (Gibco) for 3h and dissociated into single cells with 0.25% trypsin-EDTA (Gibco) for 3-5 min at 37 ºC. Cells were centrifuged (120xg for 5min) and resuspended in KCl solution (Gibco) for 15 at 37ºC. Cells were then centrifuged (120xg for 5 min) and fixed by resuspension in Methanol/Glacial acetic acid (3:1). Chromosome preparations were made by dropping cells onto glass slides. At least 20 metaphases were analysed per sample following current European Guidelines for Constitutional Cytogenetics Analysis.

3.2.2 Alkaline phosphatase staining

Culture of iPSC were washed twice with PBS and incubated with freshly made fixing solution (9ml PBS + 1ml formaldehyde 37%) for 3-4 min. Cells were then washed with substrate solution (Sigma Blue membrane, AB0300-1KT) and incubated in substrate solution in the dark for 20 min. Cells were then washed with PBS and images were taken using Leica DMI400 inverted microscope.

3.3 Quantitative real-time PCR

Total RNA was extracted from iPSC clones using the GeneJET RNA purification Kit (Thermo Fisher) following manufacturer's instructions, and 1

µg was used to synthesize cDNA using Transcriptor first-strand cDNA synthesis kit (Roche), following manufacturer's instructions. qRT-PCR was carried out using the 7900 HT Fast RT-PCR System (Applied Biosystems). Human GAPDH was used as positive control. Specific primers are listed in Table MM1.

Table MM1. List of qRT-PCR primer sequences.

Primers for gene	Forward 5'-3'	Reverse 3'-5'
ND1	ATGGCCAACCTCCTACTCCTCATT	TTATGGCGTCAGCGAAGGGTTGTA
ACTB	CATGTACGTTGCTATCCAGGC	CTCCTTAATGTCACGCACGAT
Endo hOCT4	GGAGGAAGCTGACAACAATGAAA	GGCCTGCACGAGGGTTT
Endo hSOX2	TGCGAGCGCTGCACAT	TCATGAGCGTCTTGGTTTTCC
Endo KLF4	CGAACCCACACAGGTGAGAA	GAGCGGGCGAATTTCCAT
Endo hc-MYC	AGGGTCAAGTTGGACAGTGTCA	TGGTGCATTTTCGGTTGTTG
Cripto	CGGAACTGTGAGCACGATGT	GGGCAGCCAGGTGTCATG
Nanog	ACAACTGGCCGAAGAATAGCA	GGTTCCCAGTCGGGTTCAC
Rex	CCTGCAGGCGGAAATAGAAC	GCACACATAGCCATCACATAAGG
Sendai OCT4	CCCGAAAGAGAAAGCGAACCAG	AATGTATCGAAGGTGCTCAA
Sendai SOX2	ATGCACCGCTACGACGTGAGCGC	AATGTATCGAAGGTGCTCAA
Sendai KLF4	TTCCTGCATGCCAGAGGAGCCC	AATGTATCGAAGGTGCTCAA
Sendai c-MYC	TAACTGACTAGCAGGCTTGTCG	TCCACATACAGTCCTGGATGATGATG
SeV	GGATCACTAGGTGATATCGAGC	ACCAGACAAGAGTTTAAGAGATATGTATC
GAPDH	GCACCGTCAAGGCTGAGAAC	AGGGATCTCGCTCCTGGAA

3.4 Immunofluorescence

Cells were fixed with 4% paraformaldehyde in PBS for 15 min at room temperature. After three washes with 1X TBS (5 min each), cells were incubated in blocking solution I (1X TBS, 0.5% Triton-X100 (Sigma) and 6% donkey serum (Chemicon)) for 1 hour at room temperature and incubated with primary antibodies diluted in blocking solution II (1X TBS, 0.1% Triton-X100 and 6% donkey serum) overnight at 4°C in agitation. Cells were then washed 3 times with 1X TBS for 5 min each and incubated with 0.5 µg/ml DAPI (4',6-diamino-2-phenylindole)(Invitrogen) for 10 min at room temperature. Images were taken using Leica SP5 Inverted confocal microscope (Leica) and

analysed using ImageJ free software (National Institutes of Health, USA). Table MM2 summarizes the primary and secondary antibodies used in this work.

Table MM2. List of primary and secondary antibodies.

Primary Antibodies	**Host**	**Dilution**	**Manufacturer**
Nanog (Polyclonal IgG)	Goat	1:50	R&D Systems, AF1997
Tra-1-81 (Monoclonal IgM)	Mouse	1:200	Merck-Millipore, MAB4381
OCT4 (Monoclonal IgG2b)	Mouse	1:30	Santa Cruz, sc-5279
SSEA-3 (Monoclonal IgM)	Rat	1:10	DSHB, MC-631
SOX2 (polyclonal IgG)	Rabbit	1:100	Thermo Fisher, PA1-16968
SSEA-4 (Monoclonal IgG3)	Mouse	1:100	DSHB, MC-813-70
FOXA2 (Polyclonal IgG)	Goat	1:100	R&D Systems, AF2400
αSMA (Monoclonal IgG2a)	Mouse	1:400	Sigma-Aldrich, A5228
TUJ1 (Monoclonal IgG2a)	Mouse	1:500	Biolegend, MMS-435P
GFAP (Polyclonal IgG)	Rabbit	1:500	Dako (Agilent), Z0334
Actin α-sarcomeric (Monoclonal IgM)	Mouse	1:400	Sigma-Aldrich, A2172
Troponin T (Monoclonal IgG1)	Mouse	1:100	Thermo Fisher, MS-295-P
PE-Myosin heavy chain (IgG2b)	Mouse	1:400	BD Biosciences, 564408
Alexa Fluor® 647, cardiac troponin I (IgG2b)	Mouse	1:100	BD Biosciences, 564409
PE IgG2b isotype control	Mouse	1:400	BD Biosciences, 559529
Alexa Fluor® 647 IgG2b isotype control	Mouse	1:100	BD Biosciences, 558713
Secondary Antibodies			
Alexa Fluor® 488, Mouse IgG	Goat	1:200	Jackson, 115-546-071
Cy™3, Rat IgM	Goat	1:200	Jackson, 112-165-020
Alexa Fluor® 488, Rabbit IgG	Donkey	1:200	Jackson, 711-545-152
Cy™3, Mouse IgG	Goat	1:200	Jackson, 115-165-071
DyLight™ 649, Mouse IgM	Goat	1:200	Jackson, 115-495-075
Alexa Fluor® 488, Goat IgG	Donkey	1:200	Jackson, 705-545-147
Cy™3, Mouse IgM	Donkey	1:200	Jackson, 715-165-140
Cy™3, Rabbit IgG	Donkey	1:200	Jackson, 711-165-152
Cy™3, Goat IgG	Donkey	1:200	Jackson, 705-165-147
Cy™3, Mouse IgM	Goat	1:200	Jackson, 115-165-075

3.5 Generation of CRISPR/Cas9 plasmids and donor templates

Modified CRISPR/Cas9 plasmid pSpCas9(BB)-2A-GFP (PX458)(Calatayud et al., 2019; Ran et al., 2013) with the full-lengh pCAGGS promoter was used. Custom guide RNAs were cloned into the BbsI sites as annealed oligonucleotides. The donor templates for HDR were ordered as Ultramer DNA oligos of 100-120 bases (Integrated DNA technologies).

3.6 Gene edition in iPSC

For correcting the *MYBPC3* K600Nfs*2 variant, mutant iPSC were gene-edited using CRISPR/Cas9 plasmid. The day before transfection, iPSC were disaggregated into small clumps using 0.5 mM EDTA (Invitrogen) and 400.000 cells were seeded on Matrigel-coated 6-cm plates. The day after, cells were transfected using FuGENE HD (Promega) and a mixture of 5 µg containing CRISPR/Cas9 plasmid and HDR donor template in 250 µl of OptiMEM (Invitrogen). 72 hours post-transfection, cells were pre-treated for 1 hour with 10 µM Y-27632 (Rho-associated kinase (ROCK) inhibitor, Stem Cell Technologies) and dissociated with Accutase (eBiosciences) for FACS-sorting based on GFP fluorescence (MoFlo XDP, Beckman Coulter). Approximately 15,000 cells were seeded in Matrigel-coated 10-cm plates containing RI-supplemented mTesR1 medium and maintained for 10-14 days until colonies attained enough size as to be screened. Colonies were manually picked and genotyped by restriction site polymorphism and Sanger sequencing. Colonies with the desired genotype were isolated, expanded and cryopreserved. Specific gRNA and ssODN for correcting the *MYBPC3* K600Nfs*2 mutation are listed in Table MM3.

For correcting the heterozygous I1927F variant in the *MYH7* gene, MYB1#4-iPSC were edited based on CRISPR/Cas9 ribonucleoprotein (RNP) complexes in order to achieve a higher gene-editing efficiency. For RNP

delivery, 200 pmol of annealed cr:tracrRNA (Thermo Fisher) were mixed with 100 pmol of Cas9 nuclease (Thermo Fisher) and incubated at room temperature for 10 min to allow for RNP assembly. The assembled RNP complexes were mixed with 250,000 dissociated cells in 20 µl P3 primary Cell solution (Lonza) and 100 pmol of ssODN donor template. Cells were placed into the Nucleocuvette strips (Lonza) and transfected using the Amaxa 4D-Nucleofector system (Lonza) and the electroporation protocol CA137. Transfected cells were then plated onto 48-well plates containing pre-warmed mTeSR1 medium supplemented with 10 µM Rho kinase inhibitor (Y-27632, STEMCELL technologies). 3-4 days post-transfection, cells were dissociated into single cells and plated at low density in 10-cm plates. Subsequent steps were carried out as described before. Specific sgRNA and ssODN are listed in Table MM4.

Table MM3. List of oligonucleotides and ssODN donor template for correcting c.1800delA mutation in the *MYBPC3* gene.

Oligonucleotides	**Sequence 5'-3'**	**sgRNA (Protospacer sequence 5'-3')**
MYBPC3 px458 DelA Fw	CACCGCGTCGTCAATGGTCAGTTG	ACGTCGTCAATGGTCAGTTG
MYBPC3 px458 DelA Rv	AAACCAACTGACCATTGACGACGC	
ssODN	**Sequence 5'-3'**	
MYBPC3 delA to WT	GGGGTGTGTGGCCCAGTGGGGTCCCCTGAGCCACTGCTCCCCTGCAGG GTGCACAAACTGACCATTGACGACGTCACACCTGCCGACGAGGCTGACT ACAGC	

C>G → ApaLI site

Table MM4. List of sgRNA and ssODN donor template for correcting c.5779A>T (I1927F) mutation in the *MYH7* gene.

sgRNA	**Sequence 5'-3'**
MYH7 I1917 to WT	CCGTGACTTTGGCACGAAGG
ssODN	**Sequence 5'-3'**
MYH7 I1927F to WT	GCAGAGGAGCGGGCGGACATCGCCGAGTCCCAGGTCAACAAGCTGCGG GCCAAGAGCCGTGACATTGGTACGAAGGTGGGTCCCTCTTTTGGGCTTTG CTAGTCACCCCCACAG

A>T → wild type sequence; C>T → RsaI site

3.7 iPSC differentiation towards cardiomyocytes

hiPSC were differentiated into cardiomyocytes in monolayer culture as previously described (Lian et al., 2013; Valls-Margarit et al., 2019) and represented in Figure MM1.

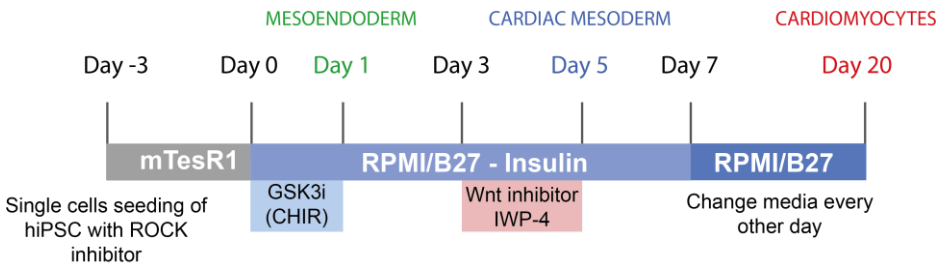

Figure MM1. Schematic protocol of cardiac differentiation from hiPSC. Cardiac specification is based on the modulation of the Wnt/β-catenin signalling pathway (Adapted from Valls-Margarit et al., 2019).

Briefly, iPSC maintained in mTeSR1 medium on Matrigel were dissociated into single cells with Accutase (eBiosciences) at 37°C for 5 min and seeded onto Matrigel-coated 12-well plate at a density of 1.5 million cells per well in mTeSR1 medium supplemented with 10 µM ROCK inhibitor (Stem Cell Technologies). Cells were maintained in mTeSR1 medium, changed daily during 3 days. When iPSC achieved confluence, cells were treated with 6-12 µM GSK3 inhibitor (CHIR99021, Stemgent) in RPMI (Invitrogen) supplemented with B27 lacking insulin (Life Technologies), 1% glutamax (Gibco), 0.5% penicilin-streptomycin (Gibco), 1% nonessential amino acids (Lonza), and 0.1 mM 2-mercaptoethanol (Gibco) (RPMI/B27- insulin medium) for 24 h (day 0 to day 1). After 24 h, the medium was changed to RPMI/B27-insulin and cultured for another 2 days. On day 3 of differentiation, cells were treated with 5 µM Wnt inhibitor IWP4 (Stemgent) in RPMI/B27-insulin medium and cultured without medium change for 2 days. Cells were maintained in RPMI supplemented with B27 (Life Technologies), 1% L-glutamine, 0.5%

penicilin/streptomycin, 1% non-essential amino acids, and 0.1 mM 2-mercaptoethanol (RPMI/B27 medium) starting from day 7, with medium change every 2 days. On day 8, contracting cardiomyocytes were obtained. Beating clusters were disaggregated by incubation with 0.25% trypsin-EDTA (Gibco) for 5-8 min at 37 ºC for subsequent characterization and *in vitro* functional studies.

3.8 Flow cytometry analysis of cardiac differentiation

Characterization of human iPSC-derived cardiomyocytes was performed by flow cytometry analysis. Cells were dissociated on day 20 of differentiation using 0.25% trypsin-EDTA at 37 ºC for 5 min and then fixed with 4% paraformaldehyde (Sigma) for 20 min at room temperature. After washing with 1X saponin (Sigma), cells were permeabilized using Cell Permeabilization Kit (Invitrogen) and blocked with 5% mouse serum during 15 min at room temperature. Then, cells were stained with the antibodies mouse PE-anti myosin heavy chain (MHC) (IgG2b, 1:400 BD Biosciences) and mouse Alexa Fluor 647 cardiac troponin I (cTnI) (IgG2b, 1:100, BD Biosciences). Mouse IgG2b PE (1:400 BD Biosciences) and mouse IgG2b Alexa Fluor 647 (1:100, BD Biosciences) antibodies were used as isotype controls. After incubation during 15 min at room temperature in the dark and washing twice with 1X saponin, cells were analysed with FACS MoFlo (Beckman Coulter) and data acquisition and analysis performed by Kaluza software (Beckman Coulter). The detailed list of antibodies are listed in Table MM1.

3.9 Transmission electron microscopy

Cardiac macrotissues were fixed with 2.5% glutaraldehyde (Electron Microscopy Sciences) for 1h at 4ºC. After washing with 0.1 M cacodylate buffer (pH = 7.2) (SigmaAldrich), cardiac macrotissues were gradually dehydrated

with ethanol and embedded in epoxy resin (Ted Pella). Semithin sections (0.25 µm) were cut with a diamond knife using an ultramicrotome (Leica UC6), and stained lightly with 1% toluidine blue (Panreac). Later, ultra-thin sections (0.08 µm) were cut with a diamond knife, contrasted with uranyl acetate (Electron Microscopy Sciences) and lead citrate (Electron Microscopy Sciences) and examined under a JEOL 1011 transmission electronic microscope (JEOL). Images were analyzed using ImageJ free software (National Institutes of Health, USA).

3.10 Traction force microscopy

iPSC-CMs at day 20 of cardiac differentiation were dissociated and seeded on a polyacrylamide substrate with finite thickness containing fluorescent beads. Traction forces were computed using Fourier transform-based traction microscopy. Gel displacements were computed using correlation-based particle imaging velocimetry software (Trepat et al., 2009).

3.11 Cell area and nucleation assessment

For cell area analysis, beating iPSC-derived cardiac monolayers were dissociated at day 20 and seeded at low density in RPMI/B27 medium supplemented with 10 µM ROCK inhibitor and 10% FBS (Invitrogen) for 24 h. Dissociated cardiomyocytes were seeded for 4-5 days before fixation and stained for the cardiac marker Troponin T (Table MM1). Randomly selected fields from differentiated cultures were taken and cell area was manually measured using ImageJ free software (National Institutes of Health, USA). Number of nuclei were manually counted for every cell measurement.

3.12 Evaluation of contraction-relaxation kinetics

Contractile kinetics analysis was performed at the indicated time-points on iPSC-derived cardiomyocytes cultured on monolayer. 8-10 days prior contractile assessment, cells were dissociated using 0.25% trypsin-EDTA and seeded into Matrigel-coated 96-well plate at a density of 100,000 cells per well in RPMI/B27 medium supplemented with 10 µM ROCK inhibitor and 10% FBS (Invitrogen) for 24 h. Cells were maintained in RPMI/B27 medium, with medium changed every other day. Contraction-relaxation movement was recorded every 56 ms for 16 seconds using an inverted microscope (Olympus CellR). During the recording process, temperature was kept at 37°C and 5% CO_2. Data was analysed with the help of the open software 'MuscleMotion' tool of ImageJ (Sala et al., 2018).

3.13 Mitochondrial assessment using the Seahorse XFe Analyzer

The Seahorse XFe96 extracellular flux analyser (Agilent) was used to assess respiration and acidification rates and mitochondrial function. Cardiomyocytes were seeded on Matrigel-coated assay plates 7 days before measurement at a density of 20,000 cells per XFe96 well. iPSC were seeded at low density in small clumps 3-4 days before measurement. Cells were washed twice in Agilent Seahorse XFe DMEM Basal Medium supplemented with 2 mM glutamine, 10 mM glucose and 1 mM Sodium Pyruvate 1 hour before the assay and for the duration of the measurement. For the standard profiling (Mito Stress test), oligomycin was injected at 1.5 µM, FCCP at 0.5 µM and rotenone/antimycin A were added at 0.5 µM. The oxygen consumption rate (OCR) and extracellular acidification rate (ECAR) values were normalized to the number of nuclei and quantified by DAPI staining. OCR, ECAR and ATP production rates were obtained using the Seahorse Wave controller Software 2.6.1 (Agilent).

3.14 Mitochondrial DNA content

Cardiac cultures at day 30 of differentiation were collected and total RNA-free DNA was extracted using the QIAmp® DNA Mini Kit (Qiagen) according to manufacturer's instructions. 10ng from isolated DNA were used for Real-time quantitative PCR using the 7900 HT Fast Real-Time PCR System (Applied Biosystems). The nuclear gene ACTB was used for normalization. Specific primers are listed in Table MM2.

3.15 Calcium transients assessment

At day 30 of cardiac differentiation, cardiomyocytes were dissociated with Trypsin/EDTA 0.25% and 80,000 cells were seeded on a gelatine-coated glass chamber that allow temperature control and electrical stimulation (Cell MicroControl). Cells were maintained for 5 days, with mediaum change every other day. Cells were loaded with 5µM of Fluo-4 (AAT Bioquest) in Tyrode's solution (129mM NaCl, 5mM KCl, 2mM CaCl2, 1mM MgCl2, 30mM Glucose, 25mM HEPES) containing Pluronic F-127 0.02% (Merck) for 30 min. Cells were washed 3 times with Tyrode's solution and images were acquired at 60 fps in a Confocal Inverted Microscope for 10s (Ex/Em = 490/525 nm) at a rate of 0.5 Hz. Fluorescence signals were recorded and data analysis was performed with ImageJ. Using the plugin ''multi kymograph'', line-based kymograph images were produced. MATLAB (Mathworks) was used to calculate the calcium kinetic parameters.

3.16 Whole Exome Sequencing

Exome sequencing was performed on probands III.7 and III.5 and their father in a research pipeline at Health in Code (A Coruña, Spain). In brief, individual's gDNA was extracted using QIAsymphony SP® (Qiagen). Library preparation was performed using the SureSelect^{XT} Library Preparation kit

(Agilent) for the Illumina multiplexed sequencing paired-end. Exome capture was performed with the Agilent Clinical Research Exome V2 probe kit (Agilent) and sequenced using the Illumina Hiseq 1500 platform. Bioinformatic analysis was carried out using an in-house pipeline for the interpretation of 405 genes within a panel for global cardiovascular diseases, in accordance with best WES analysis practices. Selected variants were confirmed by Sanger sequencing. Genetic missense variants identified in our study are listed in Supplementary Table S1.

3.17 Statistical analyses

Data presented in text and figures are as mean ± standard deviation (SD). The number of independent experiments (N) and replicated measurements per experiment (n) is indicated in the figure legends. Analysis comprising more than two experimental groups, data was evaluated using one-way ANOVA followed by a post hoc test as indicated in figure legends. For statistical analysis, GraphPad Prism 8 Software (La Jolla, Ca, USA) was used.

4 RESULTS

4.2 Description of a familial case of HCM

After presentation of an 18 years old male with a systolic murmur at medical exploration, cardiac magnetic resonance imaging (CMRI) revealed a maximal left ventricular hypertrophy (LVH) of 39 mm with moderate fibrosis in septal segments (Figure 1A-B) that required negative inotropic support. During subsequent years, the index case (individual III.7 in Figure R1G) developed non-sustained ventricular tachycardia and a syncope episode that required an implantable cardioverter-defibrillator (ICD) at 25 years old. Genetic testing of known variants using the Sequenom MassArray platform detected a previously described variant in the *MYBPC3* gene (c.1800delA) present in heterozygosis, which is predicted to produce a truncating version of the protein (K600Nfs*2).

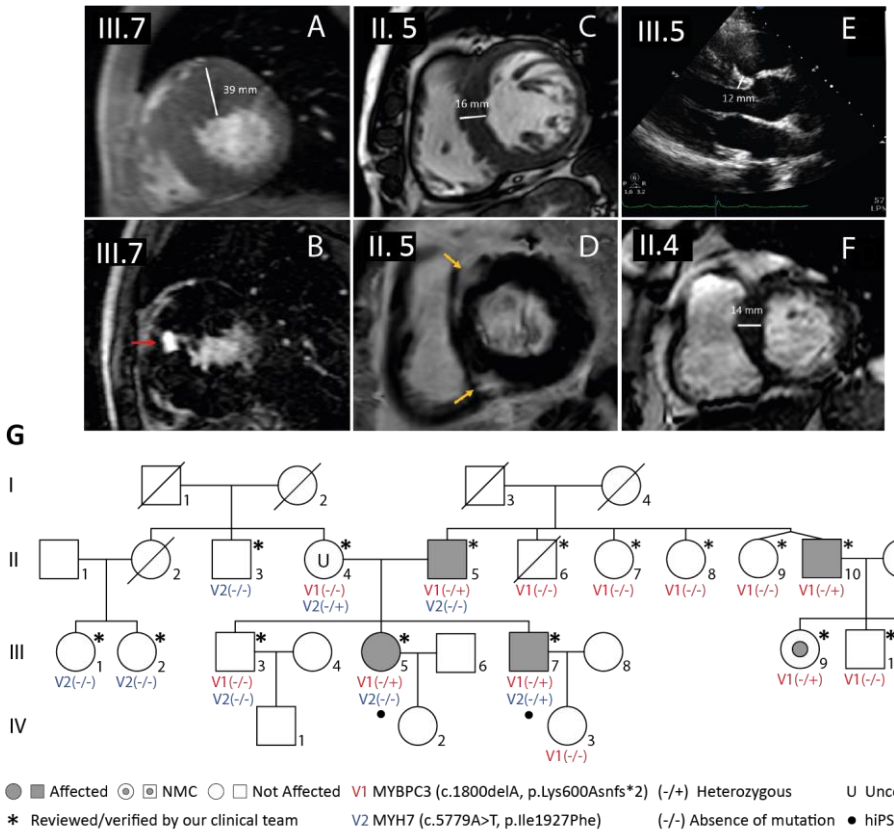

Figure R1. Description of a familial case of HCM. **A-F)** CMRI sections showing mid short axis views and echocardiogram image (E) from the proband III.7 diagnosed with severe HCM (LVH of 39 mm) and the relatives II.5, III.5, and II.4, diagnosed with mild hypertrophy. **G)** Pedigree of the HCM family. Genetic testing initially described a heterozygous truncating mutation in the *MYBPC3* gene (c.1800delA; p.K600Nfs*2) in the proband III.7, which cosegregates with the HCM affected relatives.

Expanding the clinical and genetic study into the present family unveiled that the father (individual II.5) was a carrier of the *MYBPC3* variant and had non-obstructive HCM with LVH of 16 mm and fibrosis in the septal insertion points in CMRI (Figure 1C-D). The sister of the proband (individual III.5) was also a carrier and has a borderline phenotype with septal LVH of 12 mm and mild inducible obstructive gradient at 42 years old in echocardiogram (Figure 1E).

4.3 Truncating *MYBPC3* K600Nfs*2 variant is associated with HCM pathogenicity

This variant appears with very low frequency in public databases as gnomAD (1/203524) (Lek et al., 2016). It has been reported before in several HCM probands in registries but there were no family information (Lopes et al., 2019; Mademont-Soler et al., 2017; Richard et al., 2003; Rodriguez-Garcia et al., 2010). Segregation studies within this family and in another 15 HCM families of Galicia confirm the pathogenicity of the *MYBPC3* variant and suggest a founder effect in this region. Since frameshift variants in the *MYBPC3* gene generate truncating versions of the protein that are not incorporated into the sarcomeres, it is expected a similar primary molecular mechanism and clinical outcomes (Helms et al., 2020b). Indeed, we do not see significant differences in survival rate and age of diagnosis when comparing the *MYBPC3* K600Nfs*2 variant with all *MYBPC3* truncating variants (data not shown). When analysing age at diagnosis for all *MYBPC3* truncating variants, we

observed that more than 50% of male carriers are diagnosed with HCM at the age of 50 years, while in the case of female carriers the percentage is 35% (Figure R2A). Event-free survival curves also show more cardiovascular events in male carriers at 30 years (Figure R2B). Taken together, the reasons underlying the clinical disparities between our familial variant carriers are unknown. Sex-related differences appear to account for a delayed age at diagnosis and survival rate in woman with HCM mutations (Lakdawala et al., 2021) and in the population with truncating *MYBPC3* carriers. Nevertheless, disease progression will ultimately lead to HCM pathogenicity independently of the gender in most cases.

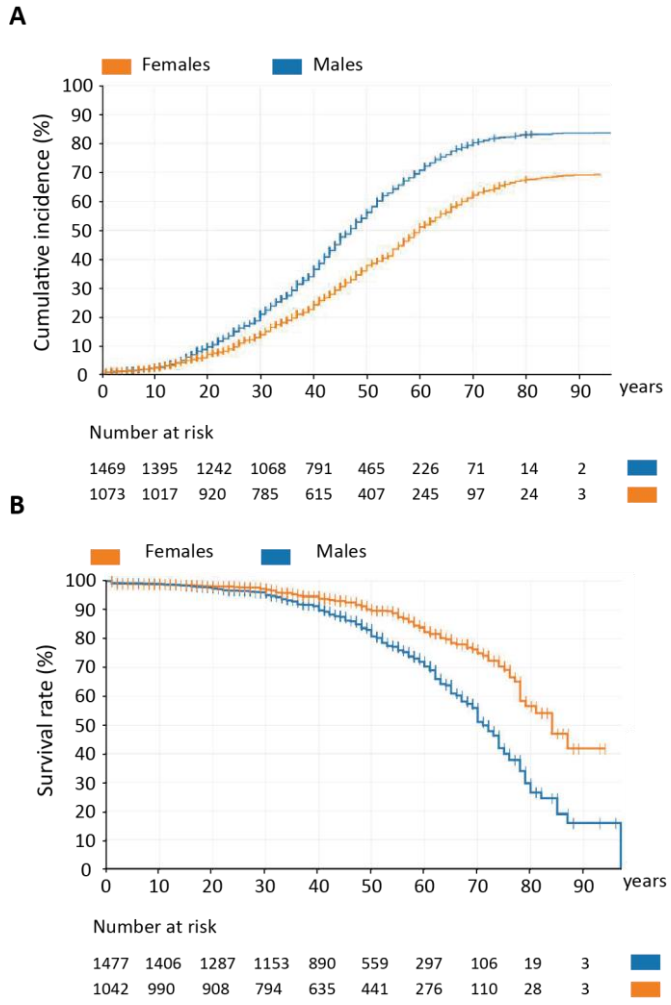

Figure R2. Kaplan-Meier curves with *MYBPC3*-truncating variants. A) Age at diagnosis of HCM probands with *MYBPC3* variants that cause truncations or affect splicing, comparing male vs female. **B)** Event-free survival rate in HCM with *MYBPC3* variants that cause truncations or affect splicing, comparing male vs female. The analysis included affected relatives.

4.4 Generation of iPSC from *MYBPC3* mutant carriers

To investigate the pathogenesis of the present HCM family in a controlled *in vitro* cellular setting, we generated iPSCs from the two siblings with a positive family history of HCM (Figure R1G).

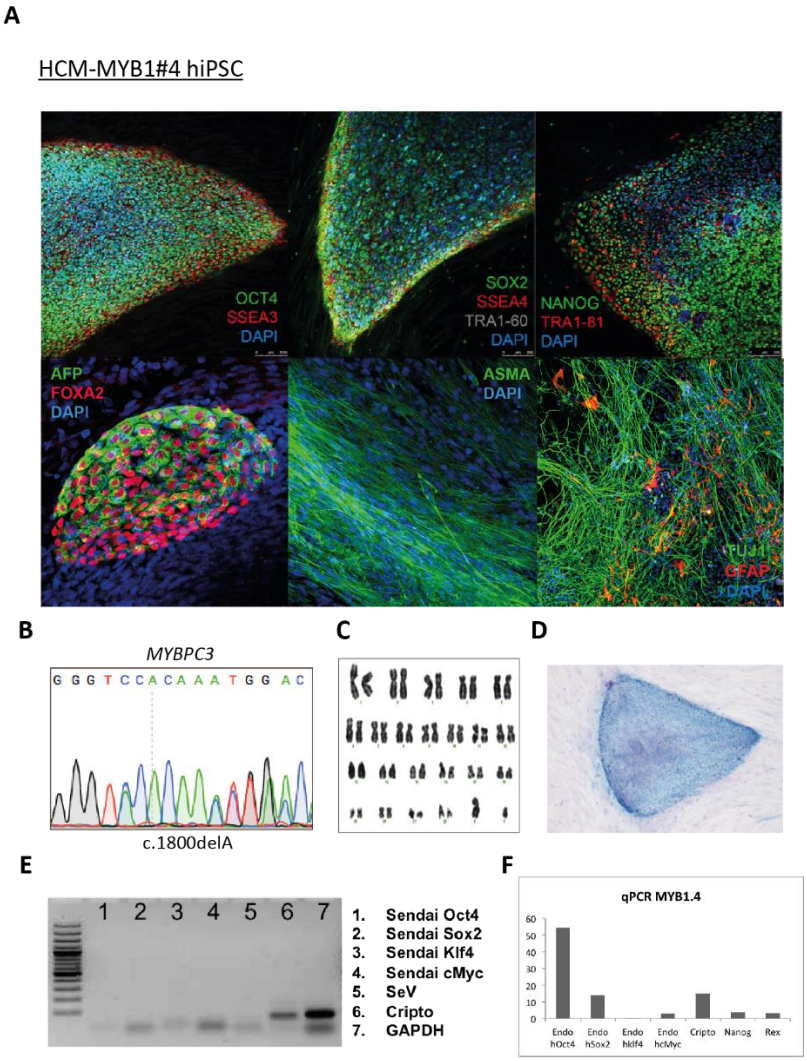

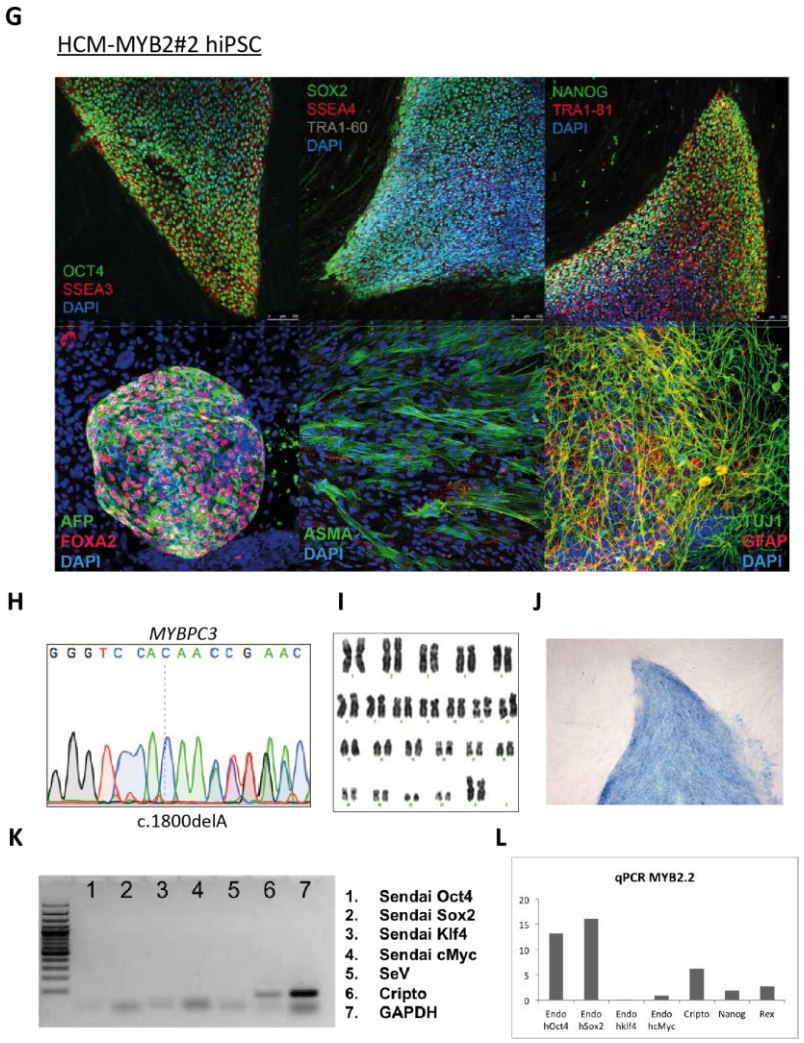

Figure R3. Characterization of patient-specific iPSC. Patient-specific induced pluripotent stem cell lines were generated from proband III.7 (MYB1#4) (A-F) and from proband III.5 (MYB2#2) (G-L). (**A, G**) Top: immunofluorescence of iPSC colonies showing expression of pluripotent markers including OCT4, SSEA3, SOX2, SSEA4, TRA1-60, NANOG and TRA1-81. Bottom: immunofluorescence analysis of cell derivatives differentiated *in vitro* to the three primary germ layers including endoderm (stained for α-fetoprotein (green) and FOXA2A (red)), mesoderm (stained for α-smooth muscle actin, ASMA (green), and ectoderm (stained for TUJ1 (green) and GFAP (red)). **(B, H)** Sanger sequencing of *MYBPC3* mutant iPSCs carrying the c.1800delA mutation. **(C, I)** Normal karyotype. **(D, J)** Staining for alkaline phosphatase (AP) activity. **(E, K)** RT-qPCR analysis of the endogenous expression levels of pluripotent genes and **(F, L)** the Sendai-derived reprogramming factors.

iPSC were generated from the proband (III.7; MYB1#4-iPSC) diagnosed with a severe hypertrophic phenotype, and his sister (III.5; MYB2#2-iPSC) with mild hypertrophy, both carrying the heterozygous c.1800delA (K600Nfs*2) in the *MYBPC3* gene. Dermal fibroblasts were isolated and reprogrammed into iPSCs as previously described (Sanchez-Danes et al., 2012). The derived human iPSC lines met all pluripotency criteria and had confirmed the c.1800delA (K600Nfs*2) heterozygous mutation in the *MYBPC3* gene (Figure R3A-L). A healthy individual without HCM mutations was used as a wild type control (FiPS).

4.5 iPSC-CMs with the *MYBPC3* K600Nfs*2 variant showed well-aligned sarcomeres

To better understand the pathogenesis of the *MYBPC3* sarcomeric mutation in the appropriate cellular context, we differentiated the iPSC into cardiomyocytes (iPSC-CMs) following a standard monolayer protocol (Figure MM1), which is based on the modulation of the Wnt/β-catenin signalling pathway with small-molecule inhibitors (Lian et al., 2013).

Differentiated iPSC-CM were produced at high efficiencies >80%, as evaluated by coexpression of myosin heavy chain (MHC) and cardiac troponin I (cTnI) proteins and immunostaining of the cardiac sarcomere protein marker troponin T (cTnT) (Figure R4A).

Since myofibrillar disarray has been reported in iPSC models of HCM (Mosqueira et al., 2018; Tanaka et al., 2014), we explored whether the sarcomeric organization was affected in HCM iPSC-CMs.

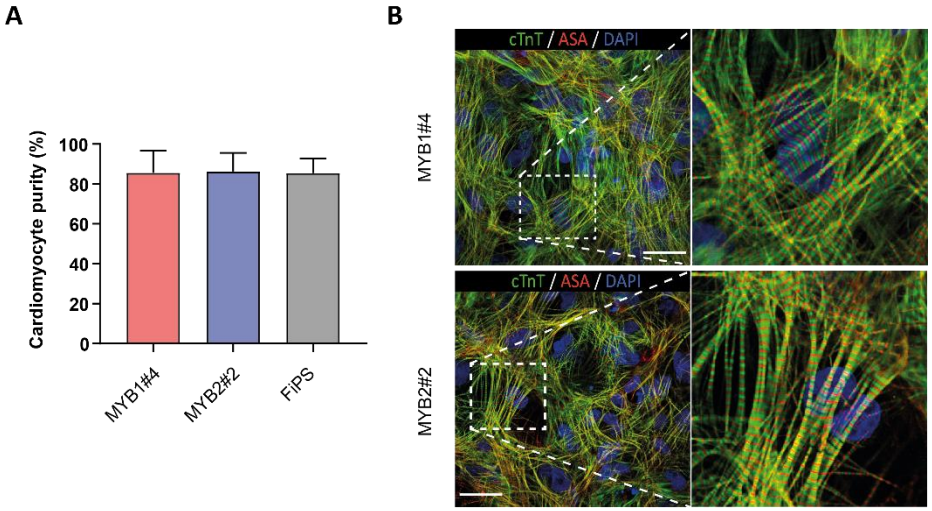

Figure R4. Generation of iPSC-derived cardiac monolayers. A) Cardiac differentiation cultures are composed off > 80% cardiomyocytes. MYB1#4 (*N* = 7), MYB2#2 (*N* = 5), FiPS (*N* = 3). **B)** Representative immunostaining of mutant iPSC-CMs staining positive for Troponin T (cTnT) and α-sarcomeric actin (ASA), showing well aligned sarcomeres. Scale bar, 200 µm.

Our results showed that cardiomyocytes stained for the sarcomeric proteins cTnT and α-sarcomeric actin (ASA) formed well-aligned sarcomeres with no apparent structural disarray for either of the *MYBPC3* mutant iPSC-derived cardiomyocytes (Figure R4B).

4.6 iPSC-CMs with the *MYBPC3* K600Nfs*2 variant do not exhibit sarcomeric structural abnormalities

In order to obtain a better resolution of the myofibrils and analyse whether the truncating *MYBPC3* mutation has an effect in the structure of the sarcomeres, we extended our analysis using transmission electron microscopy (TEM). We showed that both mutant iPSC-CMs as well as control iPSC-CMs formed organized and regular myofibrils with defined Z bands (Figure R5A). Indeed, we did not observe significant differences in sarcomere length between control and mutant lines (Figure R5B).

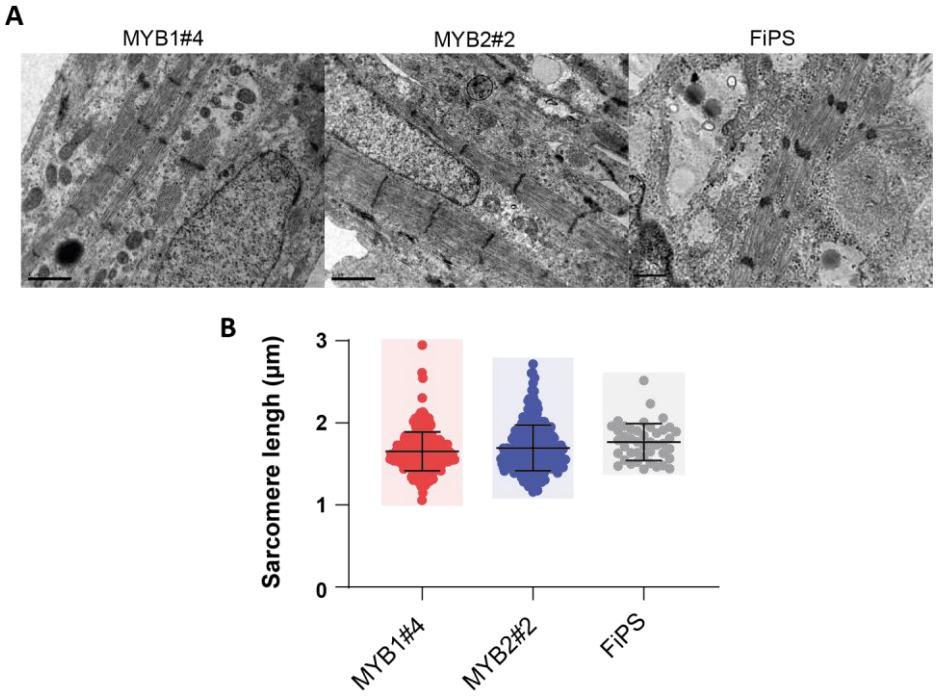

Figure R5. Ultrastructural characterization of mutant iPSC-CMs. **A)** Ultrastructural analysis of HCM mutants and controls iPSC-CMs. Representative TEM images of cardiomyocytes after 20 days in culture. Scale bar, 1µm. **B)** Quantification of sarcomere length. *n* = 266 (MYB1#4), 324 (MYB2#2) and 43 (FiPS) sarcomeres studied.

Hence, our results showed that the c.1800delA (K600Nfs*2) mutation in the *MYBPC3* gene does not produce any sarcomeric structural alterations, as in agreement with mouse and iPSC models of HCM showing that PTC mutations in the *MYBPC3* gene do not exhibit any structural alterations at the sarcomere level (Ma et al., 2018b; Seeger et al., 2019; Stohr et al., 2013).

4.7 Cellular hypertrophy is not recapitulated in HCM iPSC-CM

The most common hallmark of HCM is the presence of thicker left ventricular cardiac walls, which resulted from enlarged cardiomyocytes. To test whether cellular hypertrophy can be recapitulated *in vitro*, we assessed the morphological aspects between mutants and wild type iPSC-CMs. We did

not observed significant differences in cell area as a surrogate of cardiac hypertrophy between MYB1#4 and MYB2#2 iPSC-CMs when compared to control iPSC-CMs (Figure R6A-B).

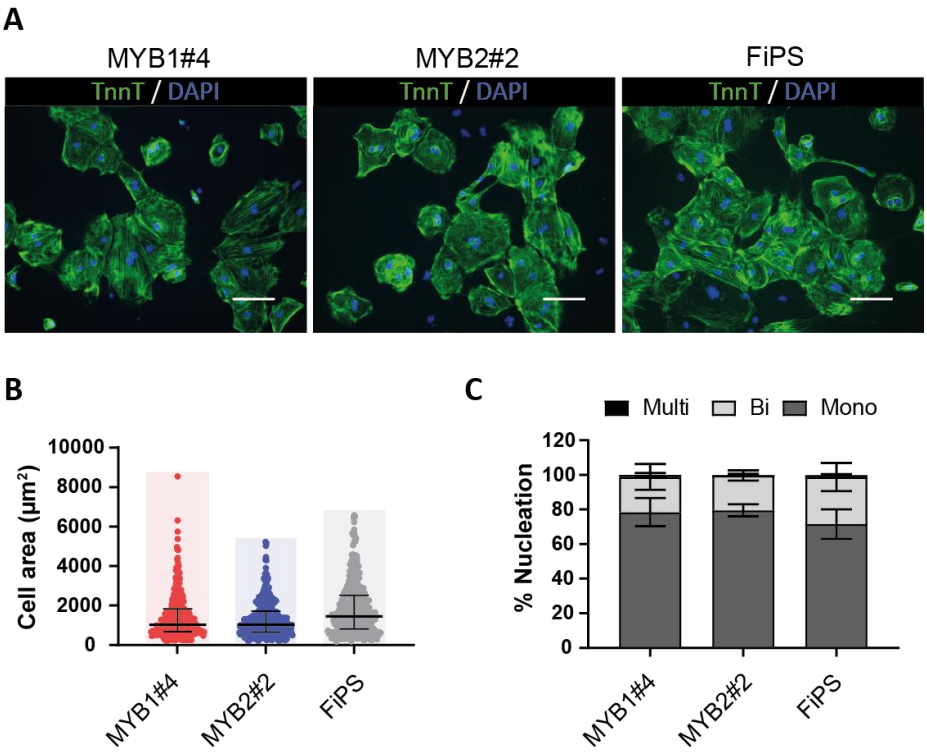

Figure R6. Morphological characterization of mutant iPSC-CMs. **A)** Representative immunofluorescence images stained for Troponin T (cTnT) from mutants and control iPSC-CMs. Scale bar 100 µm. **B-C)** morphological analysis of single iPSC-CMs showing quantification of cell area (B) and percentage of nucleation (C) distinguishing between mono-, bi- and multi-nucleated cells; *n* = 362 (MYB1#4), 351 (MYB2#2) and 335 (FiPS) cells from *N* = 3 independent differentiations.

We did not observed significant differences in multi-nucleation levels between MYB1#4 and MYB2#2 when compared to control iPSC-CMs (Figure R6C). These results are in accordance with a recent report indicating that the absence of *MYBPC3* do not produce cell shape remodelling in engineered cardiac microtissues within three weeks in culture (Ma et al., 2018b). Moreover, iPSC-CM produced by standard protocols are not fully mature,

likely hindering the appearance of pathogenic phenotypes derived from the *MYBPC3* K600Nfs*2 variant.

4.8 *MYBPC3* HCM iPSC-CMs showed contractile force deficits

cMyBP-C is a regulator of force development in myocardium. As it can interact with both actin and myosin, cMyBP-C controls the probability of cross-bridge formation, thereby controlling the kinetics and force of cardiac contraction (Moss et al., 2015).

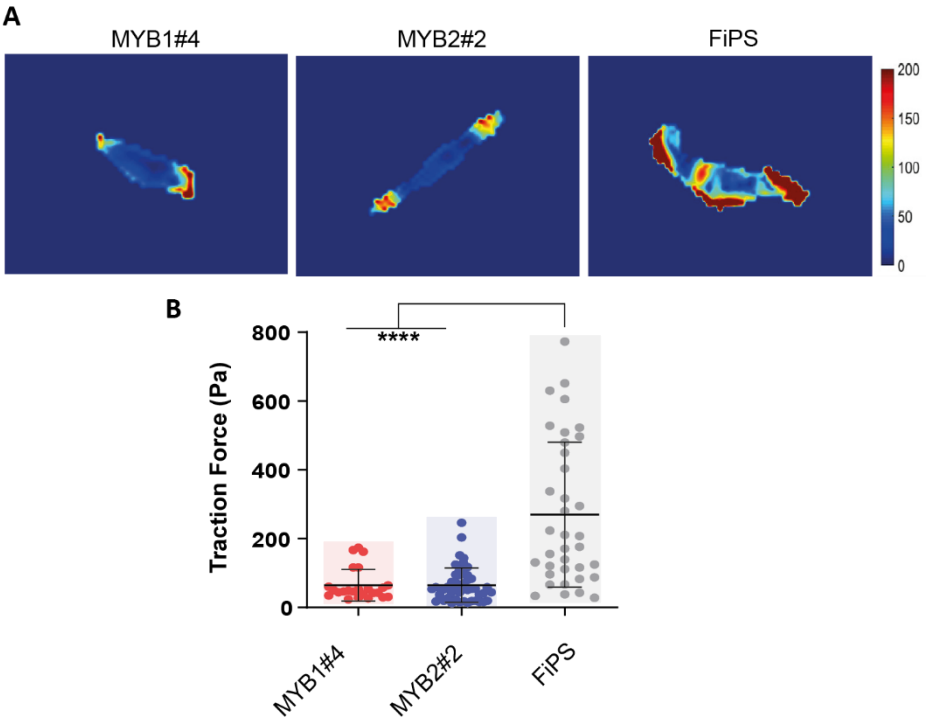

Figure R7. Traction force measurements in single cardiomyocytes. A) Representative images of single cardiomyocytes from mutant carriers and a control FiPS line showing traction force maps. **B)** Traction stress analysis of spontaneously beating iPSC-CMs from the *MYBPC3* mutated lines MYB1#4 (n = 24), MYB2#2 (n = 48) and the control line FiPS (n = 36) from N = 2 independent batches of differentiation. Data represent mean ± SD. Statistical analysis was tested with one-way ANOVA with Dunnett's correction test for multiple comparison (****P < 0.0001).

Thus, we examined contractile force of single cardiomyocytes seeded on polyacrylamide gels. Fluorescent bead displacement was recorded during spontaneous contraction (Figure R7A). We observed that CMs derived from both MYB1#4 and MYB2#2 iPSC lines exhibit lower traction forces compared to control iPSC-CMs (Figure R7B), as in agreement with several iPSC models of HCM (Birket et al., 2015; Ma et al., 2018b; Yang et al., 2018). Interestingly, the similar reduction in traction force in both mutant iPSC-CMs suggests a direct impact of the *MYBPC3* truncating mutation on force development at the *in vitro* level, independently of the pathogenic severity within the mutant carriers.

4.9 Generation of CRISPR/Cas9 gene-edited isogenic control iPSCs

Inter-individual differences are the main source of phenotypic variation among iPSC lines (Kilpinen et al., 2017). To counteract such variability, CRISPR/Cas9 has emerged as the most prominent gene-editing technology in the context of iPSC. In order to gain better insights into the genotype-phenotype relationship and overcome the limitation of the control FiPS' genomic background, we took advantage of the CRISPR/Cas9 system to correct the c.1800delA (K600Nfs*2) mutation in the *MYBPC3* gene in both mutants MYB1#4 and MYB2#2 iPSC lines, generating IsoMYB1#4 and IsoMYB2#2 iPSC, respectively (Figure R8).

To efficiently edit the pathogenic c.1800delA mutation, we designed various sgRNA overlapping the mutation and next to a protospacer adjacent motif (PAM) sequence within the exon 19 of the *MYBPC3* gene. After analysing the cutting efficiency, we decided to use the one with higher targeting efficiency (sgRNA showed in Figure R8A). After transfection of the CRISPR/Cas9 components and iPSC isolation, several iPSC clones were genotyped for the desired edition. The generated isogenic lines had a normal

karyotype, maintained their pluripotent potential and the correction of the mutation was confirmed by Sanger sequencing (Figure R8B-C).

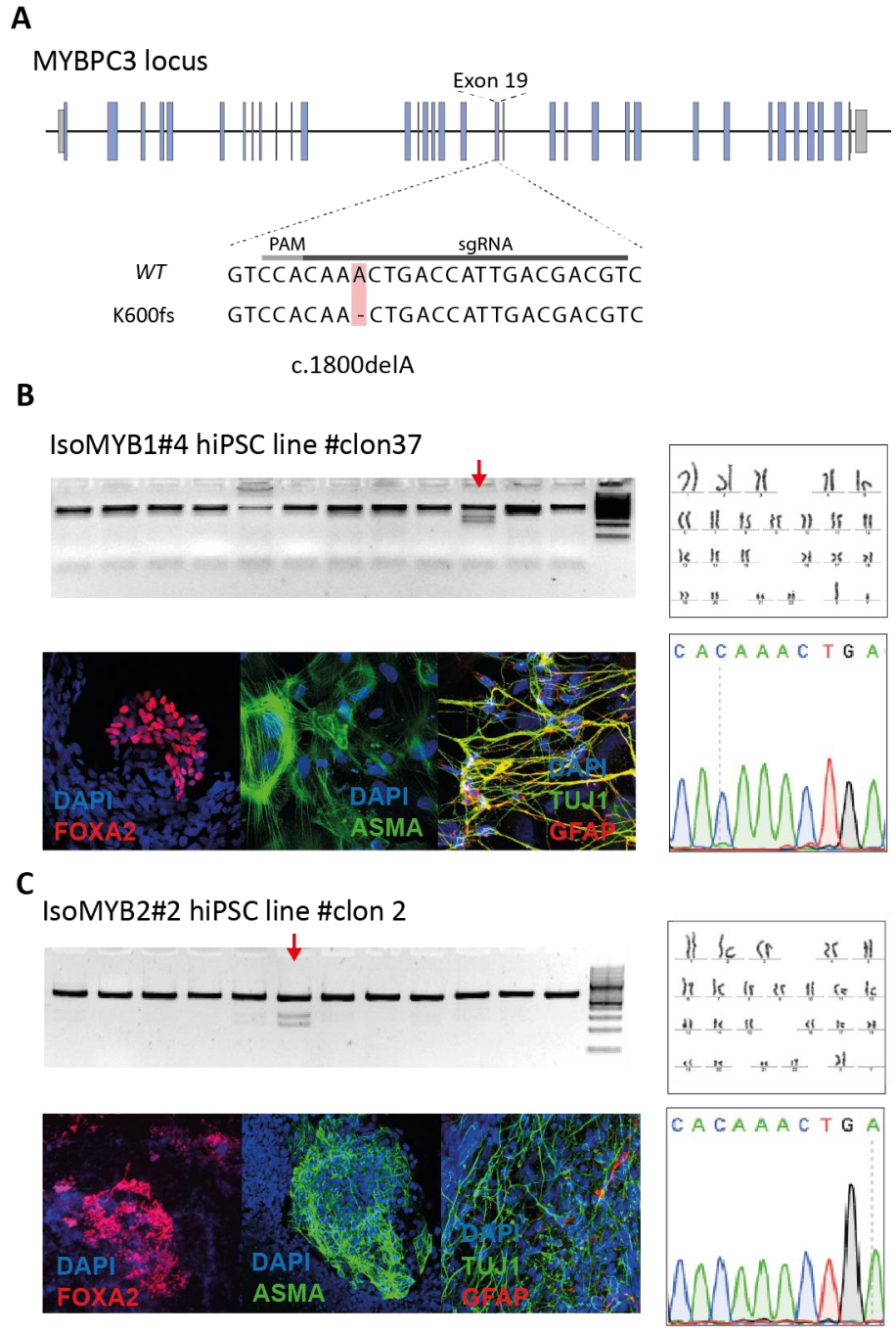

Figure R8. Characterization of CRISPR/Cas9 gene-edited isogenic controls iPSCs. A) Schematic representation of the CRISPR/Cas9 gene editing design, showing the c.1800delA mutation in the *MYBPC3* gene and the sgRNA used in our study. **B-C)** Generation and characterization of isogenic corrected IsoMYB1#4-iPSC line (B) and IsoMYB2#2-iPSC line (C) showing from top left to bottom right: Molecular analysis of the gene-edited clones (indicated by red arrows) confirming the proper restriction site integration; normal karyotype; immunofluorescence analysis of cell derivatives differentiated *in vitro* to the three primary germ layers including endoderm (stained FOXA2A (red)), mesoderm (stained for α-smooth muscle actin, ASMA (green)), and ectoderm (stained for TUJ1 (green) and GFAP (red)) and Sanger sequencing confirming the correction of the pathogenic c.1800delA mutation in the *MYBPC3* gene.

4.10 Abnormal calcium handling underlies symptomatic MYB1#4-iPSC-CMs

Calcium plays a central role in regulating the excitation-contraction coupling in cardiomyocytes (Bers, 2008). Given that alterations in intracellular calcium levels are commonly associated with the pathology of HCM and can contribute to early preclinical manifestations (Liu et al., 2017; Michels et al., 2009; Wu et al., 2019), we sought to investigate whether differing abnormal Ca^{2+} handling could be detected between the severely affected MYB1#4 and mild symptomatic MYB2#2 iPSC-CMs.

In order to gain better insights into the genotype-phenotype relationship we used as controls the previously generated isogenic corrected iPSC lines. To record Ca^{2+} transient properties, 5 weeks cardiac monolayers were labeled with the fluorescent Ca^{2+} dye Fluo-4. To avoid confounding variation due to spontaneous beating, cardiomyocytes were electrically paced at 0.5 Hz during imaging (Figure R9A).

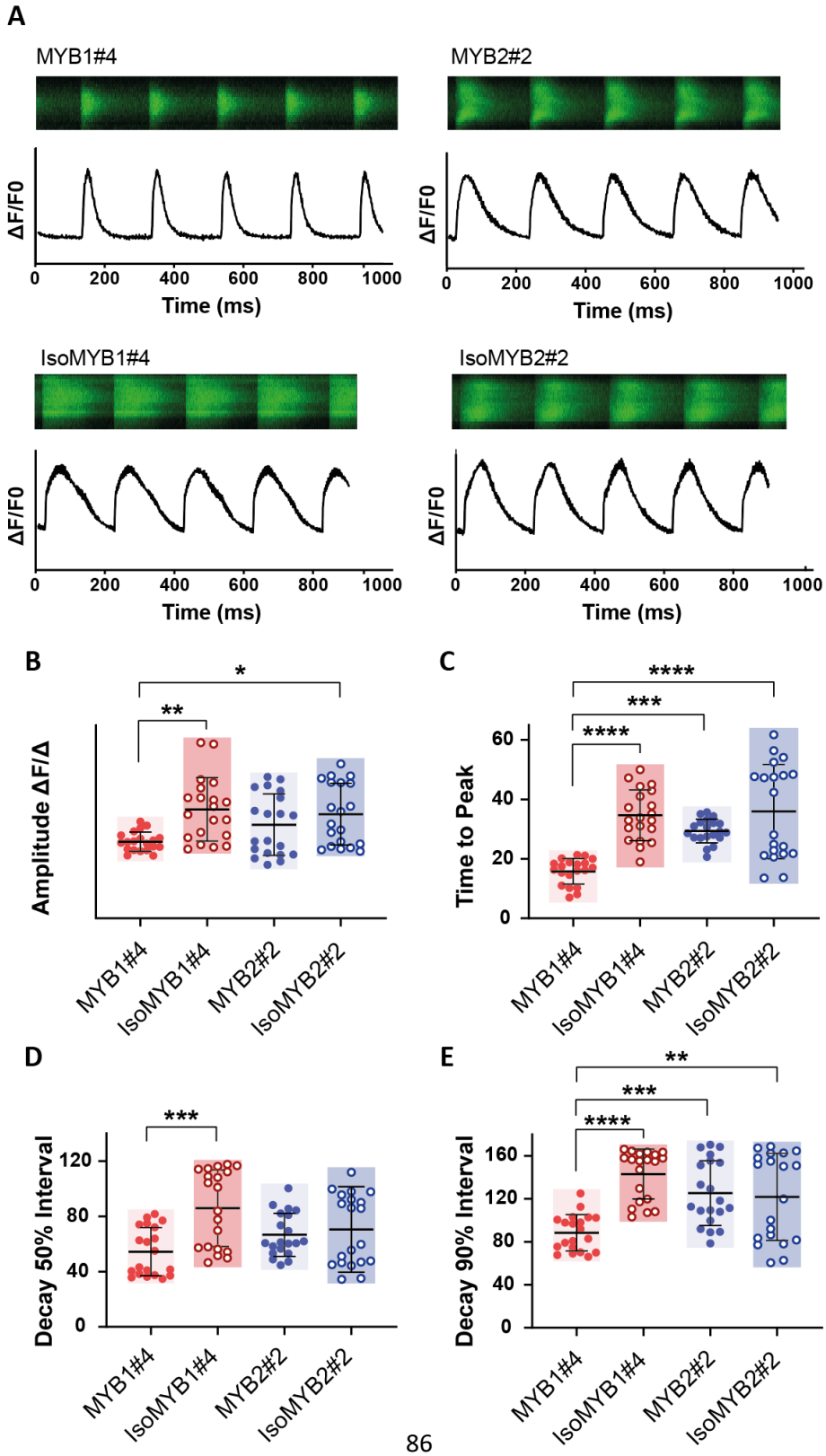
A
MYB1#4
MYB2#2
IsoMYB1#4
IsoMYB2#2
ΔF/F0
Time (ms)
0
200
400
600
800
1000
B
Amplitude ΔF/Δ
C
Time to Peak
D
Decay 50% Interval
E
Decay 90% Interval
MYB1#4
IsoMYB1#4
MYB2#2
IsoMYB2#2

Figure R9. Calcium handling of HCM mutants and isogenic controls in iPSC-derived cardiac monolayers. A) Representative traces and line-scan images of Fluo-4 Ca^{2+} transients from electrically paced (0.5 Hz) iPSC-derived cardiac monolayers. **B-E)** Quantification of calcium handling properties in HCM mutants and isogenic corrected iPSC-CMs showing peak amplitudes (B), time to reach calcium peaks (C), calcium decay at 50% interval (D) and 90% interval (E). Data represent mean ± SD. *n* = 20 cells in all groups. For each group in (A-E), data was generated from *N* = 2 independent differentiation batches. Data represent mean ± SD. Statistical analysis was tested with one-way ANOVA with Tukey correction (*P < 0.05; **P < 0.01; ***P < 0.001; ****P < 0.0001).

We found that transient amplitude was reduced in MYB1#4-CMs when compared to MYB2#2-CMs and to their isogenic *MYBPC3*-corrected iPSC-CMs (Figure R9B). Moreover, MYB1#4-CMs exhibited a significantly faster time to maximum calcium amplitude (Figure R9C). When analyzing Ca^{2+} transient decay kinetics we observed a significantly reduced time at 50% peak in MYB1#4 only when compared to IsoMYB1#4, but we did observed that MYB1#4-CMs showed a markedly reduced transient decay at 90% peak when compared to MYB2#2 and their isogenic *MYBPC3*-corrected iPSC-CMs (Figure R9D-E), suggesting that calcium reuptake may be altered. Taken together, these results indicate an increase in the severity of calcium handling phenotypes in MYB1#4 iPSC-CMs, which is not observed in the iPSC-CMs derived from the mild symptomatic MYB2#2 carrier.

4.11 Symptomatic MYB1#4 iPSC-CMs exhibit altered contraction-relaxation kinetics

Although hypercontractility is a pathological mechanism commonly found in HCM, abnormal contractile alterations in iPSC-based models carrying *MYBPC3* mutations are inconsistently described. While some reports showed altered contraction kinetics (Cohn et al., 2019; Wu et al., 2019), others showed no difference (Helms et al., 2020a; Seeger et al., 2019). To evaluate whether

cardiac contractility is similarly affected in our set of isogenic iPSC, cardiac monolayers were recorded. Using pixel-based motion analysis at day 20 of cardiac differentiation, we showed that there are no differences in contraction duration, time to peak, relaxation at 50% interval or cardiac relaxation between the mutant iPSC-CMs and their isogenic corrected counterparts (Figure R10A-D).

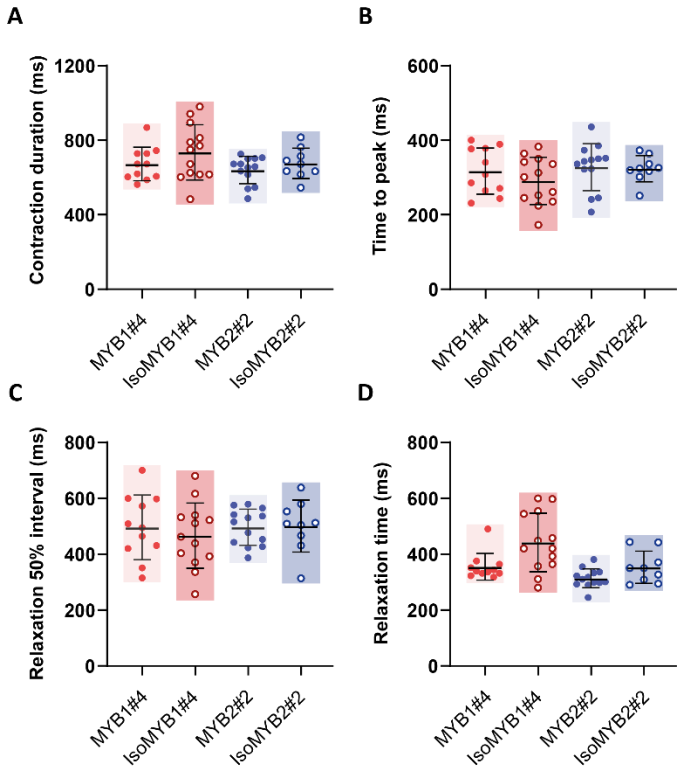

Figure R10. Contractile dynamics of HCM mutants and isogenic controls in iPSC-derived cardiac monolayers at day 20 of differentiation. (A-D) Analysis of contraction parameters from HCM mutants, control and isogenic edited iPSC-CM monolayers at Day 20 post-induction of cardiac differentiation showing quantification of contraction duration (A), time to maximum contraction (B), relaxation at 50% interval (C) and relaxation time (D). For each group in (A-D), data was generated from *N* = 3 independent differentiation batches. Data represent mean ± SD. Statistical analysis was tested with one-way ANOVA with Tukey correction.

To evaluate whether longer *in vitro* culture maturation could promote altered contractile kinetics, day 30 cardiac monolayers were analysed using high-speed imaging (Figure R11A-B). We did not observe significant differences in beating rate during spontaneous contraction among the analyzed lines (Figure R11C).

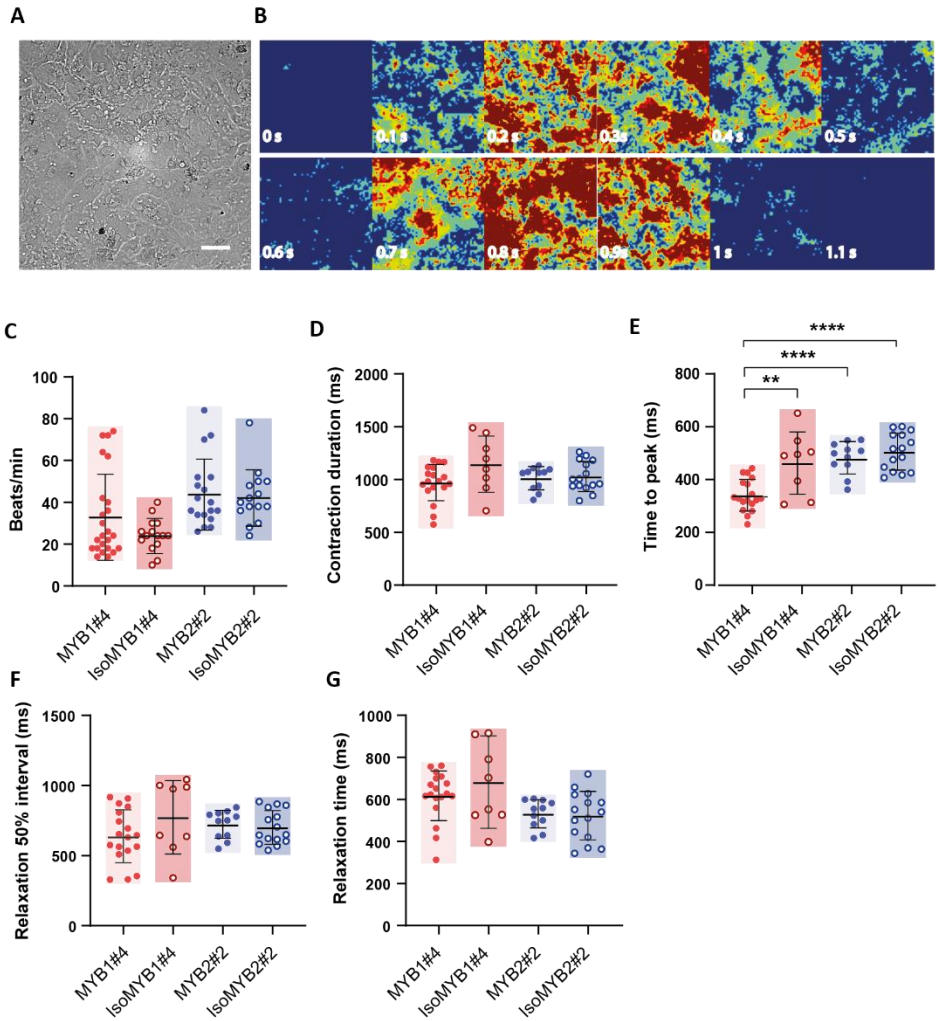

Figure R11. Contractile dynamics of HCM mutants and isogenic controls in iPSC-derived cardiac monolayers. A) Representative bright-field image of a iPSC-CM monolayer. Scale bar 100 µm. **B)** Vector-based contractile heatmap showing a homogeneous cardiac contraction and relaxation during a single beating event in a

iPSC-CM monolayer. **C)** Spontaneous beating rate at day 20 of cardiac differentiation. **(D-G)** Analysis of contraction parameters from HCM mutants, control and isogenic edited iPSC-CM monolayers at 5 weeks post-induction of cardiac differentiation showing quantification of contraction duration (D), time to maximum contraction (E), relaxation at 50% interval (F) and relaxation time (G). For each group in (D-G), data was generated from *N* = 3-5 independent differentiation batches. Data represent mean ± SD. Statistical analysis was tested with one-way ANOVA with Tukey correction (*P < 0.05; **P < 0.01; ***P < 0.001; ****P < 0.0001).

While we could not observed any difference in contraction duration nor relaxation, MYB1#4 iPSC-CMs displayed a significantly faster contraction time (Figure R11E). Of note, we could not detect any abnormalities in cardiac contraction kinetics related to MYB2#2 iPSC-CMs and its isogenic corrected IsoMYB2#2 iPSC-CMs, indicating that the *MYBPC3* mutation does not induce a pathological alteration on cardiac contraction within 30 days culture.

Thus, although the effect of *MYBPC3* K600Nfs*2 pathogenic mutation on contraction dynamics is not evident in MYB2#2-iPSC-CMs in our *in vitro* culture conditions, MYB1#4-iPSC-CMs appears to account for a severe HCM pathological phenotype at the contractile level after 30 days in culture.

4.12 *MYBPC3* mutant iPSC-CMs exhibit altered mitochondrial bioenergetics

HCM-causing mutations within myofilament proteins deregulate ATP utilization at the sarcomere level, increasing the energetic cost of contraction (van der Velden et al., 2018). Although it is still on debate whether mitochondrial energy depletion is a consequence or a cause of myocardial dysfunction, there is evidence in support for a reduced efficiency of cardiac performance in non-manifesting carriers (Crilley et al., 2003).

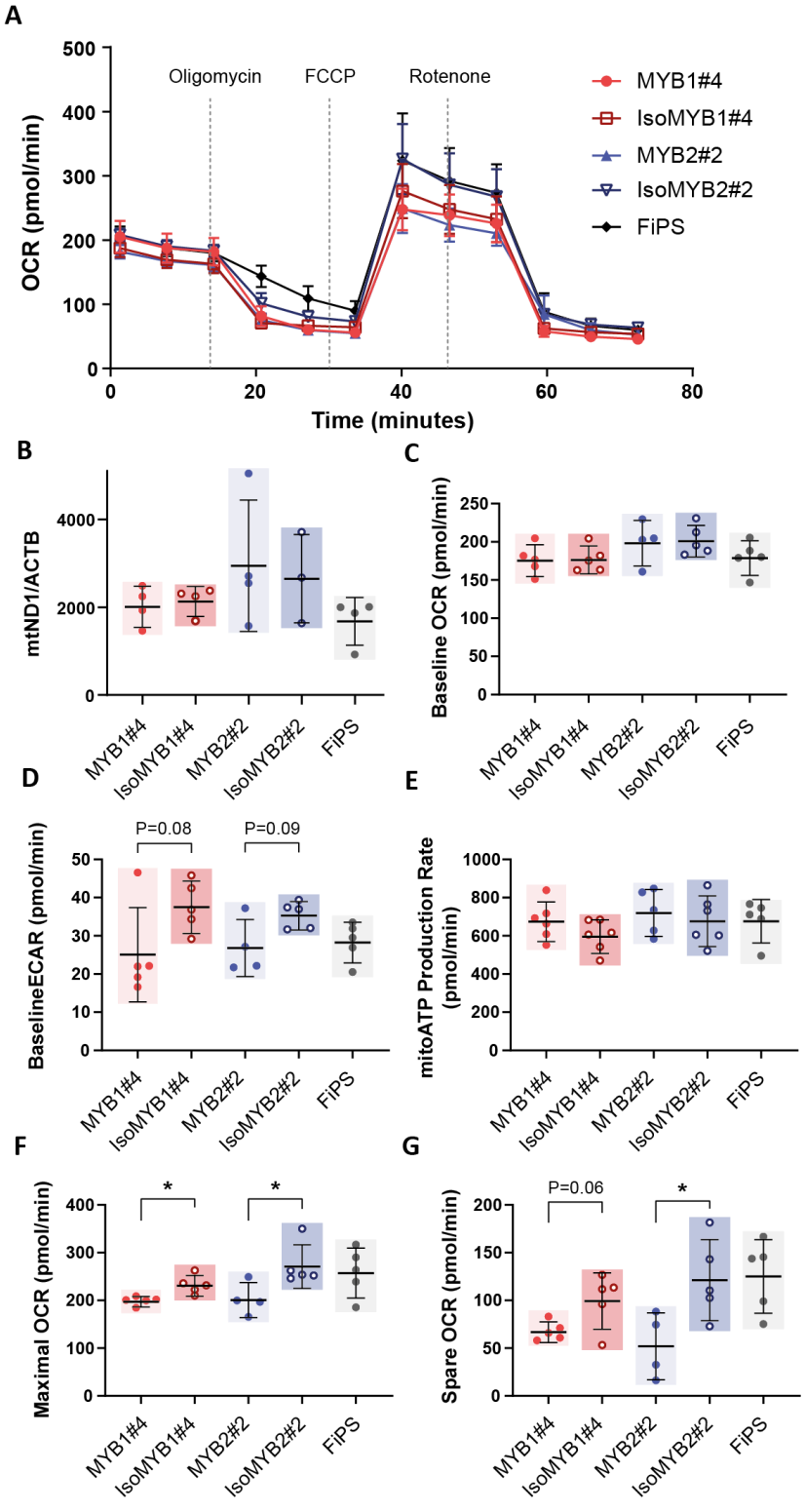
A
OCR (pmol/min)
Time (minutes)
Oligomycin
FCCP
Rotenone
MYB1#4
IsoMYB1#4
MYB2#2
IsoMYB2#2
FiPS
B
mtND1/ACTB
C
Baseline OCR (pmol/min)
D
BaselineECAR (pmol/min)
P=0.08
P=0.09
E
mitoATP Production Rate (pmol/min)
F
Maximal OCR (pmol/min)
G
Spare OCR (pmol/min)
P=0.06
MYB1#4
IsoMYB1#4
MYB2#2
IsoMYB2#2
FiPS

Figure R12. Bioenergetic analysis of *MYBPC3* mutants and isogenic controls iPSC-CMs. A) Mitochondrial respiration rates in cardiac monolayers after the sequential addition of modulators of the respiratory chain using the Seahorse Extracellular Flux Analyzer. **B)** qPCR analysis showing mitochondrial (ND1):nuclear (ACTB) DNA ratio (*N* = 3-4). Bioenergetics profile quantified for **C)** baseline OCR, **D)** ECAR, **E)** mitochondrial ATP production rate, **F)** maximal and **(G)** spare capacity. For each group, data was generated from *N* = 4-5 independent differentiation batches. Data represent mean ± SD. Statistical analysis was tested using two-tailed unpaired t-test with Welch's correction comparing between isogenic sets.

Thus, we measured mitochondrial respiration using the Seahorse extracellular flux analyzer, which determines the oxygen consumption rates (OCR) during the sequential addition of specific electron transport chain inhibitors (Figure R12A). While mitochondrial content, baseline OCR and ATP production rate were unchanged (Figure R12B-D), we observed a tendency towards a reduced ECAR in both patient-derived MYB1#4 and MYB2#2 iPSC-CMs as compared to their respective isogenic iPSC-CMs, suggesting that glycolysis might be downregulated (Figure R12E). Additionally, maximal respiration and spare capacity were reduced in both mutant iPSC-CMs as compared to their respective isogenic and control iPSC-CMs (Figure R12D, F-G). Moreover, unchanged non-mitochondrial respiration and an unaltered proton leak did not indicate notable increases in oxidative stress (Figure R13A-B).

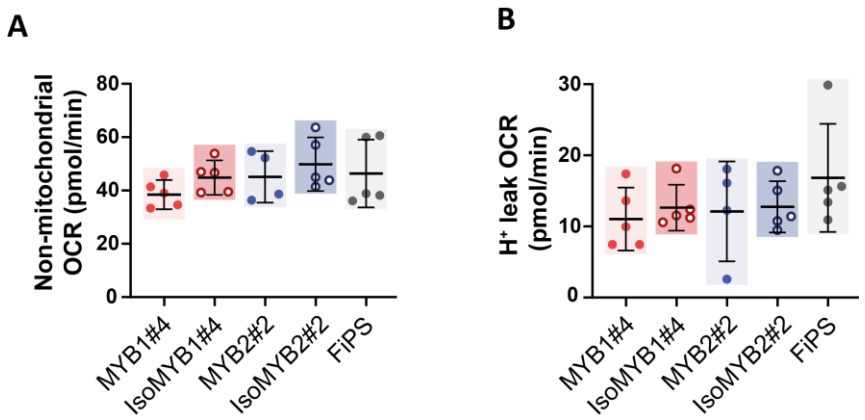

Figure R13. Oxygen consumption estimates for ROS production and ETC integrity of *MYBPC3* mutants and isogenic controls iPSC-CMs. Quantification of **A)** Non-mitochondrial OCR and **B)** proton H^+ leak. For each group, data was generated from *N* = 4-5 independent differentiation batches. Data represent mean ± SD. Statistical analysis was tested using two-tailed unpaired t-test with Welch's correction comparing between isogenic sets.

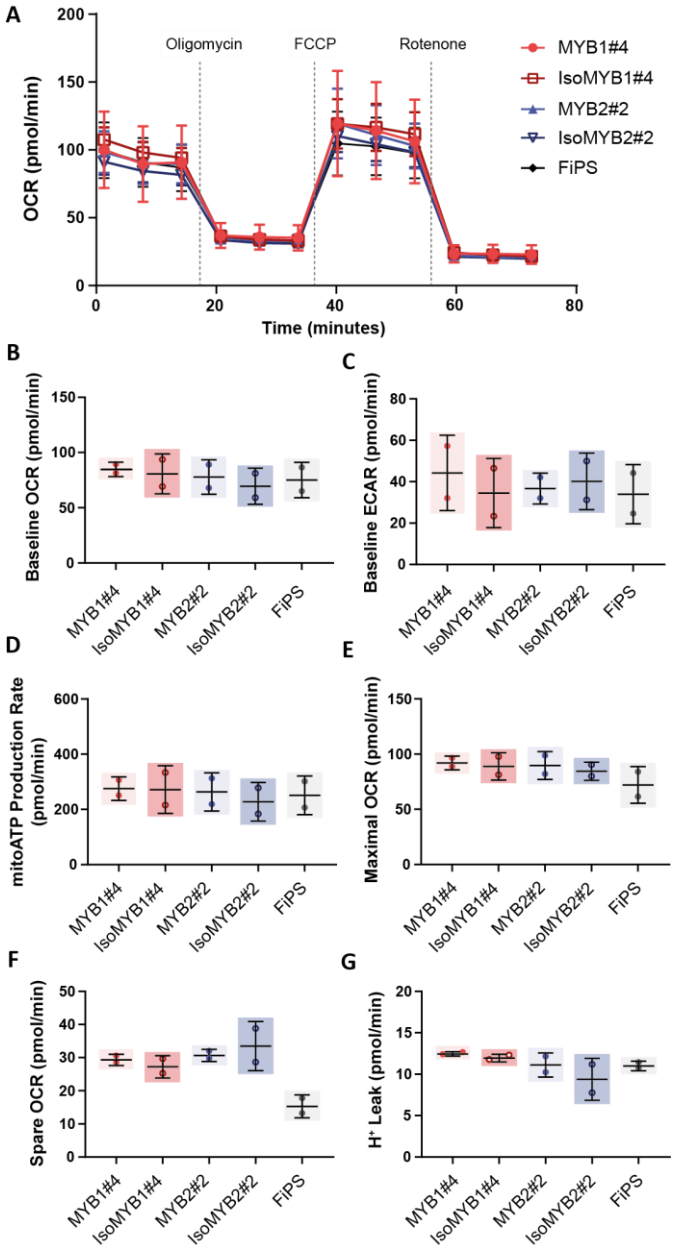

Figure R14. Bioenergetic analysis of HCM mutants and isogenic controls iPSC lines. **A)** Mitochondrial respiration rates in iPSC cultures after the sequential addition of modulators of the respiratory chain using the Seahorse Extracellular Flux Analyzer. Bioenergetics profile of iPSC quantified for **B)** baseline OCR, **C)** baseline ECAR, **D)** mitochondrial ATP production rate, **E)** maximal respiration, **F)** spare capacity and **G)** proton leak. Data represent mean ± SD (*N = 2*). Statistical analysis was tested using two-tailed unpaired t-test with Welch's correction comparing between isogenic sets.

These results suggest that mitochondria is functioning at a higher capacity to meet the elevated energetic demands in *MYBPC3* mutant iPSC-CMs, whereas these differences are not present at the undifferentiated iPSCs (Figure R14A-G).

Interestingly, the observation that mitochondrial dysfunction is present in cardiomyocytes derived from the mild symptomatic MYB2#2 carrier suggest that impaired bioenergetics may be an early pathogenic event in HCM, thus supporting the energy depletion model as a common mechanism that could potentially trigger disease progression (Ashrafian et al., 2003). Together, these results suggest that mitochondrial respiration is altered in *MYBPC3* mutant iPSC-CMs regardless of the individual's genomic background and is independent of the clinical pathological phenotypes observed in the mutant carriers.

4.13 Whole exome sequencing highlights a potential genetic modifier in the symptomatic carrier

To explore the possibility that genetic drivers are modifying the pathological outcomes in the symptomatic carrier and, therefore, would account for the recapitulation of HCM phenotypes in our iPSC-based model, we conducted a whole-exome sequencing of both probands and the HCM-affected father (Figure R15A-B).

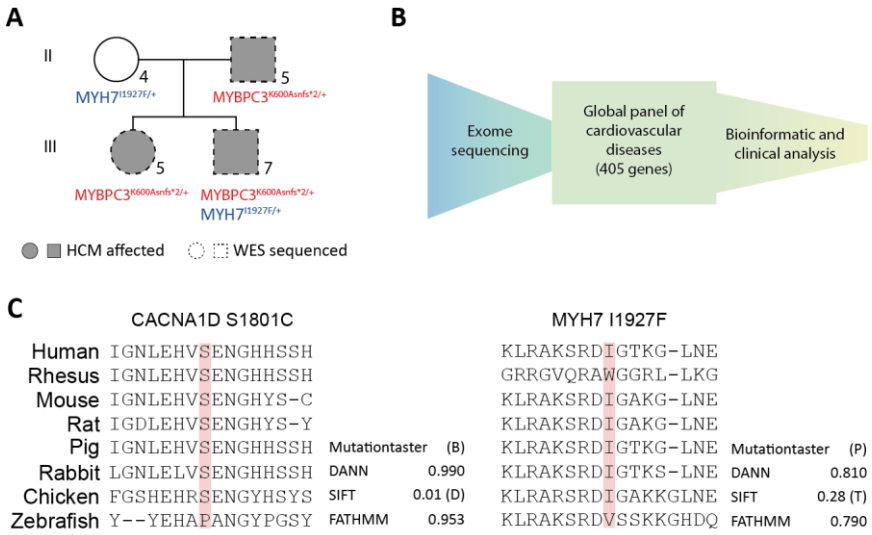

Figure R15. Exome sequencing and variant analysis of the HCM family. **A)** Pedigree of the present HCM family showing mutation carriers subjected to whole exome sequencing. **B)** Workflow for the identification and analysis of genetic variants following a cardiac-enriched gene panel. **C)** Genetic variants exclusively identified in the symptomatic individual III.7 showing amino acid conservation across species. Variants of interest are highlighted in red. Prediction analysis of the effect of the amino acid change on protein function using Mutationtaster, DANN, SIFT and FATHMM damaging algorithms. B, benign; D, damaging; P, pathogenic; T, tolerated.

From a considered panel of 405 genes associated with cardiovascular diseases, we identified two additional rare, non-synonymous, exonic VUS variants that were specific to the HCM-affected individual III.7 and not present in the mild symptomatic carrier III.5 (Table R1). The first one is a heterozygous serine to cysteine substitution in the *CACNA1D* gene (p.S1801C), not previously described in the general or HCM population cohorts, suggesting that this variant may not be implicated in HCM. The second variant is located in the myosin heavy 7 (*MYH7*) gene and involves a previously described heterozygous isoleucine-to-phenylalanine substitution at position 1927 (p.I1927F). This residue is localized at the C-terminal end within the LMM domain of the protein.

Table R1. Relevant sequence genetic variants identified by WES

Gene	Variant	Result	Pathogenicity	gnomAD frequency
Variant identified in all individuals				
MYBPC3	NP_000247.2:K600Nfs*2 NM_000256.3:c.1800delA NC_000011.9:g.47362788delT	Heterozygosis	Pathogenic (+++)	<0,001%
Considered variants identified in individual III.5; MYB1#4				
MYH7	NP_000248.2:I1927F NM_000257.3:c.5779A>T NC_000014.8:g.23882979T>A	Heterozygosis	Variant of uncertain significance, possibly pathogenic	<0,005%
C10orf71	NP_001128668.1:p.Glu1092Lys NM_001135196.1:c.3274G>A NC_000010.10:g.50533864G>A	Heterozygosis	Variant of uncertain significance	<0,001%
CACNA1D	NP_000711.1:p.Ser1801Cys NM_000720.3:c.5402C>G NC_000003.11:g.53835386C>G	Heterozygosis	Variant of uncertain significance	-
LAMA4	NM_001105206.2:c.4822-9T>C NC_000006.11:g.112439110A>G	Heterozygosis	Possibly benign	<0,001%
Considered variants identified in individual III.3; MYB2#2				
C10orf71	NP_001128668.1:p.Glu1092Lys NM_001135196.1:c.3274G>A NC_000010.10:g.50533864G>A	Heterozygosis	Variant of uncertain significance	<0,001%
CREBBP	NP_004371.2:p.Arg1081Cys NM_004380.2:c.3241C>T NC_000016.9:g.3817730G>A	Heterozygosis	Variant of uncertain significance	<0,001%
LAMA4	NM_001105206.2:c.4822-9T>C NC_000006.11:g.112439110A>G	Heterozygosis	Possibly benign	<0,001%
Considered variants identified in individual II.3				
PTPN11	NP_002825.3:p.Val382Ile NM_002834.3:c.1144G>A NC_000012.11:g.112919929G>A	Heterozygosis	Variant of uncertain significance	<0,001%
FOXF1	NP_001442.2:p.Met158Arg NM_001451.2:c.473T>G NC_000016.9:g.86544648T>G	Heterozygosis	Variant of uncertain significance	-

Although bioinformatics analysis indicate that it is not a highly conserved amino acid, multiple in-silico algorithms predict a pathogenic score (Figure R15C). Within the LMM domain, several pathogenic, likely-pathogenic and VUS nucleotide variants are found to be associated with HCM (Homburger et al., 2016). However, a significant proportion of individuals carrying variants in the LMM region do not develop HCM, suggesting and incomplete penetrance. Similarly, the *MYH7* I1927F variant has been associated with HCM. However, many of the individuals carried additional pathogenic variants that could

explain the observed phenotype and some individuals had no cardiac involvement. The fact that co-segregation studies in those families are still missing further complicates variant interpretation (Claes et al., 2016; Fokstuen et al., 2008; Jaafar et al., 2016).

Extending the genetic study to the mother of the proband confirmed the presence of the *MYH7* I1927F variant. Clinical evaluation showed mild LVH with a septum of 14 mm and no fibrosis in CMRI that could be explained by arterial hypertension (Figure R1F). No other *MYH7* carriers or HCM affected individuals were found (Figure R1G). Taken together, there is not sufficient clinical and experimental evidence to accurately assess pathogenicity of the *MYH7* I1927F variant.

4.14 CRISPR/Cas9 gene correction of the *MYH7* I1927F variant

Evaluating rare and low-penetrance genetic variants by genome population studies or co-segregation analysis is frequently insufficient to produce robust evidence for variant interpretation. To precisely evaluate the consequence of the VUS *MYH7* I1927F, we used CRISPR/Cas9 technology to correct the *MYH7* I1927F variant in the MYB1#4 genomic background, generating the isogenic corrected MYB1#4-MYH7 iPSC line (Figure R16).

We designed a sgRNA spanning the c.5779A>T (I1927F) mutation to target specifically the mutated allele and next to a PAM sequence 'NGG', which is necessary for DNA cleavage by the Cas9 endonuclease (Figure R16A). MYB1#4-iPSC were nucleofected with CRISPR/Cas9 RNP complexes and with the repair template containing the wild type sequence. Several iPSC colonies were screened for the desired genotype. The generated isogenic corrected MYB1#4-MYH7 iPSC line was genotyped, verified by Sanger sequencing and had a normal karyotype (Figure R16B).

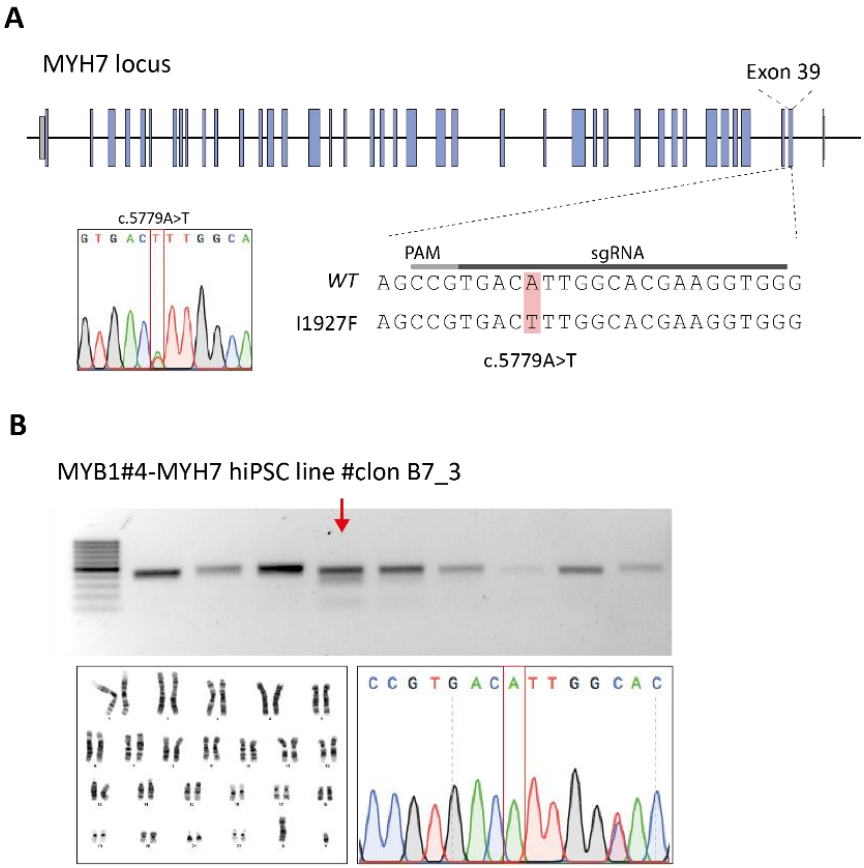

Figure R16. Generation and characterization of CRISPR/Cas9 gene-corrected isogenic iPSCs. A) Schematic representation of the CRISPR/Cas9 gene editing design, showing the c.5779A>T (I1927F) mutation in the *MYH7* gene and the sgRNA used in our study. **B)** Generation and characterization of isogenic corrected MYB1#4-MYH7 iPSC line showing: (top) molecular analysis of the gene-edited clone (indicated by red arrow) confirming the proper restriction site integration; (bottom left) normal karyotype and (bottom right) Sanger sequencing confirming the correction of the c.5779A>T (I1927F) mutation in the *MYH7* gene.

4.15 Morphological characterization of MYB1#4 and isogenic corrected iPSC-CMs

To evaluate whether the different mutational load have an impact on cellular hypertrophy, we differentiated double and isogenic single mutants iPSC lines toward cardiomyocytes and assessed various morphological aspects

(Figure R17). We did not observe any difference in cell area between double mutant MYB1#4 iPSC-CMs and their isogenic single mutant IsoMYB1#4 and MYB1#4-MYH7 iPSC-CMs at day 25 post-differentiation (Figure R17A-B).

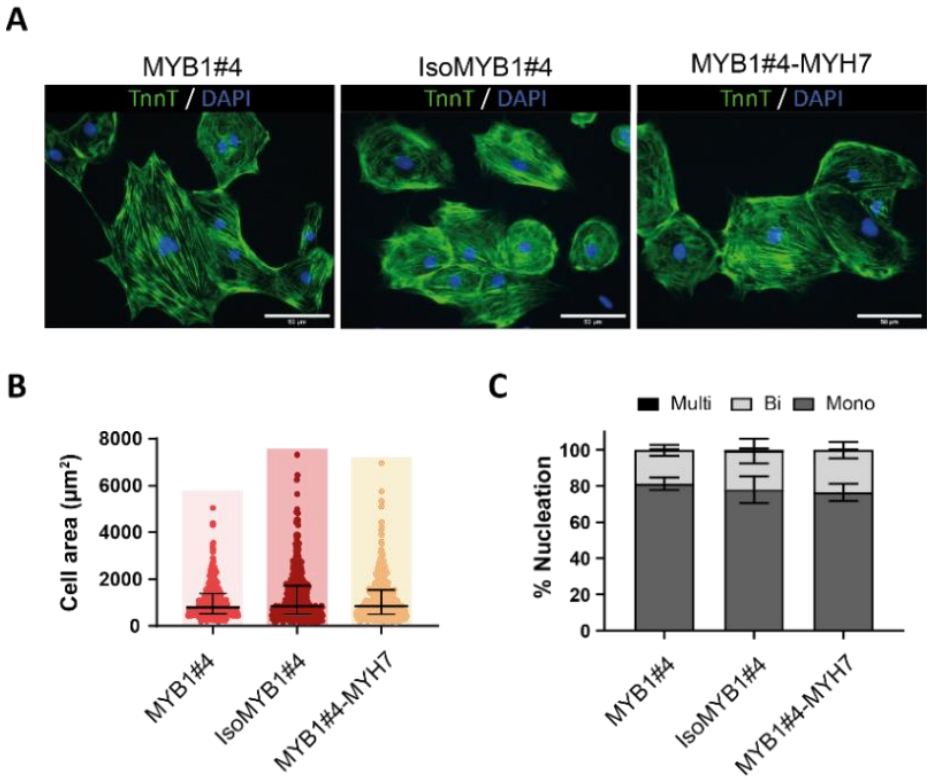

Figure R17. Morphological characterization of double and single mutants iPSC-CMs. **A)** Representative immunofluorescence images stained for Troponin T (cTnT) from double mutant MYB1#4 and isogenic single mutants iPSC-CMs. Scale bar 50 µm. **B-C)** morphological analysis of single iPSC-CMs showing quantification of cell area (B) and percentage of nucleation (C) distinguishing between mono-, bi- and multi-nucleated cells; *n* = 428 (MYB1#4), 457 (IsoMYB1#4) and 452 (MYB1#4-MYH7) cells from *N* = 3 independent differentiations.

Moreover, we were not able to observe significant differences in the multi-nucleation levels between double and single mutants iPSC-CMs (Figure R17C). These results suggest that single *MYBPC3* or *MYH7* mutations, or the presence of both in the MYB1#4 genetic background, do not produce cellular

hypertrophy nor a change in the percentage of nucleation in our *in vitro* culture at day 25 of cardiac differentiation.

4.16 *MYH7* I1927F variant enhances contraction kinetics in MYB1#4 iPSC-CMs

Since we have previously identified a faster contraction kinetics in MYB1#4 iPSC-CMs when compared to its isogenic *MYBPC3*-corrected counterparts, we hypothesize that this observation can be triggered by the additional presence of the *MYH7* I1927F variant, as we do not observe a faster contraction time in the mutant MYB2#2 when compared to its isogenic *MYBPC3*-corrected iPSC-CMs. To assess the contribution of the *MYH7* I1927F variant on cardiac contractility, we recorded cardiac monolayers from our complete set of MYB1#4 isogenic mutant lines.

While we were not able to detect differences in contraction duration nor relaxation, MYB1#4 iPSC-CMs showed a significantly faster contraction time when compared with its isogenic single mutant IsoMYB1#4 iPSC-CMs (Figure R18B), as previously revealed in Figure R11E and suggesting that the pathological contractile phenotype can be recapitulated robustly in our iPSC *in vitro* model. Importantly, MYB1#4-MYH7 cardiac monolayers displayed a significantly slower contraction time when compared to the double mutant MYB1#4, but did not differed significantly when compared with IsoMYB1#4, suggesting that the *MYH7* I1927F variant have a pathogenic role.

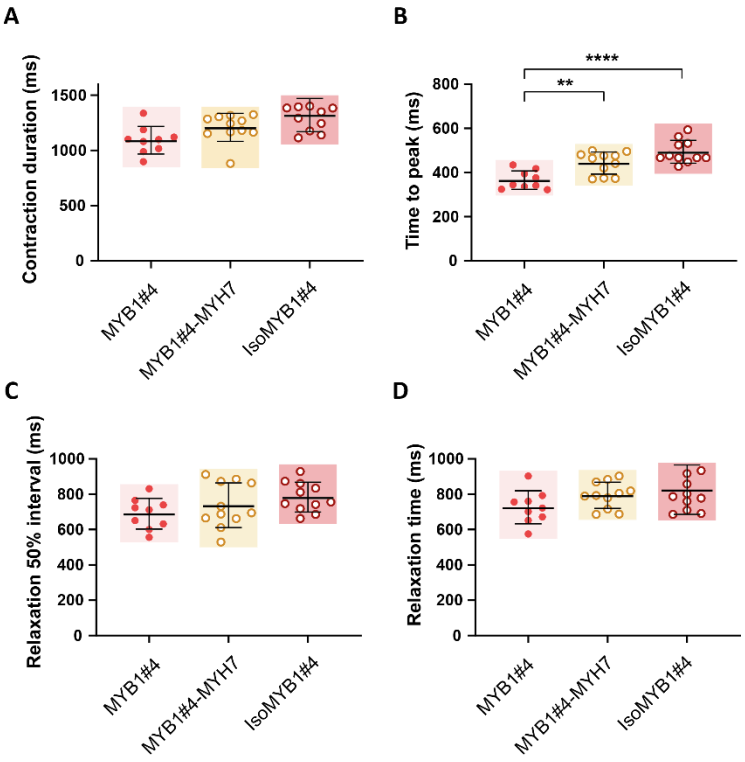

Figure R18. Contractile dynamics of double and single mutants iPSC-derived cardiac monolayers. (A-D) Analysis of contraction parameters from double mutant MYB1#4 and isogenic single mutants iPSC-CMs monolayers at 5 weeks post-induction of cardiac differentiation showing quantification of contraction duration (A), time to maximum contraction (B), relaxation at 50% interval (C) and relaxation time (D). For each group in (A-D), data was generated from *N* = 3 independent differentiation batches. Data represent mean ± SD. Statistical analysis was tested with one-way ANOVA with Tukey correction (**P < 0.01; ****P < 0.0001).

Taken together, these results indicate that the presence of both *MYBPC3* K600Nfs*2 and the *MYH7* I1927F variants in the MYB1#4 iPSC-CMs accounts for a severe cardiac contractile deficit. Additionally, gene-correction of either *MYBPC3* or *MYH7* mutations rescues the enhanced contractile dynamics at the same level, indicating that the particular effect of the single mutations on contraction kinetics is not evident after 30 days in culture.

5 DISCUSSION

Hypertrophic cardiomyopathy (HCM) is the most common inherited cardiac disease and a frequent cause of heart failure and sudden cardiac death in the young population (Authors/Task Force et al., 2014; Ho et al., 2018). HCM is a complex condition defined by heterogeneous clinical manifestations, ranging from severely affected to asymptomatic individuals (Marian and Braunwald, 2017). It is also a genetically complex disease for which a plethora of pathogenic variants in several sarcomeric and non-sarcomeric genes has been recognised (Sabater-Molina et al., 2018; Teekakirikul et al., 2019). Over the last decades, invaluable insights has propelled our understanding into the genetic landscape of HCM (Maron et al., 2012). However, the wide clinical spectrum observed among HCM individuals harbouring the same gene mutation reinforces the importance of identifying and interpreting genetic and environmental modifiers for better disease management and risk stratification. In this sense, increased technological advances in next-generation sequencing (NGS) is facilitating the discovery of thousands of missense VUS variants whose clinical interpretation remains a critical bottleneck (Starita et al., 2017). To advance into precision medicine, in the present thesis we have combined clinical data, iPSC-based disease modelling and CRISPR/Cas9-mediated gene editing technology to develop a unique platform assay to interrogate the pathogenic effect of a variant of unknown significance presented in a symptomatic genotype-positive HCM carrier. Here, we were able to recapitulate *in vitro* the distinct clinical severity of two genotype-positive HCM siblings using patient-specific iPSC-derived cardiomyocytes. Using whole-exome sequencing, we identified a variant of unknown significance in the severely affected HCM proband and provided functional evidence supporting that such missense VUS, localized in the *MYH7* gene (p.I1927F), contributes to a severe phenotype when present in combination with a pathogenic *MYBPC3* mutation, highlighting the

importance of functional assays to undoubtedly ascribe genotype-phenotype correlations.

In the present work, we were able to recruit several related individuals with a large family history of HCM. The clinical diversity commonly observed in HCM patients was also mirrored in this family, as genetic testing and clinical assessment revealed both highly severe and very mild HCM phenotypes in two siblings carrying the same pathogenic c.1800delA (p.K600Nfs*2) mutation in the *MYBPC3* gene. This truncating variant in the *MYBPC3* gene was inherited from their father, who was diagnosed with non-obstructive HCM during familial evaluation at 60 years-old. He presented left ventricular hypertrophy of 16 mm and fibrosis in CMRI images and was subjected to a pacemaker implantation because of symptomatic bradycardia at 74 years-old. A paternal uncle was also a carrier of the *MYBPC3* variant and had similar mild phenotype. From a clinical point of view, *MYBPC3*-mutant HCM carriers have a later disease onset as compared to individuals having mutations in other relevant sarcomeric genes, such as *MYH7* or thin filament genes (Lakdawala et al., 2021; Sedaghat-Hamedani et al., 2018). In both works by Lakdawala and Sedaghat-Hamedani et al., the mean age of diagnosis in *MYBPC3*-mutant carriers was around the fourth decade of life. However, in our large population cohort carrying truncating *MYBPC3* variants, around 35% of male patients and 25% of female patients are diagnosed by HCM at 40 years-old, indicating that *MYBPC3* truncating variants generally produce a later disease onset with milder phenotypes. The 27-years-old sister of the proband was initially described as a non-manifesting carrier at the time of the familial study. However, during subsequent clinical evaluations, she developed a borderline phenotype with septal left ventricular hypertrophy of 12 mm at 42 years-old in echocardiogram. It is not uncommon that the index case present the more severe phenotype, as in our HCM family. Sources of such phenotypic differences between the aforementioned siblings can be explain by several

factors, including environmental, epigenetic or genetic modifiers. Numerous studies, and observed as well in our population data, have shown that gender-based differences may be one important factor that modify clinical outcomes and disease progression. Woman are underrepresented in cohorts of HCM patients, and are diagnosed at an older age when compared with men, which may indicate that sarcomeric variants have a reduced penetrance in woman (Lakdawala et al., 2021; Page et al., 2012; Terauchi et al., 2015). However, it is still not known whether this finding may reflect a lack of gender-specific criteria for HCM diagnosis, the influence of sex hormones or sex-specific differences in cardiac physiology (Butters et al., 2021).

To investigate whether different mechanistic or genetic factors between the siblings are contributing to the diverse clinical outcomes, we sought to generate iPSC as a unique platform to model the complex genetic peculiarities of the patients in a dish. Human iPSC are characterized by self-renewal and by their ability to differentiate towards any cell type of the human body. This unique model offers the possibility to obtain, theoretically, an unlimited amounts of patient-specific cells, including cardiomyocytes. Despite the current disadvantages of the iPSC approach, such as the immaturity of iPSC-derivatives and the lack of complex environmental cues, the generation of iPSC-based disease models overcomes the main limitation regarding the use of animal models, which do not represent human biology. The drawbacks of the animal models are also exemplified within the cardiovascular field. At the genetic level, HCM mouse models with heterozygous mutations do not seem to recapitulate all aspects of human HCM pathophysiology (Barefield et al., 2014; Flenner et al., 2021; Fraysse et al., 2012). At the molecular level, several prominent differences may limit the clinical translation to humans: mouse predominantly express the fast α-MHC while humans ventricles express the slow β-MHC, the action potential duration in mouse is shorter as compared to humans, calcium removal for relaxation is mostly driven by SERCA in mouse

cardiomyocytes while in human cardiomyocytes the NCX channel greatly contributes to calcium removal, among many others (Milani-Nejad and Janssen, 2014). Thus, in the present work we used iPSC as a model to decipher the functional consequences of a familial HCM mutation in the *MYBPC3* gene that are particular at the patient level. We generated iPSC from the severely affected HCM proband (individual III.7) and from his sister with a mild hypertrophy (individual III.5), both carrying the same pathogenic truncating variant in the *MYBPC3* gene (c.1800delA, p.Lys600Ansfs*2).

In the literature, it has been described several procedures to differentiate iPSC towards cardiomyocytes. For the present work, we have implemented a robust and widely used cardiac differentiation protocol based on the modulation of the Wnt/β-catenin signalling pathway (Lian et al., 2013). Although it is a simple and stepwise protocol, certain parameters require iPSC line-dependent optimization, such as the initial cell density and the concentration of the Gsk3 inhibitor. This is especially convenient when working with several lines to reduce batch-dependent variability. Despite of inconsistencies and low reproducibility of cardiac specification efficiencies (Laco et al., 2018), we were able to generate highly pure cultures of cardiomyocytes from all iPSC lines presented in the current thesis (and from many other iPSC lines not shown).

Here, we used a comprehensive phenotypic characterization of iPSC-CMs at both morphological and at the functional level. At the morphological level, we showed that neither double mutant MYB1#4 iPSC-CMs nor single *MYBPC3* mutant MYB2#2 iPSC-CMs revealed any abnormalities in sarcomere structure as revealed by immunostaining and transmission electron microscopy (TEM). First, our observations are in line with recent iPSC models indicating that cMyBP-C protein is not a constraint for sarcomere assembly and organization (Helms et al., 2020a; Ma et al., 2018b; Seeger et al., 2019).

Second, although *MYH7* I1927F missense variant and surrounding variants within the LMM domain has been associated with myopathy, likely by impacting LMM domain's structure and function (Atemin et al., 2021; Lamont et al., 2014; Parker et al., 2018), the affected proband does not show clinical signs of muscle weakness, indicating that *MYH7* I1927F does not seem to severely impair sarcomere assembly. However, additional biomechanical and biophysical studies on protein folding or stability of *MYH7* VUS in the LMM domain will be necessary to fully understand their functional consequences. We also observed that *MYH7* I1927F does not impact contractile force generation and that the marked reduction in traction stress was directly due to the *MYBPC3* frameshift variant (K600Nfs*2), as both mutant iPSC-CMs showed similar contractile force deficits. Previous *MYBPC3*-related iPSC studies have also shown lower systolic contractile force both at the single cell level (Birket et al., 2015; Ribeiro et al., 2017), in engineered microtissues after external mechanical load (Ma et al., 2018b) and also shown in an heterozygous *MYBPC3*-KI mouse model (Barefield et al., 2014). However, as in our study, they do not observe structural deficiencies or hypertrophic remodelling in iPSC-CMs.

Measurements of cell area, a surrogate of cardiac hypertrophy commonly evaluated in cell-based models *in vitro*, revealed no differences between both patient-specific iPSC-CMs. Despite of the marked hypertrophic remodelling in the proband (individual III. 7) at a younger age, we were not able to recapitulate this HCM hallmark using iPSC-derived cardiomyocytes. We tested various protocols and conditions aimed to improve the maturation of iPSC-CMs (not shown in the present thesis). Specifically, we tested the addition of three known factors that improve the maturation status of iPSC-CMs (T_3: Triiodothyronine, IGF-1: insulin growth factor 1, and dexamethasone)(Birket et al., 2015). We also evaluated whether 3D cardiac spheroids promoted a hypertrophic response. However, we could not observed any difference in cell

area between both mutant carriers iPSC-CMs, highlighting the need for better maturation protocols that could potentially reveal morphological phenotypes.

As a strategy to functionally assess the effect of the *MYBPC3* K600Nfs*2 variant and to evaluate disease-specific changes, we created a series of isogenic iPSC using CRISPR/Cas9-mediated genome editing. These included isogenic corrected iPSCs for the heterozygous pathogenic *MYBPC3* K600Nfs*2 mutation in both carriers. CRISPR/Cas9 technology has revolutionized completely the biomedical field and opened the door for better cell therapies and disease models. Because of its simplicity, CRISPR/Cas9 editing has rapidly been adapted by many laboratories. Our first attempts to edit a genetic variant in iPSC lines were based on the transfection of a plasmid containing the expression of Cas9-P2A-GFP and the custom sgRNA sequences. Since iPSC are considered 'hard-to-transfect' cells with high sensitivity to external stresses, our initial editing efficiencies were really low (~0,5- 2,1%), implying that hundreds of iPSC colonies had to be genotyped. With the continuous progress towards the democratization of CRISPR/Cas9 gene editing, more affordable protein versions of Cas9 and sgRNA products were available. The direct transfection of the ribonucleotide (RNP) Cas9-sgRNA complexes allowed us to increase transfection and editing efficiencies, while reducing the timings and the screening process.

Previous *MYBPC3*-deficient iPSC-CMs and animal models have reported impaired contractile dynamics and calcium mishandling as key pathological phenotypes observed in HCM, often with contradictory results (de Lange et al., 2011; Fraysse et al., 2012; Seeger et al., 2019), indicating the complex correlation between genotype and phenotype caused by HCM mutations.

Our data showed a hyper-contractile phenotype with faster calcium transients in the iPSC-CMs derived from the symptomatic patient at day 30 of cardiac differentiation, which is rescued when the *MYBPC3* mutation is corrected. It therefore indicates that the *MYH7* I1927F variant is not sufficient, but exacerbates disease phenotype. In a related report from Mosqueira et al., similar conclusions were made. They showed that severe phenotypic dysfunctions were associated with the mutational load in iPSC-CMs (Mosqueira et al., 2018). They observed that iPSC-CMs with a known pathogenic mutation in homozygosis in the *MYH7* gene displayed lower contractile force and a severe calcium mishandling when compared with its heterozygous counterpart (Mosqueira et al., 2018). Similar conclusions could be obtained from our familiar evaluation: the proband has a severe phenotype while the rest of the *MYBPC3* variant carriers have a milder phenotype. The lack of contractile deficits in iPSCs-CMs derived from the mild HCM patient indicates that our platform can faithfully recapitulate the diverse clinical phenotypes in a dish, as shown in a recent report in which the phenotypes caused by different VUS in the MYL3 gene could be recapitulated using iPSC (Ma et al., 2018a).

Our results in mitochondrial function using the isogenic sets revealed a metabolic derangement that supports the energy depletion model (Ashrafian et al., 2003). Since our data showed that iPSC-CMs derived from the mild symptomatic HCM individual also developed mitochondrial bioenergetics alterations, and because we could not detect any other deficits in calcium handling or contraction kinetics, we theorise that mitochondrial dysfunction may be an early phenotype that precedes HCM progression. Although it is a controversial paradigm, many studies have reported energetic or metabolic imbalances in HCM iPSC-CMs carrying different sarcomeric mutations (Bhagwan et al., 2020; Cohn et al., 2019; Mosqueira et al., 2018; Toepfer et al., 2020). A clinical study also reported that not only symptomatic HCM

patients carrying sarcomeric mutations, but also mutant carriers with undetected clinical symptoms present a bioenergetics deficit. (Crilley et al., 2003). Mechanistically, reduced levels of cMyBP-C results in augmented myosin contractility by altering myosin dynamic conformations (Toepfer et al., 2019), imposing an inefficient ATP usage and an increased energetic demand that can compromise ATP-dependent cellular processes, such as the calcium influx by the SERCA2a ATPase towards the sarco/endoplasmic reticulum (SR). However, whether HCM-linked missense variants or VUS have an evident impact on mitochondrial respiration remains to be fully elucidated.

By using whole-exome sequencing, we were able to identify dozens of variants in probands III.5 and III.3. Most of them were shared between both individuals and frequently found in the general population. Only two were specific to the HCM-affected proband III.5. We identified a p.Ser1801Cys missense variant in the *CACNA1D* gene. The *CACNA1D* p.Ser1801Cys variant has not been detected previously in population or HCM databases. The *CACNA1D* gene codifies for the L-type calcium channel Cav1.3, expressed in the atria and sinoatrial node of the heart and absent in the ventricles (Mesirca et al., 2015). Since variants within this gene has been associated with channelopathies of heart automaticity and deafness (Torrente et al., 2020), not observed in our proband, we hypothesize that the CACNA1D p.Ser1801Cys variant may not be related with HCM. Nevertheless, we cannot completely discard that such CACNA1D variant is not affecting the function of the protein nor contributing to HCM, as the serine amino acid at position 1801 is highly conserved among species. We also identified the missense VUS I1927F in the *MYH7* gene, the second most common mutated gene in HCM after *MYBPC3* (Marian and Braunwald, 2017). This variant is localized at the C-terminal end within the repetitive heptad sequence within the LMM domain, essential for thick filament assembly. Based on the ClinVar database, missense variants surrounding the codon 1927 of the *MYH7* protein are mostly interpreted as

variants of uncertain significance with no assertion criteria provided, although many of them has been found in association with cardiomyopathies. In silico metrics (e.g. Polyphen or MutationTaster), have been generated to predict the impact of an amino acid substitution on protein function (Adzhubei et al., 2010; Schwarz et al., 2014). However, such predictions may not truly reflect the actual consequence of a variant, as for the *MYH7* I1927F (Adzhubei et al., 2013). Furthermore, scoring the epistatic contribution of multiple genetic changes is challenging (Papadimitriou et al., 2019).

Clinical data also provides clues regarding pathogenicity of *MYH7* I1927F. In the literature, it was first described in a male individual diagnosed with HCM at 61 years-old with moderate septal hypertrophy and a positive family history of HCM (Fokstuen et al., 2008). Later, it was also found in isolated HCM probands from different ethnicities, some of them associated with additional sarcomeric variants that may further contribute to their phenotype (Claes et al., 2016). From those studies providing clinical details, Jaafar et al. found the *MYH7* variant in a 36 years-old male with heart palpitations and a mild septal hypertrophy of 15 mm (Jaafar et al., 2016). In a later study, Mademont-Soler et al. the variant was found in a 12 years-old girl with HCM. No other familial relatives were studied (Mademont-Soler et al., 2017). In no case, cosegregation studies were made and the variant was considered as uncertain significance. In our clinical database, the *MYH7* p.I1297F variant has been identified in 10 index cases of more than 23.000 unrelated probands (0,047%) sequenced by NGS. Six of them were clinically diagnosed with HCM. Among these, the *MYH7* variant was identified in 65 years-old woman with an additional pathogenic variant in the *MYBPC3* gene (p.Glyc531Arg) that could explained the phenotype. Another proband was a 61 years-old woman with no family history of sudden cardiac death. She also carried and additional VUS in the *MYBPC3* gene (p.Pro16Ser). The rest 4 index cases were male individuals with no additional genetic variants. The rest index cases had other non-related

phenotypes (Marfan syndrome, long QT syndrome and heart conduction disorder). The fact that co-segregation studies in those families are still missing further complicates variant interpretation. In our familial case described in the present thesis the variant *MYH7* I1927F found in our index case was inherited from his mother. CMRI imaging revealed a mild left ventricular hypertrophy. Although it could be secondary to arterial hypertension, we cannot discard that it represents a mild phenotype of HCM.

In this sense, rapid advancements in high-throughput DNA sequencing have revolutionized genetic screening and the ability to analyse genetic variation of Mendelian disorders, both in healthy and diseased individuals (Lek et al., 2016). Therefore, a vast increase of novel genetic variants has been associated to HCM, often with insufficient evidence (Ingles et al., 2019; Walsh et al., 2017). This ever-increasing collection of sequence changes has raised important challenges in variant interpretation (Richards et al., 2015). Except for deletions, insertions, pathogenic nonsense or splice-site variants, the predictable consequences of most missense SNPs variants identified by whole-exome or genome sequencing are difficult to determine. Furthermore, many of them are only present in a small number of individuals, making variant interpretation even challenging. For numerous rare novel variants there is not sufficient information to ascertain pathogenicity and they are thus classified as variants of unknown significance (VUS), creating uncertainty and adverse consequences for the patients and their relatives (Manrai et al., 2016; Mazzarotto et al., 2020). Determining the pathogenicity of genetic variants is an imperative hallmark for precision medicine of cardiomyopathies, especially when the presence of double or multiple variants can greatly modulate disease onset and clinical outcomes (Alfares et al., 2015; Girolami et al., 2010; Ingles et al., 2005). Thus, new experimental evidence to functionally assess the potential pathogenicity of VUS is urgently needed.

With this end, we corrected the *MYH7* I1927F variant in the double mutant MYB1#4 iPSC using CRISPR/Cas9 gene editing, creating a complete series of isogenic corrected control iPSCs. Morphological characterization did not revealed variant-specific differences in cell hypertrophy, emphasizing the importance for developing better maturation protocols. As a strategy to functionally validate and understand variant pathogenicity in genetically defined conditions and in the absence of environmental cues, we measured cardiac contractility, as we observed significant differences within iPSC-CMs in previous analysis. We observed that single variant isogenic iPSC-CMs had similar contraction kinetics, while the double variant carrier MYB1#4-CMs displayed faster contraction time. We conclude that the *MYH7* I1927F variant contributes to a severe contractile phenotype in iPSC-CMs when present in combination with the *MYBPC3* K600Nfs*2 variant, as observed in our familial case of HCM.

In summary, we demonstrated the robustness of the iPSC disease-modelling platform when combined with clinical data and CRISPR/Cas9 genome editing technology to functionally explore the effect of genetic modifiers of unknown significance. Although important limitations in our study include the use of iPSC-CMs, which do not resemble fully mature adult cardiomyocytes, and it relies on cost-expensive and slow methodologies, the work presented here will help to elucidate VUS risk assessment and improve the diagnosis and prognosis of HCM patients.

6 CONCLUSIONS

- Within a large familial case of HCM, the clinical manifestation between two siblings carrying the same heterozygous *MYBPC3* K600Nfs*2 pathogenic mutation differ in severity.

- We generated two iPSC lines representing the mutant carriers of the *MYBPC3* K600Nfs*2 mutation.

- Morphological characterization of iPSC-derived cardiomyocytes from the *MYBPC3* K600Nfs*2 mutant carriers do not show structural alterations at the sarcomere level but show reduced traction force as compared to the control line.

- We generated isogenic clones differing in the presence of *MYBPC3* K600Nfs*2 mutation by gene edition of two mutant lines.

- MYB1#4 cardiomyocytes present faster calcium transients and contraction time compared to those derived from MYB2#2. Alternatively, both mutant cardiomyocytes present reduced mitochondrial bioenergetics capacity compared to the control line.

- Correction of the *MYBPC3* K600Nfs*2 mutation alleviates the aforementioned phenotypes in MYB1#4 cardiomyocytes, while the MYB2#2 contractile phenotypes resemble those of the isogenic lines.

- We identified a *MYH7* variant predicted as uncertain significance in the severe HCM mutant carrier.

- Correction of the *MYH7* I1927F variant reverses the faster contractile defects in MYB1#4 cardiomyocytes, confirming its pathogenic role when present in combination with the *MYBPC3* mutation.

7 REFERENCES

Aasen, T., Raya, A., Barrero, M.J., Garreta, E., Consiglio, A., Gonzalez, F., Vassena, R., Bilic, J., Pekarik, V., Tiscornia, G*., et al.* (2008). Efficient and rapid generation of induced pluripotent stem cells from human keratinocytes. Nat Biotechnol *26*, 1276-1284.

Adhikari, A.S., Kooiker, K.B., Sarkar, S.S., Liu, C., Bernstein, D., Spudich, J.A., and Ruppel, K.M. (2016). Early-Onset Hypertrophic Cardiomyopathy Mutations Significantly Increase the Velocity, Force, and Actin-Activated ATPase Activity of Human beta-Cardiac Myosin. Cell Rep *17*, 2857-2864.

Adhikari, A.S., Trivedi, D.V., Sarkar, S.S., Song, D., Kooiker, K.B., Bernstein, D., Spudich, J.A., and Ruppel, K.M. (2019). beta-Cardiac myosin hypertrophic cardiomyopathy mutations release sequestered heads and increase enzymatic activity. Nat Commun *10*, 2685.

Adzhubei, I., Jordan, D.M., and Sunyaev, S.R. (2013). Predicting functional effect of human missense mutations using PolyPhen-2. Curr Protoc Hum Genet *Chapter 7*, Unit7 20.

Adzhubei, I.A., Schmidt, S., Peshkin, L., Ramensky, V.E., Gerasimova, A., Bork, P., Kondrashov, A.S., and Sunyaev, S.R. (2010). A method and server for predicting damaging missense mutations. Nat Methods *7*, 248-249.

Alfares, A.A., Kelly, M.A., McDermott, G., Funke, B.H., Lebo, M.S., Baxter, S.B., Shen, J., McLaughlin, H.M., Clark, E.H., Babb, L.J*., et al.* (2015). Results of clinical genetic testing of 2,912 probands with hypertrophic cardiomyopathy: expanded panels offer limited additional sensitivity. Genet Med *17*, 880-888.

Allen, D.G., and Kurihara, S. (1980). Calcium transients in mammalian ventricular muscle. Eur Heart J *Suppl A*, 5-15.

Alpert, N.R., Mohiddin, S.A., Tripodi, D., Jacobson-Hatzell, J., Vaughn-Whitley, K., Brosseau, C., Warshaw, D.M., and Fananapazir, L. (2005). Molecular and phenotypic effects of heterozygous, homozygous, and compound heterozygote myosin heavy-chain mutations. Am J Physiol Heart Circ Physiol *288*, H1097-1102.

Arbustini, E., Narula, N., Dec, G.W., Reddy, K.S., Greenberg, B., Kushwaha, S., Marwick, T., Pinney, S., Bellazzi, R., Favalli, V*., et al.* (2013). The MOGE(S) Classification for a Phenotype-Genotype Nomenclature of Cardiomyopathy: Endorsed by the World Heart Federation. Glob Heart *8*, 355-382.

Aronsen, J.M., Swift, F., and Sejersted, O.M. (2013). Cardiac sodium transport and excitation-contraction coupling. J Mol Cell Cardiol *61*, 11-19.

Ashrafian, H., Redwood, C., Blair, E., and Watkins, H. (2003). Hypertrophic cardiomyopathy:a paradigm for myocardial energy depletion. Trends Genet *19*, 263-268.

Atemin, S., Todorov, T., Maver, A., Chamova, T., Georgieva, B., Tincheva, S., Pacheva, I., Ivanov, I., Taneva, A., Zlatareva, D*., et al.* (2021). MYH7-related disorders in two Bulgarian families: Novel variants in the same region associated with different clinical manifestation and disease penetrance. Neuromuscul Disord *31*, 633-641.

Authors/Task Force, m., Elliott, P.M., Anastasakis, A., Borger, M.A., Borggrefe, M., Cecchi, F., Charron, P., Hagege, A.A., Lafont, A., Limongelli, G.*, et al.* (2014). 2014 ESC Guidelines on diagnosis and management of hypertrophic cardiomyopathy: the Task Force for the Diagnosis and Management of Hypertrophic Cardiomyopathy of the European Society of Cardiology (ESC). Eur Heart J *35*, 2733-2779.

Baker, D.E., Harrison, N.J., Maltby, E., Smith, K., Moore, H.D., Shaw, P.J., Heath, P.R., Holden, H., and Andrews, P.W. (2007). Adaptation to culture of human embryonic stem cells and oncogenesis in vivo. Nat Biotechnol *25*, 207-215.

Barefield, D., Kumar, M., de Tombe, P.P., and Sadayappan, S. (2014). Contractile dysfunction in a mouse model expressing a heterozygous MYBPC3 mutation associated with hypertrophic cardiomyopathy. Am J Physiol Heart Circ Physiol *306*, H807-815.

Barefield, D., and Sadayappan, S. (2010). Phosphorylation and function of cardiac myosin binding protein-C in health and disease. J Mol Cell Cardiol *48*, 866-875.

Baudenbacher, F., Schober, T., Pinto, J.R., Sidorov, V.Y., Hilliard, F., Solaro, R.J., Potter, J.D., and Knollmann, B.C. (2008). Myofilament Ca2+ sensitization causes susceptibility to cardiac arrhythmia in mice. J Clin Invest *118*, 3893-3903.

Behrens-Gawlik, V., Mearini, G., Gedicke-Hornung, C., Richard, P., and Carrier, L. (2014). MYBPC3 in hypertrophic cardiomyopathy: from mutation identification to RNA-based correction. Pflugers Arch *466*, 215-223.

Bers, D.M. (2002). Cardiac excitation-contraction coupling. Nature *415*, 198-205.

Bers, D.M. (2008). Calcium cycling and signaling in cardiac myocytes. Annu Rev Physiol *70*, 23-49.

Bessman, S.P., and Geiger, P.J. (1981). Transport of energy in muscle: the phosphorylcreatine shuttle. Science *211*, 448-452.

Bhagwan, J.R., Mosqueira, D., Chairez-Cantu, K., Mannhardt, I., Bodbin, S.E., Bakar, M., Smith, J.G.W., and Denning, C. (2020). Isogenic models of hypertrophic cardiomyopathy unveil differential phenotypes and mechanism-driven therapeutics. J Mol Cell Cardiol *145*, 43-53.

Biesiadecki, B.J., Davis, J.P., Ziolo, M.T., and Janssen, P.M.L. (2014). Tri-modal regulation of cardiac muscle relaxation; intracellular calcium decline, thin filament deactivation, and cross-bridge cycling kinetics. Biophys Rev *6*, 273-289.

Birket, M.J., Ribeiro, M.C., Kosmidis, G., Ward, D., Leitoguinho, A.R., van de Pol, V., Dambrot, C., Devalla, H.D., Davis, R.P., Mastroberardino, P.G.*, et al.* (2015). Contractile Defect Caused by Mutation in MYBPC3 Revealed under Conditions Optimized for Human PSC-Cardiomyocyte Function. Cell Rep *13*, 733-745.

Bonne, G., Carrier, L., Bercovici, J., Cruaud, C., Richard, P., Hainque, B., Gautel, M., Labeit, S., James, M., Beckmann, J.*, et al.* (1995). Cardiac myosin binding protein-C gene splice acceptor site mutation is associated with familial hypertrophic cardiomyopathy. Nat Genet *11*, 438-440.

Brand, M.D., and Nicholls, D.G. (2011). Assessing mitochondrial dysfunction in cells. Biochem J *435*, 297-312.

Briasoulis, A., Mallikethi-Reddy, S., Palla, M., Alesh, I., and Afonso, L. (2015). Myocardial fibrosis on cardiac magnetic resonance and cardiac outcomes in hypertrophic cardiomyopathy: a meta-analysis. Heart *101*, 1406-1411.

Burkhardt, M.F., Martinez, F.J., Wright, S., Ramos, C., Volfson, D., Mason, M., Garnes, J., Dang, V., Lievers, J., Shoukat-Mumtaz, U.*, et al.* (2013). A cellular model for sporadic ALS using patient-derived induced pluripotent stem cells. Mol Cell Neurosci *56*, 355-364.

Burridge, P.W., Matsa, E., Shukla, P., Lin, Z.C., Churko, J.M., Ebert, A.D., Lan, F., Diecke, S., Huber, B., Mordwinkin, N.M.*, et al.* (2014). Chemically defined generation of human cardiomyocytes. Nat Methods *11*, 855-860.

Butters, A., Lakdawala, N.K., and Ingles, J. (2021). Sex Differences in Hypertrophic Cardiomyopathy: Interaction With Genetics and Environment. Curr Heart Fail Rep *18*, 264-273.

Cahill, T.J., Ashrafian, H., and Watkins, H. (2013). Genetic cardiomyopathies causing heart failure. Circ Res *113*, 660-675.

Calatayud, C., Carola, G., Fernandez-Carasa, I., Valtorta, M., Jimenez-Delgado, S., Diaz, M., Soriano-Fradera, J., Cappelletti, G., Garcia-Sancho, J., Raya, A.*, et al.* (2019). CRISPR/Cas9-mediated generation of a tyrosine hydroxylase reporter iPSC line for live imaging and isolation of dopaminergic neurons. Sci Rep *9*, 6811.

Campos, P.B., Sartore, R.C., Abdalla, S.N., and Rehen, S.K. (2009). Chromosomal spread preparation of human embryonic stem cells for karyotyping. J Vis Exp.

Cao, F., Zervou, S., and Lygate, C.A. (2018). The creatine kinase system as a therapeutic target for myocardial ischaemia-reperfusion injury. Biochem Soc Trans *46*, 1119-1127.

Carrier, L., Bonne, G., Bahrend, E., Yu, B., Richard, P., Niel, F., Hainque, B., Cruaud, C., Gary, F., Labeit, S.*, et al.* (1997). Organization and sequence of human cardiac myosin binding protein C gene (MYBPC3) and identification of mutations predicted to produce truncated proteins in familial hypertrophic cardiomyopathy. Circ Res *80*, 427-434.

Carvajal-Vergara, X., Sevilla, A., D'Souza, S.L., Ang, Y.S., Schaniel, C., Lee, D.F., Yang, L., Kaplan, A.D., Adler, E.D., Rozov, R.*, et al.* (2010). Patient-specific induced pluripotent stem-cell-derived models of LEOPARD syndrome. Nature *465*, 808-812.

Cazorla, O., Szilagyi, S., Vignier, N., Salazar, G., Kramer, E., Vassort, G., Carrier, L., and Lacampagne, A. (2006). Length and protein kinase A modulations of myocytes in cardiac myosin binding protein C-deficient mice. Cardiovasc Res *69*, 370-380.

Cho, G.S., Lee, D.I., Tampakakis, E., Murphy, S., Andersen, P., Uosaki, H., Chelko, S., Chakir, K., Hong, I., Seo, K.*, et al.* (2017). Neonatal Transplantation Confers Maturation of PSC-Derived Cardiomyocytes Conducive to Modeling Cardiomyopathy. Cell Rep *18*, 571-582.

Chung, S., Arrell, D.K., Faustino, R.S., Terzic, A., and Dzeja, P.P. (2010). Glycolytic network restructuring integral to the energetics of embryonic stem cell cardiac differentiation. J Mol Cell Cardiol *48*, 725-734.

Claes, G.R., van Tienen, F.H., Lindsey, P., Krapels, I.P., Helderman-van den Enden, A.T., Hoos, M.B., Barrois, Y.E., Janssen, J.W., Paulussen, A.D., Sels, J.W.*, et al.* (2016). Hypertrophic remodelling in cardiac regulatory myosin light chain (MYL2) founder mutation carriers. Eur Heart J *37*, 1815-1822.

Cohn, R., Thakar, K., Lowe, A., Ladha, F.A., Pettinato, A.M., Romano, R., Meredith, E., Chen, Y.S., Atamanuk, K., Huey, B.D.*, et al.* (2019). A Contraction Stress Model of Hypertrophic Cardiomyopathy due to Sarcomere Mutations. Stem Cell Reports *12*, 71-83.

Colan, S.D., Lipshultz, S.E., Lowe, A.M., Sleeper, L.A., Messere, J., Cox, G.F., Lurie, P.R., Orav, E.J., and Towbin, J.A. (2007). Epidemiology and cause-specific outcome of hypertrophic cardiomyopathy in children: findings from the Pediatric Cardiomyopathy Registry. Circulation *115*, 773-781.

Colegrave, M., and Peckham, M. (2014). Structural implications of beta-cardiac myosin heavy chain mutations in human disease. Anat Rec (Hoboken) *297*, 1670-1680.

Cong, L., Ran, F.A., Cox, D., Lin, S., Barretto, R., Habib, N., Hsu, P.D., Wu, X., Jiang, W., Marraffini, L.A.*, et al.* (2013). Multiplex genome engineering using CRISPR/Cas systems. Science *339*, 819-823.

Crilley, J.G., Boehm, E.A., Blair, E., Rajagopalan, B., Blamire, A.M., Styles, P., McKenna, W.J., Ostman-Smith, I., Clarke, K., and Watkins, H. (2003). Hypertrophic cardiomyopathy due to sarcomeric gene mutations is characterized by impaired energy metabolism irrespective of the degree of hypertrophy. J Am Coll Cardiol *41*, 1776-1782.

Czepluch, F.S., Wollnik, B., and Hasenfuss, G. (2018). Genetic determinants of heart failure: facts and numbers. ESC Heart Fail *5*, 211-217.

Davis, J., Davis, L.C., Correll, R.N., Makarewich, C.A., Schwanekamp, J.A., Moussavi-Harami, F., Wang, D., York, A.J., Wu, H., Houser, S.R.*, et al.* (2016). A Tension-Based Model Distinguishes Hypertrophic versus Dilated Cardiomyopathy. Cell *165*, 1147-1159.

de Lange, W.J., Hegge, L.F., Grimes, A.C., Tong, C.W., Brost, T.M., Moss, R.L., and Ralphe, J.C. (2011). Neonatal mouse-derived engineered cardiac tissue: a novel model system for studying genetic heart disease. Circ Res *109*, 8-19.

Decker, R.S., Decker, M.L., Kulikovskaya, I., Nakamura, S., Lee, D.C., Harris, K., Klocke, F.J., and Winegrad, S. (2005). Myosin-binding protein C phosphorylation, myofibril structure, and contractile function during low-flow ischemia. Circulation *111*, 906-912.

DeWitt, M.M., MacLeod, H.M., Soliven, B., and McNally, E.M. (2006). Phospholamban R14 deletion results in late-onset, mild, hereditary dilated cardiomyopathy. J Am Coll Cardiol *48*, 1396-1398.

di Domenico, A., Carola, G., Calatayud, C., Pons-Espinal, M., Munoz, J.P., Richaud-Patin, Y., Fernandez-Carasa, I., Gut, M., Faella, A., Parameswaran, J.*, et al.* (2019). Patient-Specific iPSC-Derived Astrocytes Contribute to Non-Cell-Autonomous Neurodegeneration in Parkinson's Disease. Stem Cell Reports *12*, 213-229.

Doudna, J.A., and Charpentier, E. (2014). Genome editing. The new frontier of genome engineering with CRISPR-Cas9. Science *346*, 1258096.

Duran, J., Martinez, A., and Adler, E. (2019). Cardiovascular Manifestations of Mitochondrial Disease. Biology (Basel) *8*.

Eisner, D.A., Caldwell, J.L., Kistamas, K., and Trafford, A.W. (2017). Calcium and Excitation-Contraction Coupling in the Heart. Circ Res *121*, 181-195.

Elitt, M.S., Barbar, L., and Tesar, P.J. (2018). Drug screening for human genetic diseases using iPSC models. Hum Mol Genet *27*, R89-R98.

Elliott, P., Andersson, B., Arbustini, E., Bilinska, Z., Cecchi, F., Charron, P., Dubourg, O., Kuhl, U., Maisch, B., McKenna, W.J.*, et al.* (2008). Classification of the cardiomyopathies: a position statement from the European Society Of Cardiology Working Group on Myocardial and Pericardial Diseases. Eur Heart J *29*, 270-276.

Eschenhagen, T., and Carrier, L. (2019). Cardiomyopathy phenotypes in human-induced pluripotent stem cell-derived cardiomyocytes-a systematic review. Pflugers Arch *471*, 755-768.

Fan, H., He, Z., Huang, H., Zhuang, H., Liu, H., Liu, X., Yang, S., He, P., Yang, H., and Feng, D. (2020). Mitochondrial Quality Control in Cardiomyocytes: A Critical Role in the Progression of Cardiovascular Diseases. Front Physiol *11*, 252.

Ferrick, D.A., Neilson, A., and Beeson, C. (2008). Advances in measuring cellular bioenergetics using extracellular flux. Drug Discov Today *13*, 268-274.

Flenner, F., Jungen, C., Kupker, N., Ibel, A., Kruse, M., Koivumaki, J.T., Rinas, A., Zech, A.T.L., Rhoden, A., Wijnker, P.J.M.*, et al.* (2021). Translational investigation of electrophysiology in hypertrophic cardiomyopathy. J Mol Cell Cardiol *157*, 77-89.

Fokstuen, S., Lyle, R., Munoz, A., Gehrig, C., Lerch, R., Perrot, A., Osterziel, K.J., Geier, C., Beghetti, M., Mach, F.*, et al.* (2008). A DNA resequencing array for pathogenic mutation detection in hypertrophic cardiomyopathy. Hum Mutat *29*, 879-885.

Frank-Hansen, R., Page, S.P., Syrris, P., McKenna, W.J., Christiansen, M., and Andersen, P.S. (2008). Micro-exons of the cardiac myosin binding protein C gene: flanking introns contain a disproportionately large number of hypertrophic cardiomyopathy mutations. Eur J Hum Genet *16*, 1062-1069.

Fraysse, B., Weinberger, F., Bardswell, S.C., Cuello, F., Vignier, N., Geertz, B., Starbatty, J., Kramer, E., Coirault, C., Eschenhagen, T.*, et al.* (2012). Increased myofilament Ca2+ sensitivity and diastolic dysfunction as early consequences of Mybpc3 mutation in heterozygous knock-in mice. J Mol Cell Cardiol *52*, 1299-1307.

Frey, N., Luedde, M., and Katus, H.A. (2011). Mechanisms of disease: hypertrophic cardiomyopathy. Nat Rev Cardiol *9*, 91-100.

Geeves, M.A. (2016). Review: The ATPase mechanism of myosin and actomyosin. Biopolymers *105*, 483-491.

Geier, C., Gehmlich, K., Ehler, E., Hassfeld, S., Perrot, A., Hayess, K., Cardim, N., Wenzel, K., Erdmann, B., Krackhardt, F.*, et al.* (2008). Beyond the sarcomere: CSRP3 mutations cause hypertrophic cardiomyopathy. Hum Mol Genet *17*, 2753-2765.

Geisterfer-Lowrance, A.A., Christe, M., Conner, D.A., Ingwall, J.S., Schoen, F.J., Seidman, C.E., and Seidman, J.G. (1996). A mouse model of familial hypertrophic cardiomyopathy. Science *272*, 731-734.

Geisterfer-Lowrance, A.A., Kass, S., Tanigawa, G., Vosberg, H.P., McKenna, W., Seidman, C.E., and Seidman, J.G. (1990). A molecular basis for familial hypertrophic cardiomyopathy: a beta cardiac myosin heavy chain gene missense mutation. Cell *62*, 999-1006.

Giacomelli, E., Bellin, M., Sala, L., van Meer, B.J., Tertoolen, L.G., Orlova, V.V., and Mummery, C.L. (2017). Three-dimensional cardiac microtissues composed of cardiomyocytes and endothelial cells co-differentiated from human pluripotent stem cells. Development *144*, 1008-1017.

Gifford, C.A., Ranade, S.S., Samarakoon, R., Salunga, H.T., de Soysa, T.Y., Huang, Y., Zhou, P., Elfenbein, A., Wyman, S.K., Bui, Y.K.*, et al.* (2019). Oligogenic inheritance of a human heart disease involving a genetic modifier. Science *364*, 865-870.

Ginsburg, K.S., and Bers, D.M. (2004). Modulation of excitation-contraction coupling by isoproterenol in cardiomyocytes with controlled SR Ca2+ load and Ca2+ current trigger. J Physiol *556*, 463-480.

Giorgetti, A., Montserrat, N., Aasen, T., Gonzalez, F., Rodriguez-Piza, I., Vassena, R., Raya, A., Boue, S., Barrero, M.J., Corbella, B.A.*, et al.* (2009). Generation of induced pluripotent stem cells from human cord blood using OCT4 and SOX2. Cell Stem Cell *5*, 353-357.

Girolami, F., Ho, C.Y., Semsarian, C., Baldi, M., Will, M.L., Baldini, K., Torricelli, F., Yeates, L., Cecchi, F., Ackerman, M.J.*, et al.* (2010). Clinical features and outcome of hypertrophic cardiomyopathy associated with triple sarcomere protein gene mutations. J Am Coll Cardiol *55*, 1444-1453.

Gordon, A.M., Homsher, E., and Regnier, M. (2000). Regulation of contraction in striated muscle. Physiol Rev *80*, 853-924.

Guenther, M.G., Frampton, G.M., Soldner, F., Hockemeyer, D., Mitalipova, M., Jaenisch, R., and Young, R.A. (2010). Chromatin structure and gene expression programs of human embryonic and induced pluripotent stem cells. Cell Stem Cell *7*, 249-257.

Gupta, M.P. (2007). Factors controlling cardiac myosin-isoform shift during hypertrophy and heart failure. J Mol Cell Cardiol *43*, 388-403.

Gyorke, I., Hester, N., Jones, L.R., and Gyorke, S. (2004). The role of calsequestrin, triadin, and junctin in conferring cardiac ryanodine receptor responsiveness to luminal calcium. Biophys J *86*, 2121-2128.

Hamman, B.L., Bittl, J.A., Jacobus, W.E., Allen, P.D., Spencer, R.S., Tian, R., and Ingwall, J.S. (1995). Inhibition of the creatine kinase reaction decreases the contractile reserve of isolated rat hearts. Am J Physiol *269*, H1030-1036.

Harris, S.P., Bartley, C.R., Hacker, T.A., McDonald, K.S., Douglas, P.S., Greaser, M.L., Powers, P.A., and Moss, R.L. (2002). Hypertrophic cardiomyopathy in cardiac myosin binding protein-C knockout mice. Circ Res *90*, 594-601.

Hayashi, T., Arimura, T., Itoh-Satoh, M., Ueda, K., Hohda, S., Inagaki, N., Takahashi, M., Hori, H., Yasunami, M., Nishi, H.*, et al.* (2004). Tcap gene mutations in hypertrophic cardiomyopathy and dilated cardiomyopathy. J Am Coll Cardiol *44*, 2192-2201.

He, H., Javadpour, M.M., Latif, F., Tardiff, J.C., and Ingwall, J.S. (2007). R-92L and R-92W mutations in cardiac troponin T lead to distinct energetic phenotypes in intact mouse hearts. Biophys J *93*, 1834-1844.

Heggermont, W.A., Papageorgiou, A.P., Heymans, S., and van Bilsen, M. (2016). Metabolic support for the heart: complementary therapy for heart failure? Eur J Heart Fail *18*, 1420-1429.

Helms, A.S., Tang, V.T., O'Leary, T.S., Friedline, S., Wauchope, M., Arora, A., Wasserman, A.H., Smith, E.D., Lee, L.M., Wen, X.W.*, et al.* (2020a). Effects of MYBPC3 loss-of-function mutations preceding hypertrophic cardiomyopathy. JCI Insight *5*.

Helms, A.S., Thompson, A.D., Glazier, A.A., Hafeez, N., Kabani, S., Rodriguez, J., Yob, J.M., Woolcock, H., Mazzarotto, F., Lakdawala, N.K.*, et al.* (2020b). Spatial and Functional Distribution of MYBPC3 Pathogenic Variants and Clinical Outcomes in Patients With Hypertrophic Cardiomyopathy. Circ Genom Precis Med *13*, 396-405.

Henderson, C.A., Gomez, C.G., Novak, S.M., Mi-Mi, L., and Gregorio, C.C. (2017). Overview of the Muscle Cytoskeleton. Compr Physiol *7*, 891-944.

Herman, D.S., Lam, L., Taylor, M.R., Wang, L., Teekakirikul, P., Christodoulou, D., Conner, L., DePalma, S.R., McDonough, B., Sparks, E.*, et al.* (2012). Truncations of titin causing dilated cardiomyopathy. N Engl J Med *366*, 619-628.

Hirano, M., Davidson, M., and DiMauro, S. (2001). Mitochondria and the heart. Curr Opin Cardiol *16*, 201-210.

Ho, C.Y., Charron, P., Richard, P., Girolami, F., Van Spaendonck-Zwarts, K.Y., and Pinto, Y. (2015). Genetic advances in sarcomeric cardiomyopathies: state of the art. Cardiovasc Res *105*, 397-408.

Ho, C.Y., Day, S.M., Ashley, E.A., Michels, M., Pereira, A.C., Jacoby, D., Cirino, A.L., Fox, J.C., Lakdawala, N.K., Ware, J.S.*, et al.* (2018). Genotype and Lifetime Burden of Disease in Hypertrophic Cardiomyopathy: Insights from the Sarcomeric Human Cardiomyopathy Registry (SHaRe). Circulation *138*, 1387-1398.

Ho, C.Y., Sweitzer, N.K., McDonough, B., Maron, B.J., Casey, S.A., Seidman, J.G., Seidman, C.E., and Solomon, S.D. (2002). Assessment of diastolic function with Doppler tissue imaging to predict genotype in preclinical hypertrophic cardiomyopathy. Circulation *105*, 2992-2997.

Hockemeyer, D., Wang, H., Kiani, S., Lai, C.S., Gao, Q., Cassady, J.P., Cost, G.J., Zhang, L., Santiago, Y., Miller, J.C*., et al.* (2011). Genetic engineering of human pluripotent cells using TALE nucleases. Nat Biotechnol *29*, 731-734.

Holmgren, D., Wahlander, H., Eriksson, B.O., Oldfors, A., Holme, E., and Tulinius, M. (2003). Cardiomyopathy in children with mitochondrial disease; clinical course and cardiological findings. Eur Heart J *24*, 280-288.

Homburger, J.R., Green, E.M., Caleshu, C., Sunitha, M.S., Taylor, R.E., Ruppel, K.M., Metpally, R.P., Colan, S.D., Michels, M., Day, S.M*., et al.* (2016). Multidimensional structure-function relationships in human beta-cardiac myosin from population-scale genetic variation. Proc Natl Acad Sci U S A *113*, 6701-6706.

Hooijman, P., Stewart, M.A., and Cooke, R. (2011). A new state of cardiac myosin with very slow ATP turnover: a potential cardioprotective mechanism in the heart. Biophys J *100*, 1969-1976.

Horn, M., Remkes, H., Stromer, H., Dienesch, C., and Neubauer, S. (2001). Chronic phosphocreatine depletion by the creatine analogue beta-guanidinopropionate is associated with increased mortality and loss of ATP in rats after myocardial infarction. Circulation *104*, 1844-1849.

Hoskins, A.C., Jacques, A., Bardswell, S.C., McKenna, W.J., Tsang, V., dos Remedios, C.G., Ehler, E., Adams, K., Jalilzadeh, S., Avkiran, M*., et al.* (2010). Normal passive viscoelasticity but abnormal myofibrillar force generation in human hypertrophic cardiomyopathy. J Mol Cell Cardiol *49*, 737-745.

Houdusse, A., and Sweeney, H.L. (2016). How Myosin Generates Force on Actin Filaments. Trends Biochem Sci *41*, 989-997.

Hu, B.Y., Weick, J.P., Yu, J., Ma, L.X., Zhang, X.Q., Thomson, J.A., and Zhang, S.C. (2010). Neural differentiation of human induced pluripotent stem cells follows developmental principles but with variable potency. Proc Natl Acad Sci U S A *107*, 4335-4340.

Huxley, H.E. (1957). The double array of filaments in cross-striated muscle. J Biophys Biochem Cytol *3*, 631-648.

Iglesias-Garcia, O., Baumgartner, S., Macri-Pellizzeri, L., Rodriguez-Madoz, J.R., Abizanda, G., Guruceaga, E., Albiasu, E., Corbacho, D., Benavides-Vallve, C., Soriano-Navarro, M*., et al.* (2015). Neuregulin-1beta induces mature ventricular cardiac differentiation from induced pluripotent stem cells contributing to cardiac tissue repair. Stem Cells Dev *24*, 484-496.

Ingles, J., Doolan, A., Chiu, C., Seidman, J., Seidman, C., and Semsarian, C. (2005). Compound and double mutations in patients with hypertrophic cardiomyopathy: implications for genetic testing and counselling. J Med Genet *42*, e59.

Ingles, J., Goldstein, J., Thaxton, C., Caleshu, C., Corty, E.W., Crowley, S.B., Dougherty, K., Harrison, S.M., McGlaughon, J., Milko, L.V*., et al.* (2019). Evaluating the Clinical Validity of Hypertrophic Cardiomyopathy Genes. Circ Genom Precis Med *12*, e002460.

Ingles, J., McGaughran, J., Scuffham, P.A., Atherton, J., and Semsarian, C. (2012). A cost-effectiveness model of genetic testing for the evaluation of families with hypertrophic cardiomyopathy. Heart *98*, 625-630.

Ingwall, J.S. (2014). The energetic cost of contraction is higher in the myocardium of patients with hypertrophic cardiomyopathy. Cardiovasc Res *103*, 192-193.

Itzhaki, I., Maizels, L., Huber, I., Zwi-Dantsis, L., Caspi, O., Winterstern, A., Feldman, O., Gepstein, A., Arbel, G., Hammerman, H.*, et al.* (2011). Modelling the long QT syndrome with induced pluripotent stem cells. Nature *471*, 225-229.

Jaafar, N., Gomez, J., Kammoun, I., Zairi, I., Amara, W.B., Kachboura, S., Kraiem, S., Hammami, M., Iglesias, S., Alonso, B.*, et al.* (2016). Spectrum of Mutations in Hypertrophic Cardiomyopathy Genes Among Tunisian Patients. Genet Test Mol Biomarkers *20*, 674-679.

Jacques, A.M., Copeland, O., Messer, A.E., Gallon, C.E., King, K., McKenna, W.J., Tsang, V.T., and Marston, S.B. (2008). Myosin binding protein C phosphorylation in normal, hypertrophic and failing human heart muscle. J Mol Cell Cardiol *45*, 209-216.

Jensen, M.K., and Bundgaard, H. (2012). Cardiomyopathy in Friedreich ataxia: exemplifying the challenges faced by cardiologists in the management of rare diseases. Circulation *125*, 1591-1593.

Jiang, Y., Park, P., Hong, S.M., and Ban, K. (2018). Maturation of Cardiomyocytes Derived from Human Pluripotent Stem Cells: Current Strategies and Limitations. Mol Cells *41*, 613-621.

Jinek, M., Chylinski, K., Fonfara, I., Hauer, M., Doudna, J.A., and Charpentier, E. (2012). A programmable dual-RNA-guided DNA endonuclease in adaptive bacterial immunity. Science *337*, 816-821.

Jung, W.I., Sieverding, L., Breuer, J., Hoess, T., Widmaier, S., Schmidt, O., Bunse, M., van Erckelens, F., Apitz, J., Lutz, O.*, et al.* (1998). 31P NMR spectroscopy detects metabolic abnormalities in asymptomatic patients with hypertrophic cardiomyopathy. Circulation *97*, 2536-2542.

Kajiwara, M., Aoi, T., Okita, K., Takahashi, R., Inoue, H., Takayama, N., Endo, H., Eto, K., Toguchida, J., Uemoto, S.*, et al.* (2012). Donor-dependent variations in hepatic differentiation from human-induced pluripotent stem cells. Proc Natl Acad Sci U S A *109*, 12538-12543.

Kamakura, T., Makiyama, T., Sasaki, K., Yoshida, Y., Wuriyanghai, Y., Chen, J., Hattori, T., Ohno, S., Kita, T., Horie, M.*, et al.* (2013). Ultrastructural maturation of human-induced pluripotent stem cell-derived cardiomyocytes in a long-term culture. Circ J *77*, 1307-1314.

Kang, T.M., and Hilgemann, D.W. (2004). Multiple transport modes of the cardiac Na+/Ca2+ exchanger. Nature *427*, 544-548.

Kawana, M., Sarkar, S.S., Sutton, S., Ruppel, K.M., and Spudich, J.A. (2017). Biophysical properties of human beta-cardiac myosin with converter mutations that cause hypertrophic cardiomyopathy. Sci Adv *3*, e1601959.

Kehat, I., Kenyagin-Karsenti, D., Snir, M., Segev, H., Amit, M., Gepstein, A., Livne, E., Binah, O., Itskovitz-Eldor, J., and Gepstein, L. (2001). Human embryonic stem cells can differentiate into myocytes with structural and functional properties of cardiomyocytes. J Clin Invest *108*, 407-414.

Khan, M., Xu, Y., Hua, S., Johnson, J., Belevych, A., Janssen, P.M., Gyorke, S., Guan, J., and Angelos, M.G. (2015). Evaluation of Changes in Morphology and Function of Human Induced Pluripotent Stem Cell Derived Cardiomyocytes (HiPSC-CMs) Cultured on an Aligned-Nanofiber Cardiac Patch. PLoS One *10*, e0126338.

Kiani, F.A., and Fischer, S. (2016). ATP-dependent interplay between local and global conformational changes in the myosin motor. Cytoskeleton (Hoboken) *73*, 643-651.

Kilpinen, H., Goncalves, A., Leha, A., Afzal, V., Alasoo, K., Ashford, S., Bala, S., Bensaddek, D., Casale, F.P., Culley, O.J.*, et al.* (2017). Common genetic variation drives molecular heterogeneity in human iPSCs. Nature *546*, 370-375.

Kimura, A., Harada, H., Park, J.E., Nishi, H., Satoh, M., Takahashi, M., Hiroi, S., Sasaoka, T., Ohbuchi, N., Nakamura, T.*, et al.* (1997). Mutations in the cardiac troponin I gene associated with hypertrophic cardiomyopathy. Nat Genet *16*, 379-382.

Kletzl, H., Marquet, A., Gunther, A., Tang, W., Heuberger, J., Groeneveld, G.J., Birkhoff, W., Mercuri, E., Lochmuller, H., Wood, C.*, et al.* (2019). The oral splicing modifier RG7800 increases full length survival of motor neuron 2 mRNA and survival of motor neuron protein: Results from trials in healthy adults and patients with spinal muscular atrophy. Neuromuscul Disord *29*, 21-29.

Kraft, T., and Montag, J. (2019). Altered force generation and cell-to-cell contractile imbalance in hypertrophic cardiomyopathy. Pflugers Arch *471*, 719-733.

Kranias, E.G., and Hajjar, R.J. (2012). Modulation of cardiac contractility by the phospholamban/SERCA2a regulatome. Circ Res *110*, 1646-1660.

Kulikovskaya, I., McClellan, G., Flavigny, J., Carrier, L., and Winegrad, S. (2003). Effect of MyBP-C binding to actin on contractility in heart muscle. J Gen Physiol *122*, 761-774.

Laco, F., Woo, T.L., Zhong, Q., Szmyd, R., Ting, S., Khan, F.J., Chai, C.L.L., Reuveny, S., Chen, A., and Oh, S. (2018). Unraveling the Inconsistencies of Cardiac Differentiation Efficiency Induced by the GSK3beta Inhibitor CHIR99021 in Human Pluripotent Stem Cells. Stem Cell Reports *10*, 1851-1866.

Lakdawala, N.K., Olivotto, I., Day, S.M., Han, L., Ashley, E.A., Michels, M., Ingles, J., Semsarian, C., Jacoby, D., Jefferies, J.L.*, et al.* (2021). Associations Between Female Sex, Sarcomere Variants, and Clinical Outcomes in Hypertrophic Cardiomyopathy. Circ Genom Precis Med *14*, e003062.

Lamont, P.J., Wallefeld, W., Hilton-Jones, D., Udd, B., Argov, Z., Barboi, A.C., Bonneman, C., Boycott, K.M., Bushby, K., Connolly, A.M.*, et al.* (2014). Novel mutations widen the phenotypic spectrum of slow skeletal/beta-cardiac myosin (MYH7) distal myopathy. Hum Mutat *35*, 868-879.

Landstrom, A.P., and Ackerman, M.J. (2012). Beyond the cardiac myofilament: hypertrophic cardiomyopathy- associated mutations in genes that encode calcium-handling proteins. Curr Mol Med *12*, 507-518.

Lee, G., Ramirez, C.N., Kim, H., Zeltner, N., Liu, B., Radu, C., Bhinder, B., Kim, Y.J., Choi, I.Y., Mukherjee-Clavin, B.*, et al.* (2012). Large-scale screening using familial dysautonomia induced pluripotent stem cells identifies compounds that rescue IKBKAP expression. Nat Biotechnol *30*, 1244-1248.

Lee, G., and Studer, L. (2010). Induced pluripotent stem cell technology for the study of human disease. Nat Methods *7*, 25-27.

Lehman, W. (2016). Thin Filament Structure and the Steric Blocking Model. Compr Physiol *6*, 1043-1069.

Lehman, W., Craig, R., and Vibert, P. (1994). Ca(2+)-induced tropomyosin movement in Limulus thin filaments revealed by three-dimensional reconstruction. Nature *368*, 65-67.

Lek, M., Karczewski, K.J., Minikel, E.V., Samocha, K.E., Banks, E., Fennell, T., O'Donnell-Luria, A.H., Ware, J.S., Hill, A.J., Cummings, B.B.*, et al.* (2016). Analysis of protein-coding genetic variation in 60,706 humans. Nature *536*, 285-291.

Li, S., Pan, H., Tan, C., Sun, Y., Song, Y., Zhang, X., Yang, W., Wang, X., Li, D., Dai, Y.*, et al.* (2018). Mitochondrial Dysfunctions Contribute to Hypertrophic Cardiomyopathy in Patient iPSC-Derived Cardiomyocytes with MT-RNR2 Mutation. Stem Cell Reports *10*, 808-821.

Lian, X., Hsiao, C., Wilson, G., Zhu, K., Hazeltine, L.B., Azarin, S.M., Raval, K.K., Zhang, J., Kamp, T.J., and Palecek, S.P. (2012). Robust cardiomyocyte differentiation from human pluripotent stem cells via temporal modulation of canonical Wnt signaling. Proc Natl Acad Sci U S A *109*, E1848-1857.

Lian, X., Zhang, J., Azarin, S.M., Zhu, K., Hazeltine, L.B., Bao, X., Hsiao, C., Kamp, T.J., and Palecek, S.P. (2013). Directed cardiomyocyte differentiation from human pluripotent stem cells by modulating Wnt/beta-catenin signaling under fully defined conditions. Nat Protoc *8*, 162-175.

Limongelli, G., Masarone, D., and Pacileo, G. (2017). Mitochondrial disease and the heart. Heart *103*, 390-398.

Lin, B.L., Song, T., and Sadayappan, S. (2017). Myofilaments: Movers and Rulers of the Sarcomere. Compr Physiol *7*, 675-692.

Linke, W.A. (2018). Titin Gene and Protein Functions in Passive and Active Muscle. Annu Rev Physiol *80*, 389-411.

Lionetti, V., Stanley, W.C., and Recchia, F.A. (2011). Modulating fatty acid oxidation in heart failure. Cardiovasc Res *90*, 202-209.

Liu, W., Sun, D., and Yang, J. (2017). Diastolic Dysfunction of Hypertrophic Cardiomyopathy Genotype-Positive Subjects Without Hypertrophy Is Detected by Tissue Doppler Imaging: A Systematic Review and Meta-analysis. J Ultrasound Med *36*, 2093-2103.

Lopaschuk, G.D., and Jaswal, J.S. (2010). Energy metabolic phenotype of the cardiomyocyte during development, differentiation, and postnatal maturation. J Cardiovasc Pharmacol *56*, 130-140.

Lopes, L.R., Brito, D., Belo, A., Cardim, N., and Portuguese Registry of Hypertrophic, C. (2019). Genetic characterization and genotype-phenotype associations in a large cohort of patients with hypertrophic cardiomyopathy - An ancillary study of the Portuguese registry of hypertrophic cardiomyopathy. Int J Cardiol *278*, 173-179.

Lopes, L.R., and Elliott, P.M. (2013). New approaches to the clinical diagnosis of inherited heart muscle disease. Heart *99*, 1451-1461.

Lundy, S.D., Zhu, W.Z., Regnier, M., and Laflamme, M.A. (2013). Structural and functional maturation of cardiomyocytes derived from human pluripotent stem cells. Stem Cells Dev *22*, 1991-2002.

Luther, P.K., Bennett, P.M., Knupp, C., Craig, R., Padron, R., Harris, S.P., Patel, J., and Moss, R.L. (2008). Understanding the organisation and role of myosin binding protein C in normal striated muscle by comparison with MyBP-C knockout cardiac muscle. J Mol Biol *384*, 60-72.

Ma, N., Zhang, J.Z., Itzhaki, I., Zhang, S.L., Chen, H., Haddad, F., Kitani, T., Wilson, K.D., Tian, L., Shrestha, R*., et al.* (2018a). Determining the Pathogenicity of a Genomic Variant of Uncertain Significance Using CRISPR/Cas9 and Human-Induced Pluripotent Stem Cells. Circulation *138*, 2666-2681.

Ma, Z., Huebsch, N., Koo, S., Mandegar, M.A., Siemons, B., Boggess, S., Conklin, B.R., Grigoropoulos, C.P., and Healy, K.E. (2018b). Contractile deficits in engineered cardiac microtissues as a result of MYBPC3 deficiency and mechanical overload. Nat Biomed Eng *2*, 955-967.

Mademont-Soler, I., Mates, J., Yotti, R., Espinosa, M.A., Perez-Serra, A., Fernandez-Avila, A.I., Coll, M., Mendez, I., Iglesias, A., Del Olmo, B*., et al.* (2017). Additional value of screening for minor genes and copy number variants in hypertrophic cardiomyopathy. PLoS One *12*, e0181465.

Mali, P., Yang, L., Esvelt, K.M., Aach, J., Guell, M., DiCarlo, J.E., Norville, J.E., and Church, G.M. (2013). RNA-guided human genome engineering via Cas9. Science *339*, 823-826.

Malinchik, S., Xu, S., and Yu, L.C. (1997). Temperature-induced structural changes in the myosin thick filament of skinned rabbit psoas muscle. Biophys J *73*, 2304-2312.

Manrai, A.K., Funke, B.H., Rehm, H.L., Olesen, M.S., Maron, B.A., Szolovits, P., Margulies, D.M., Loscalzo, J., and Kohane, I.S. (2016). Genetic Misdiagnoses and the Potential for Health Disparities. N Engl J Med *375*, 655-665.

Marian, A.J., and Braunwald, E. (2017). Hypertrophic Cardiomyopathy: Genetics, Pathogenesis, Clinical Manifestations, Diagnosis, and Therapy. Circ Res *121*, 749-770.

Maron, B.J. (2018). Clinical Course and Management of Hypertrophic Cardiomyopathy. N Engl J Med *379*, 655-668.

Maron, B.J., Gardin, J.M., Flack, J.M., Gidding, S.S., Kurosaki, T.T., and Bild, D.E. (1995). Prevalence of hypertrophic cardiomyopathy in a general population of young adults. Echocardiographic analysis of 4111 subjects in the CARDIA Study. Coronary Artery Risk Development in (Young) Adults. Circulation *92*, 785-789.

Maron, B.J., Maron, M.S., and Semsarian, C. (2012). Genetics of hypertrophic cardiomyopathy after 20 years: clinical perspectives. J Am Coll Cardiol *60*, 705-715.

Maron, M.S., Olivotto, I., Zenovich, A.G., Link, M.S., Pandian, N.G., Kuvin, J.T., Nistri, S., Cecchi, F., Udelson, J.E., and Maron, B.J. (2006). Hypertrophic cardiomyopathy is predominantly a disease of left ventricular outflow tract obstruction. Circulation *114*, 2232-2239.

Marston, S., Copeland, O., Jacques, A., Livesey, K., Tsang, V., McKenna, W.J., Jalilzadeh, S., Carballo, S., Redwood, C., and Watkins, H. (2009). Evidence from human myectomy samples that MYBPC3 mutations cause hypertrophic cardiomyopathy through haploinsufficiency. Circ Res *105*, 219-222.

Mazzarotto, F., Olivotto, I., Boschi, B., Girolami, F., Poggesi, C., Barton, P.J.R., and Walsh, R. (2020). Contemporary Insights Into the Genetics of Hypertrophic Cardiomyopathy: Toward a New Era in Clinical Testing? J Am Heart Assoc *9*, e015473.

McGonigle, P., and Ruggeri, B. (2014). Animal models of human disease: challenges in enabling translation. Biochem Pharmacol *87*, 162-171.

McNally, E.M., Barefield, D.Y., and Puckelwartz, M.J. (2015). The genetic landscape of cardiomyopathy and its role in heart failure. Cell Metab *21*, 174-182.

McNamara, J.W., Li, A., Smith, N.J., Lal, S., Graham, R.M., Kooiker, K.B., van Dijk, S.J., Remedios, C.G.D., Harris, S.P., and Cooke, R. (2016). Ablation of cardiac myosin binding protein-C disrupts the super-relaxed state of myosin in murine cardiomyocytes. J Mol Cell Cardiol *94*, 65-71.

McNamara, J.W., Singh, R.R., and Sadayappan, S. (2019). Cardiac myosin binding protein-C phosphorylation regulates the super-relaxed state of myosin. Proc Natl Acad Sci U S A *116*, 11731-11736.

Mesirca, P., Torrente, A.G., and Mangoni, M.E. (2015). Functional role of voltage gated Ca(2+) channels in heart automaticity. Front Physiol *6*, 19.

Michele, D.E., Albayya, F.P., and Metzger, J.M. (1999). Direct, convergent hypersensitivity of calcium-activated force generation produced by hypertrophic cardiomyopathy mutant alpha-tropomyosins in adult cardiac myocytes. Nat Med *5*, 1413-1417.

Michels, M., Soliman, O.I., Kofflard, M.J., Hoedemaekers, Y.M., Dooijes, D., Majoor-Krakauer, D., and ten Cate, F.J. (2009). Diastolic abnormalities as the first feature of hypertrophic cardiomyopathy in Dutch myosin-binding protein C founder mutations. JACC Cardiovasc Imaging *2*, 58-64.

Milani-Nejad, N., and Janssen, P.M. (2014). Small and large animal models in cardiac contraction research: advantages and disadvantages. Pharmacol Ther *141*, 235-249.

Mogensen, J., Kubo, T., Duque, M., Uribe, W., Shaw, A., Murphy, R., Gimeno, J.R., Elliott, P., and McKenna, W.J. (2003). Idiopathic restrictive cardiomyopathy is part of the clinical expression of cardiac troponin I mutations. J Clin Invest *111*, 925-925.

Moore, J.R., Leinwand, L., and Warshaw, D.M. (2012). Understanding cardiomyopathy phenotypes based on the functional impact of mutations in the myosin motor. Circ Res *111*, 375-385.

Moretti, A., Bellin, M., Welling, A., Jung, C.B., Lam, J.T., Bott-Flugel, L., Dorn, T., Goedel, A., Hohnke, C., Hofmann, F.*, et al.* (2010). Patient-specific induced pluripotent stem-cell models for long-QT syndrome. N Engl J Med *363*, 1397-1409.

Mortality, G.B.D., and Causes of Death, C. (2015). Global, regional, and national age-sex specific all-cause and cause-specific mortality for 240 causes of death, 1990-2013: a systematic analysis for the Global Burden of Disease Study 2013. Lancet *385*, 117-171.

Mosqueira, D., Mannhardt, I., Bhagwan, J.R., Lis-Slimak, K., Katili, P., Scott, E., Hassan, M., Prondzynski, M., Harmer, S.C., Tinker, A.*, et al.* (2018). CRISPR/Cas9 editing in human pluripotent stem cell-cardiomyocytes highlights arrhythmias, hypocontractility, and energy depletion as potential therapeutic targets for hypertrophic cardiomyopathy. Eur Heart J *39*, 3879-3892.

Moss, R.L., Fitzsimons, D.P., and Ralphe, J.C. (2015). Cardiac MyBP-C regulates the rate and force of contraction in mammalian myocardium. Circ Res *116*, 183-192.

Mullard, A. (2015). Stem-cell discovery platforms yield first clinical candidates. Nat Rev Drug Discov *14*, 589-591.

Murphy, R.T., Mogensen, J., Shaw, A., Kubo, T., Hughes, S., and McKenna, W.J. (2004). Novel mutation in cardiac troponin I in recessive idiopathic dilated cardiomyopathy. Lancet *363*, 371-372.

Nag, S., Sommese, R.F., Ujfalusi, Z., Combs, A., Langer, S., Sutton, S., Leinwand, L.A., Geeves, M.A., Ruppel, K.M., and Spudich, J.A. (2015). Contractility parameters of human beta-cardiac myosin with the hypertrophic cardiomyopathy mutation R403Q show loss of motor function. Sci Adv *1*, e1500511.

Nag, S., and Trivedi, D.V. (2021). To lie or not to lie: Super-relaxing with myosins. Elife *10*.

Nag, S., Trivedi, D.V., Sarkar, S.S., Adhikari, A.S., Sunitha, M.S., Sutton, S., Ruppel, K.M., and Spudich, J.A. (2017). The myosin mesa and the basis of hypercontractility caused by hypertrophic cardiomyopathy mutations. Nat Struct Mol Biol *24*, 525-533.

Naryshkin, N.A., Weetall, M., Dakka, A., Narasimhan, J., Zhao, X., Feng, Z., Ling, K.K., Karp, G.M., Qi, H., Woll, M.G.*, et al.* (2014). Motor neuron disease. SMN2 splicing modifiers improve motor function and longevity in mice with spinal muscular atrophy. Science *345*, 688-693.

Nelson, S.R., Li, A., Beck-Previs, S., Kennedy, G.G., and Warshaw, D.M. (2020). Imaging ATP Consumption in Resting Skeletal Muscle: One Molecule at a Time. Biophys J *119*, 1050-1055.

Neubauer, S. (2007). The failing heart--an engine out of fuel. N Engl J Med *356*, 1140-1151.

O'Leary, T.S., Snyder, J., Sadayappan, S., Day, S.M., and Previs, M.J. (2019). MYBPC3 truncation mutations enhance actomyosin contractile mechanics in human hypertrophic cardiomyopathy. J Mol Cell Cardiol *127*, 165-173.

Oliva-Sandoval, M.J., Ruiz-Espejo, F., Monserrat, L., Hermida-Prieto, M., Sabater, M., Garcia-Molina, E., Ortiz, M., Rodriguez-Garcia, M.I., Nunez, L., Gimeno, J.R.*, et al.* (2010). Insights into genotype-phenotype correlation in hypertrophic cardiomyopathy. Findings from 18 Spanish families with a single mutation in MYBPC3. Heart *96*, 1980-1984.

Omole, A.E., and Fakoya, A.O.J. (2018). Ten years of progress and promise of induced pluripotent stem cells: historical origins, characteristics, mechanisms, limitations, and potential applications. PeerJ *6*, e4370.

Ong, S.B., Subrayan, S., Lim, S.Y., Yellon, D.M., Davidson, S.M., and Hausenloy, D.J. (2010). Inhibiting mitochondrial fission protects the heart against ischemia/reperfusion injury. Circulation *121*, 2012-2022.

Ormerod, J.O., Frenneaux, M.P., and Sherrid, M.V. (2016). Myocardial energy depletion and dynamic systolic dysfunction in hypertrophic cardiomyopathy. Nat Rev Cardiol *13*, 677-687.

Osadchii, O.E. (2007). Cardiac hypertrophy induced by sustained beta-adrenoreceptor activation: pathophysiological aspects. Heart Fail Rev *12*, 66-86.

Page, S.P., Kounas, S., Syrris, P., Christiansen, M., Frank-Hansen, R., Andersen, P.S., Elliott, P.M., and McKenna, W.J. (2012). Cardiac myosin binding protein-C mutations in families with hypertrophic cardiomyopathy: disease expression in relation to age, gender, and long term outcome. Circ Cardiovasc Genet *5*, 156-166.

Pandit, B., Sarkozy, A., Pennacchio, L.A., Carta, C., Oishi, K., Martinelli, S., Pogna, E.A., Schackwitz, W., Ustaszewska, A., Landstrom, A.*, et al.* (2007). Gain-of-function RAF1 mutations cause Noonan and LEOPARD syndromes with hypertrophic cardiomyopathy. Nat Genet *39*, 1007-1012.

Papadimitriou, S., Gazzo, A., Versbraegen, N., Nachtegael, C., Aerts, J., Moreau, Y., Van Dooren, S., Nowe, A., Smits, G., and Lenaerts, T. (2019). Predicting disease-causing variant combinations. Proc Natl Acad Sci U S A *116*, 11878-11887.

Parker, F., Batchelor, M., Wolny, M., Hughes, R., Knight, P.J., and Peckham, M. (2018). A1603P and K1617del, Mutations in beta-Cardiac Myosin Heavy Chain that Cause Laing Early-Onset Distal Myopathy, Affect Secondary Structure and Filament Formation In Vitro and In Vivo. J Mol Biol *430*, 1459-1478.

Ponikowski, P., Voors, A.A., Anker, S.D., Bueno, H., Cleland, J.G.F., Coats, A.J.S., Falk, V., Gonzalez-Juanatey, J.R., Harjola, V.P., Jankowska, E.A.*, et al.* (2016). 2016 ESC Guidelines for the diagnosis and treatment of acute and chronic heart failure: The Task Force for the diagnosis and treatment of acute and chronic heart failure of the European Society of Cardiology (ESC)Developed with the special contribution of the Heart Failure Association (HFA) of the ESC. Eur Heart J *37*, 2129-2200.

Ponnam, S., Sevrieva, I., Sun, Y.B., Irving, M., and Kampourakis, T. (2019). Site-specific phosphorylation of myosin binding protein-C coordinates thin and thick filament activation in cardiac muscle. Proc Natl Acad Sci U S A *116*, 15485-15494.

Previs, M.J., Beck Previs, S., Gulick, J., Robbins, J., and Warshaw, D.M. (2012). Molecular mechanics of cardiac myosin-binding protein C in native thick filaments. Science *337*, 1215-1218.

Ran, F.A., Hsu, P.D., Wright, J., Agarwala, V., Scott, D.A., and Zhang, F. (2013). Genome engineering using the CRISPR-Cas9 system. Nat Protoc *8*, 2281-2308.

Rao, C., Prodromakis, T., Kolker, L., Chaudhry, U.A., Trantidou, T., Sridhar, A., Weekes, C., Camelliti, P., Harding, S.E., Darzi, A.*, et al.* (2013). The effect of microgrooved culture substrates on calcium cycling of cardiac myocytes derived from human induced pluripotent stem cells. Biomaterials *34*, 2399-2411.

Rapezzi, C., Arbustini, E., Caforio, A.L., Charron, P., Gimeno-Blanes, J., Helio, T., Linhart, A., Mogensen, J., Pinto, Y., Ristic, A.*, et al.* (2013). Diagnostic work-up in cardiomyopathies: bridging the gap between clinical phenotypes and final diagnosis. A position statement from the ESC Working Group on Myocardial and Pericardial Diseases. Eur Heart J *34*, 1448-1458.

Raya, A., Rodriguez-Piza, I., Aran, B., Consiglio, A., Barri, P.N., Veiga, A., and Izpisua Belmonte, J.C. (2008). Generation of cardiomyocytes from new human embryonic stem cell lines derived from poor-quality blastocysts. Cold Spring Harb Symp Quant Biol *73*, 127-135.

Rayment, I., Holden, H.M., Whittaker, M., Yohn, C.B., Lorenz, M., Holmes, K.C., and Milligan, R.A. (1993). Structure of the actin-myosin complex and its implications for muscle contraction. Science *261*, 58-65.

Ribeiro, A.J.S., Schwab, O., Mandegar, M.A., Ang, Y.S., Conklin, B.R., Srivastava, D., and Pruitt, B.L. (2017). Multi-Imaging Method to Assay the Contractile Mechanical Output of Micropatterned Human iPSC-Derived Cardiac Myocytes. Circ Res *120*, 1572-1583.

Richard, P., Charron, P., Carrier, L., Ledeuil, C., Cheav, T., Pichereau, C., Benaiche, A., Isnard, R., Dubourg, O., Burban, M.*, et al.* (2003). Hypertrophic cardiomyopathy: distribution of disease genes, spectrum of mutations, and implications for a molecular diagnosis strategy. Circulation *107*, 2227-2232.

Richards, S., Aziz, N., Bale, S., Bick, D., Das, S., Gastier-Foster, J., Grody, W.W., Hegde, M., Lyon, E., Spector, E.*, et al.* (2015). Standards and guidelines for the interpretation of sequence variants: a joint consensus recommendation of the American College of Medical Genetics and Genomics and the Association for Molecular Pathology. Genet Med *17*, 405-424.

Rodriguez-Garcia, M.I., Monserrat, L., Ortiz, M., Fernandez, X., Cazon, L., Nunez, L., Barriales-Villa, R., Maneiro, E., Veira, E., Castro-Beiras, A.*, et al.* (2010). Screening mutations in myosin binding protein C3 gene in a cohort of patients with Hypertrophic Cardiomyopathy. BMC Med Genet *11*, 67.

Ronaldson-Bouchard, K., Ma, S.P., Yeager, K., Chen, T., Song, L., Sirabella, D., Morikawa, K., Teles, D., Yazawa, M., and Vunjak-Novakovic, G. (2018). Advanced maturation of human cardiac tissue grown from pluripotent stem cells. Nature *556*, 239-243.

Sabater-Molina, M., Perez-Sanchez, I., Hernandez Del Rincon, J.P., and Gimeno, J.R. (2018). Genetics of hypertrophic cardiomyopathy: A review of current state. Clin Genet *93*, 3-14.

Sadayappan, S., and de Tombe, P.P. (2012). Cardiac myosin binding protein-C: redefining its structure and function. Biophys Rev *4*, 93-106.

Sala, L., van Meer, B.J., Tertoolen, L.G.J., Bakkers, J., Bellin, M., Davis, R.P., Denning, C., Dieben, M.A.E., Eschenhagen, T., Giacomelli, E.*, et al.* (2018). MUSCLEMOTION: A Versatile Open Software Tool to Quantify Cardiomyocyte and Cardiac Muscle Contraction In Vitro and In Vivo. Circ Res *122*, e5-e16.

Salle, L., and Brette, F. (2007). T-tubules: a key structure of cardiac function and dysfunction. Arch Mal Coeur Vaiss *100*, 225-230.

Sanchez-Danes, A., Richaud-Patin, Y., Carballo-Carbajal, I., Jimenez-Delgado, S., Caig, C., Mora, S., Di Guglielmo, C., Ezquerra, M., Patel, B., Giralt, A.*, et al.* (2012). Disease-specific phenotypes in dopamine neurons from human iPS-based models of genetic and sporadic Parkinson's disease. EMBO Mol Med *4*, 380-395.

Sankaranarayanan, R., E, J.F., and C, J.G. (2013). Mimics of Hypertrophic Cardiomyopathy - Diagnostic Clues to Aid Early Identification of Phenocopies. Arrhythm Electrophysiol Rev *2*, 36-40.

Santos Mateo, J.J., Sabater Molina, M., and Gimeno Blanes, J.R. (2018). Hypertrophic cardiomyopathy. Med Clin (Barc) *150*, 434-442.

Schlossarek, S., Mearini, G., and Carrier, L. (2011). Cardiac myosin-binding protein C in hypertrophic cardiomyopathy: mechanisms and therapeutic opportunities. J Mol Cell Cardiol *50*, 613-620.

Schwarz, J.M., Cooper, D.N., Schuelke, M., and Seelow, D. (2014). MutationTaster2: mutation prediction for the deep-sequencing age. Nat Methods *11*, 361-362.

Scriven, D.R., Dan, P., and Moore, E.D. (2000). Distribution of proteins implicated in excitation-contraction coupling in rat ventricular myocytes. Biophys J *79*, 2682-2691.

Sedaghat-Hamedani, F., Kayvanpour, E., Tugrul, O.F., Lai, A., Amr, A., Haas, J., Proctor, T., Ehlermann, P., Jensen, K., Katus, H.A.*, et al.* (2018). Clinical outcomes associated with sarcomere mutations in hypertrophic cardiomyopathy: a meta-analysis on 7675 individuals. Clin Res Cardiol *107*, 30-41.

Seeger, T., Shrestha, R., Lam, C.K., Chen, C., McKeithan, W.L., Lau, E., Wnorowski, A., McMullen, G., Greenhaw, M., Lee, J.*, et al.* (2019). A Premature Termination Codon Mutation in MYBPC3 Causes Hypertrophic Cardiomyopathy via Chronic Activation of Nonsense-Mediated Decay. Circulation *139*, 799-811.

Semsarian, C., Ingles, J., Maron, M.S., and Maron, B.J. (2015). New perspectives on the prevalence of hypertrophic cardiomyopathy. J Am Coll Cardiol *65*, 1249-1254.

Sequeira, V., Bertero, E., and Maack, C. (2019). Energetic drain driving hypertrophic cardiomyopathy. FEBS Lett *593*, 1616-1626.

Sequeira, V., Najafi, A., McConnell, M., Fowler, E.D., Bollen, I.A., Wust, R.C., dos Remedios, C., Helmes, M., White, E., Stienen, G.J.*, et al.* (2015a). Synergistic role of ADP and Ca(2+) in diastolic myocardial stiffness. J Physiol *593*, 3899-3916.

Sequeira, V., Najafi, A., Wijnker, P.J., Dos Remedios, C.G., Michels, M., Kuster, D.W., and van der Velden, J. (2015b). ADP-stimulated contraction: A predictor of thin-filament activation in cardiac disease. Proc Natl Acad Sci U S A *112*, E7003-7012.

Sewanan, L.R., Schwan, J., Kluger, J., Park, J., Jacoby, D.L., Qyang, Y., and Campbell, S.G. (2019). Extracellular Matrix From Hypertrophic Myocardium Provokes Impaired Twitch Dynamics in Healthy Cardiomyocytes. JACC Basic Transl Sci *4*, 495-505.

Shadrin, I.Y., Allen, B.W., Qian, Y., Jackman, C.P., Carlson, A.L., Juhas, M.E., and Bursac, N. (2017). Cardiopatch platform enables maturation and scale-up of human pluripotent stem cell-derived engineered heart tissues. Nat Commun *8*, 1825.

Shcheglovitov, A., Shcheglovitova, O., Yazawa, M., Portmann, T., Shu, R., Sebastiano, V., Krawisz, A., Froehlich, W., Bernstein, J.A., Hallmayer, J.F.*, et al.* (2013). SHANK3 and IGF1 restore synaptic deficits in neurons from 22q13 deletion syndrome patients. Nature *503*, 267-271.

Shi, Y., Inoue, H., Wu, J.C., and Yamanaka, S. (2017). Induced pluripotent stem cell technology: a decade of progress. Nat Rev Drug Discov *16*, 115-130.

Solaro, R.J. (2008). Multiplex kinase signaling modifies cardiac function at the level of sarcomeric proteins. J Biol Chem *283*, 26829-26833.

Sommese, R.F., Sung, J., Nag, S., Sutton, S., Deacon, J.C., Choe, E., Leinwand, L.A., Ruppel, K., and Spudich, J.A. (2013). Molecular consequences of the R453C hypertrophic cardiomyopathy mutation on human beta-cardiac myosin motor function. Proc Natl Acad Sci U S A *110*, 12607-12612.

Spindler, M., Saupe, K.W., Christe, M.E., Sweeney, H.L., Seidman, C.E., Seidman, J.G., and Ingwall, J.S. (1998). Diastolic dysfunction and altered energetics in the alphaMHC403/+ mouse model of familial hypertrophic cardiomyopathy. J Clin Invest *101*, 1775-1783.

Spudich, J.A. (2014). Hypertrophic and dilated cardiomyopathy: four decades of basic research on muscle lead to potential therapeutic approaches to these devastating genetic diseases. Biophys J *106*, 1236-1249.

Spudich, J.A. (2019). Three perspectives on the molecular basis of hypercontractility caused by hypertrophic cardiomyopathy mutations. Pflugers Arch *471*, 701-717.

Stanfield, C.L. (2013). Principles of human physiology, 5th edn (Boston: Pearson Education).

Stanley, W.C., Recchia, F.A., and Lopaschuk, G.D. (2005). Myocardial substrate metabolism in the normal and failing heart. Physiol Rev *85*, 1093-1129.

Starita, L.M., Ahituv, N., Dunham, M.J., Kitzman, J.O., Roth, F.P., Seelig, G., Shendure, J., and Fowler, D.M. (2017). Variant Interpretation: Functional Assays to the Rescue. Am J Hum Genet *101*, 315-325.

Stewart, M.A., Franks-Skiba, K., Chen, S., and Cooke, R. (2010). Myosin ATP turnover rate is a mechanism involved in thermogenesis in resting skeletal muscle fibers. Proc Natl Acad Sci U S A *107*, 430-435.

Stohr, A., Friedrich, F.W., Flenner, F., Geertz, B., Eder, A., Schaaf, S., Hirt, M.N., Uebeler, J., Schlossarek, S., Carrier, L.*, et al.* (2013). Contractile abnormalities and altered drug response in engineered heart tissue from Mybpc3-targeted knock-in mice. J Mol Cell Cardiol *63*, 189-198.

Su, R.J., Neises, A., and Zhang, X.B. (2016). Generation of iPS Cells from Human Peripheral Blood Mononuclear Cells Using Episomal Vectors. Methods Mol Biol *1357*, 57-69.

Suzuki, T., Palmer, B.M., James, J., Wang, Y., Chen, Z., VanBuren, P., Maughan, D.W., Robbins, J., and LeWinter, M.M. (2009). Effects of cardiac myosin isoform variation on myofilament function and crossbridge kinetics in transgenic rabbits. Circ Heart Fail *2*, 334-341.

Sweeney, H.L., Feng, H.S., Yang, Z., and Watkins, H. (1998). Functional analyses of troponin T mutations that cause hypertrophic cardiomyopathy: insights into disease pathogenesis and troponin function. Proc Natl Acad Sci U S A *95*, 14406-14410.

Taanman, J.W. (1999). The mitochondrial genome: structure, transcription, translation and replication. Biochim Biophys Acta *1410*, 103-123.

Takahashi, K., Tanabe, K., Ohnuki, M., Narita, M., Ichisaka, T., Tomoda, K., and Yamanaka, S. (2007). Induction of pluripotent stem cells from adult human fibroblasts by defined factors. Cell *131*, 861-872.

Takahashi, K., and Yamanaka, S. (2006). Induction of pluripotent stem cells from mouse embryonic and adult fibroblast cultures by defined factors. Cell *126*, 663-676.

Tanaka, A., Yuasa, S., Mearini, G., Egashira, T., Seki, T., Kodaira, M., Kusumoto, D., Kuroda, Y., Okata, S., Suzuki, T.*, et al.* (2014). Endothelin-1 induces myofibrillar disarray and contractile vector variability in hypertrophic cardiomyopathy-induced pluripotent stem cell-derived cardiomyocytes. J Am Heart Assoc *3*, e001263.

Teare, D. (1958). Asymmetrical hypertrophy of the heart in young adults. Br Heart J *20*, 1-8.

Teekakirikul, P., Zhu, W., Huang, H.C., and Fung, E. (2019). Hypertrophic Cardiomyopathy: An Overview of Genetics and Management. Biomolecules *9*.

Terauchi, Y., Kubo, T., Baba, Y., Hirota, T., Tanioka, K., Yamasaki, N., Furuno, T., and Kitaoka, H. (2015). Gender differences in the clinical features of hypertrophic cardiomyopathy caused by cardiac myosin-binding protein C gene mutations. J Cardiol *65*, 423-428.

Thierfelder, L., Watkins, H., MacRae, C., Lamas, R., McKenna, W., Vosberg, H.P., Seidman, J.G., and Seidman, C.E. (1994). Alpha-tropomyosin and cardiac troponin T

mutations cause familial hypertrophic cardiomyopathy: a disease of the sarcomere. Cell *77*, 701-712.

Thomson, J.A., Itskovitz-Eldor, J., Shapiro, S.S., Waknitz, M.A., Swiergiel, J.J., Marshall, V.S., and Jones, J.M. (1998). Embryonic stem cell lines derived from human blastocysts. Science *282*, 1145-1147.

Timmer, S.A., Germans, T., Brouwer, W.P., Lubberink, M., van der Velden, J., Wilde, A.A., Christiaans, I., Lammertsma, A.A., Knaapen, P., and van Rossum, A.C. (2011). Carriers of the hypertrophic cardiomyopathy MYBPC3 mutation are characterized by reduced myocardial efficiency in the absence of hypertrophy and microvascular dysfunction. Eur J Heart Fail *13*, 1283-1289.

Toepfer, C.N., Garfinkel, A.C., Venturini, G., Wakimoto, H., Repetti, G., Alamo, L., Sharma, A., Agarwal, R., Ewoldt, J.F., Cloonan, P.*, et al.* (2020). Myosin Sequestration Regulates Sarcomere Function, Cardiomyocyte Energetics, and Metabolism, Informing the Pathogenesis of Hypertrophic Cardiomyopathy. Circulation *141*, 828-842.

Toepfer, C.N., Wakimoto, H., Garfinkel, A.C., McDonough, B., Liao, D., Jiang, J., Tai, A.C., Gorham, J.M., Lunde, I.G., Lun, M.*, et al.* (2019). Hypertrophic cardiomyopathy mutations in MYBPC3 dysregulate myosin. Sci Transl Med *11*.

Tong, C.W., Stelzer, J.E., Greaser, M.L., Powers, P.A., and Moss, R.L. (2008). Acceleration of crossbridge kinetics by protein kinase A phosphorylation of cardiac myosin binding protein C modulates cardiac function. Circ Res *103*, 974-982.

Torrente, A.G., Mesirca, P., Bidaud, I., and Mangoni, M.E. (2020). Channelopathies of voltage-gated L-type Cav1.3/alpha1D and T-type Cav3.1/alpha1G Ca(2+) channels in dysfunction of heart automaticity. Pflugers Arch *472*, 817-830.

Trepat, X., Wasserman, M.R., Angelini, T.E., Millet, E., Weitz, D.A., Butler, J.P., and Fredberg, J.J. (2009). Physical forces during collective cell migration. Nature Physics *5*, 426-430.

Trivedi, D.V., Adhikari, A.S., Sarkar, S.S., Ruppel, K.M., and Spudich, J.A. (2018). Hypertrophic cardiomyopathy and the myosin mesa: viewing an old disease in a new light. Biophys Rev *10*, 27-48.

Urnov, F.D., Miller, J.C., Lee, Y.L., Beausejour, C.M., Rock, J.M., Augustus, S., Jamieson, A.C., Porteus, M.H., Gregory, P.D., and Holmes, M.C. (2005). Highly efficient endogenous human gene correction using designed zinc-finger nucleases. Nature *435*, 646-651.

Valls-Margarit, M., Iglesias-Garcia, O., Di Guglielmo, C., Sarlabous, L., Tadevosyan, K., Paoli, R., Comelles, J., Blanco-Almazan, D., Jimenez-Delgado, S., Castillo-Fernandez, O.*, et al.* (2019). Engineered Macroscale Cardiac Constructs Elicit Human Myocardial Tissue-like Functionality. Stem Cell Reports *13*, 207-220.

van Bilsen, M., van Nieuwenhoven, F.A., and van der Vusse, G.J. (2009). Metabolic remodelling of the failing heart: beneficial or detrimental? Cardiovasc Res *81*, 420-428.

van der Bliek, A.M., Sedensky, M.M., and Morgan, P.G. (2017). Cell Biology of the Mitochondrion. Genetics *207*, 843-871.

van der Velden, J., Tocchetti, C.G., Varricchi, G., Bianco, A., Sequeira, V., Hilfiker-Kleiner, D., Hamdani, N., Leite-Moreira, A.F., Mayr, M., Falcao-Pires, I.*, et al.* (2018). Metabolic changes in hypertrophic cardiomyopathies: scientific update from the Working Group of Myocardial Function of the European Society of Cardiology. Cardiovasc Res *114*, 1273-1280.

van der Zwaag, P.A., van Rijsingen, I.A., Asimaki, A., Jongbloed, J.D., van Veldhuisen, D.J., Wiesfeld, A.C., Cox, M.G., van Lochem, L.T., de Boer, R.A., Hofstra, R.M.*, et al.* (2012). Phospholamban R14del mutation in patients diagnosed with dilated cardiomyopathy or arrhythmogenic right ventricular cardiomyopathy: evidence supporting the concept of arrhythmogenic cardiomyopathy. Eur J Heart Fail *14*, 1199-1207.

van Dijk, S.J., Dooijes, D., dos Remedios, C., Michels, M., Lamers, J.M., Winegrad, S., Schlossarek, S., Carrier, L., ten Cate, F.J., Stienen, G.J.*, et al.* (2009). Cardiac myosin-binding protein C mutations and hypertrophic cardiomyopathy: haploinsufficiency, deranged phosphorylation, and cardiomyocyte dysfunction. Circulation *119*, 1473-1483.

Velicki, L., Jakovljevic, D.G., Preveden, A., Golubovic, M., Bjelobrk, M., Ilic, A., Stojsic, S., Barlocco, F., Tafelmeier, M., Okwose, N.*, et al.* (2020). Genetic determinants of clinical phenotype in hypertrophic cardiomyopathy. BMC Cardiovasc Disord *20*, 516.

Wallimann, T., Tokarska-Schlattner, M., and Schlattner, U. (2011). The creatine kinase system and pleiotropic effects of creatine. Amino Acids *40*, 1271-1296.

Walsh, R., Buchan, R., Wilk, A., John, S., Felkin, L.E., Thomson, K.L., Chiaw, T.H., Loong, C.C.W., Pua, C.J., Raphael, C.*, et al.* (2017). Defining the genetic architecture of hypertrophic cardiomyopathy: re-evaluating the role of non-sarcomeric genes. Eur Heart J *38*, 3461-3468.

Wang, L., Geist, J., Grogan, A., Hu, L.R., and Kontrogianni-Konstantopoulos, A. (2018). Thick Filament Protein Network, Functions, and Disease Association. Compr Physiol *8*, 631-709.

Watkins, H., Conner, D., Thierfelder, L., Jarcho, J.A., MacRae, C., McKenna, W.J., Maron, B.J., Seidman, J.G., and Seidman, C.E. (1995). Mutations in the cardiac myosin binding protein-C gene on chromosome 11 cause familial hypertrophic cardiomyopathy. Nat Genet *11*, 434-437.

Weinberger, F., Mannhardt, I., and Eschenhagen, T. (2017). Engineering Cardiac Muscle Tissue: A Maturating Field of Research. Circ Res *120*, 1487-1500.

Wen, Z., Nguyen, H.N., Guo, Z., Lalli, M.A., Wang, X., Su, Y., Kim, N.S., Yoon, K.J., Shin, J., Zhang, C.*, et al.* (2014). Synaptic dysregulation in a human iPS cell model of mental disorders. Nature *515*, 414-418.

Werner, J.C., and Sicard, R.E. (1987). Lactate metabolism of isolated, perfused fetal, and newborn pig hearts. Pediatr Res *22*, 552-556.

Wessels, M.W., Herkert, J.C., Frohn-Mulder, I.M., Dalinghaus, M., van den Wijngaard, A., de Krijger, R.R., Michels, M., de Coo, I.F., Hoedemaekers, Y.M., and Dooijes, D. (2015). Compound heterozygous or homozygous truncating MYBPC3 mutations cause lethal cardiomyopathy with features of noncompaction and septal defects. Eur J Hum Genet *23*, 922-928.

Wijnker, P.J., Foster, D.B., Tsao, A.L., Frazier, A.H., dos Remedios, C.G., Murphy, A.M., Stienen, G.J., and van der Velden, J. (2013). Impact of site-specific phosphorylation of protein kinase A sites Ser23 and Ser24 of cardiac troponin I in human cardiomyocytes. Am J Physiol Heart Circ Physiol *304*, H260-268.

Wilson, C., Naber, N., Pate, E., and Cooke, R. (2014). The myosin inhibitor blebbistatin stabilizes the super-relaxed state in skeletal muscle. Biophys J *107*, 1637-1646.

Witjas-Paalberends, E.R., Ferrara, C., Scellini, B., Piroddi, N., Montag, J., Tesi, C., Stienen, G.J., Michels, M., Ho, C.Y., Kraft, T.*, et al.* (2014). Faster cross-bridge detachment and increased tension cost in human hypertrophic cardiomyopathy with the R403Q MYH7 mutation. J Physiol *592*, 3257-3272.

Wu, H., Yang, H., Rhee, J.W., Zhang, J.Z., Lam, C.K., Sallam, K., Chang, A.C.Y., Ma, N., Lee, J., Zhang, H.*, et al.* (2019). Modelling diastolic dysfunction in induced pluripotent stem cell-derived cardiomyocytes from hypertrophic cardiomyopathy patients. Eur Heart J *40*, 3685-3695.

Yamada, Y., Namba, K., and Fujii, T. (2020). Cardiac muscle thin filament structures reveal calcium regulatory mechanism. Nat Commun *11*, 153.

Yang, K.C., Breitbart, A., De Lange, W.J., Hofsteen, P., Futakuchi-Tsuchida, A., Xu, J., Schopf, C., Razumova, M.V., Jiao, A., Boucek, R.*, et al.* (2018). Novel Adult-Onset Systolic Cardiomyopathy Due to MYH7 E848G Mutation in Patient-Derived Induced Pluripotent Stem Cells. JACC Basic Transl Sci *3*, 728-740.

Yang, X., Pabon, L., and Murry, C.E. (2014). Engineering adolescence: maturation of human pluripotent stem cell-derived cardiomyocytes. Circ Res *114*, 511-523.

Yu, J., Vodyanik, M.A., Smuga-Otto, K., Antosiewicz-Bourget, J., Frane, J.L., Tian, S., Nie, J., Jonsdottir, G.A., Ruotti, V., Stewart, R.*, et al.* (2007). Induced pluripotent stem cell lines derived from human somatic cells. Science *318*, 1917-1920.

Zhang, D., Shadrin, I.Y., Lam, J., Xian, H.Q., Snodgrass, H.R., and Bursac, N. (2013). Tissue-engineered cardiac patch for advanced functional maturation of human ESC-derived cardiomyocytes. Biomaterials *34*, 5813-5820.

Zhang, R., Zhao, J., and Potter, J.D. (1995). Phosphorylation of both serine residues in cardiac troponin I is required to decrease the Ca2+ affinity of cardiac troponin C. J Biol Chem *270*, 30773-30780.

Ziaeian, B., and Fonarow, G.C. (2016). Epidemiology and aetiology of heart failure. Nat Rev Cardiol *13*, 368-378.

APPENDIX

APPENDIX I

The Supplementary Table S1 summarizes all the HCM models using hiPSC for the most common mutated genes.

Supplementary Table S1. HCM iPSC models for mutations in *MYH7* and *MYBPC3* genes.

Gene/Mutation	Disease phenotype	Gene Editing	Therapeutic strategy	Reference
MYH7				
R663H	Cellular enlargement, multinucleation, contractile arrhythmia, DADs, irregular Ca^{2+} cycling, increased $[Ca^{2+}]_i$, increased expression of NPPA and MYH7.	No	Propanolol, verapamil, diltiazem	Lan 2013
R442Gly	Cellular enlargement, nuclear NFAT, arrhythmias, APD prolongation, increased diastolic $[Ca^{2+}]_i$, decreased SR Ca^{2+} storage.	No	Metoprolol, verapamil	Han 2014
R663H	Increased contractile tension, reduced Ca^{2+} amplitude.	No	No	Davis 2016
E848G	Reduced fractional shortening, reduced force of contraction.	CRISPR/Cas9	No	Yang 2018
R403Q; V606M	Increased twitch force production, resting tension (R403Q), contraction velocity and relaxation time, cellular enlargement, increased ERK2 and AKT signalling, oxidative stress.	CRISPR/Cas9	Verapamil, blebbistatin	Cohn 2019
R663H	Shorter diastolic sarcomere length, prolonged relaxation, increased diastolic $[Ca^{2+}]_i$, enhanced myofilament Ca^{2+} sensitivity, increased Cav1.2, MYH7, NPPA expression, increased CaMKIId phosphorylation.	No	Verapamil, diltiazem, ranolazine, eleclazine, Pyr3	Wu 2019
R403Q; V606M; R719Q	Reduced myosin SRX/DRX ratio, hypercontractility, prolonged relaxation, increased ATP requirements, reduced PCr/ATP ratio, increased NAD^+/NADH ratio.	CRISPR/Cas9	MYK-461	Toepfer 2020
MYBPC3				
c.2373dupG	Cellular enlargement, no further hypertrophic response to stimuli.	No	No	Dambrot 2014
G999Q1004 del	Cellular enlargement, stronger hypertrophic response to Endothelin-1, contractile abnormalities, nuclear NFAT, increased NPPA expression.	No	ET-1 blocker	Tanaka 2014
c.2373dupG	Decreased force contraction, cMyBP-C haploinsufficiency.	No	No	Birket 2015
R943X	Increased contractile tension, reduced Ca^{2+} amplitude.	No	No	Davis 2016
Q1061X	Cellular enlargement, increased arrythmogenic events (DADs and EADs), longer APDs.	No	No	Ojala 2016
p.V454C fsX21	Cellular enlargement, cMyBP-C haploinsufficiency.	No	Lentiviral cMyBP-C transfer	Prondzynski 2017

APPENDIX I

Gene/Mutation	Disease phenotype	Gene Editing	Therapeutic strategy	Reference
MYBPC3				
cMyBP-C -/-	Decreased contractile force in microtissues, higher contraction velocity, faster decay Ca^{2+} dynamics, Ca^{2+} desensitization.	TALENs	No	Ma 2018
V321M	NPPA expression, faster contraction velocity, arrhythmias, DADs.	CRISPR/Cas9	No	Ma N 2018
Q1061X	Arrythmogenic events (DADs and EADs).	No	Bisoprolol	Prajapati 2018
R943X; R1073P	Elevated diastolic Ca^{2+} levels, prolonged relaxation, sustained activation of NMD pathway.	CRISPR/Cas9		Seeger 2019
W792VfsX41; R502W	Increased twitch force production increased resting tension, increased contraction velocity and relaxation time, cMyBP-C haploinsufficiency (W792VfsX41), oxidative stress.	CRISPR/Cas9	No	Cohn 2019
V321M; V219L	Shorter diastolic sarcomere length, prolonged relaxation, increased diastolic $[Ca^{2+}]_i$, enhanced myofilament Ca^{2+} sensitivity, increased Cav1.2, MYH7 and NPPA expression, increased CaMKIId phosphorylation.	No	Verapamil, diltiazem, ranolazine, eleclazine, Pyr3	Wu 2019
c.2373dupG	Reduced *MYBPC3* mRNA levels, unchanged cMyBP-C protein levels and myofibrillar organization, enhance contractile function with homozygous mutation, unaltered calcium dynamics, reduced cMyBP-C synthesis rate.	CRISPR/Cas9	No	Helms 2020

APPENDIX II

The present appendix II shows accepted publications during this thesis:

Review article

Escribá R, Ferrer-Lorente R, Raya Á. Inborn errors of metabolism: Lessons from iPSC models. Rev Endocr Metab Disord. 2021 Jul 9. doi: 10.1007/s11154-021-09671-z. PMID: 34241766.

Article I

Sánchez-Botet A, Quandt E, Masip N, **Escribá R**, Novellasdemunt L, Gasa L, Li VSW, Raya Á, Clotet J, Ribeiro MPC. Atypical cyclin P regulates cancer cell stemness through activation of the WNT pathway. Cell Oncol (Dordr). 2021 Dec;44(6):1273-1286. doi: 10.1007/s13402-021-00636-7. Epub 2021 Oct 4. PMID: 34604945.

Article II

Casanova JD, Carrillo JG, Jiménez JM, Muñoz JC, Esparza CM, Alvárez MS, **Escribá R**, Milla EB, de la Pompa JL, Raya Á, Gimeno JR, Molina MS, García GB. Trabeculated Myocardium in Hypertrophic Cardiomyopathy: Clinical Consequences. J Clin Med. 2020 Sep 30;9(10):3171. doi: 10.3390/jcm9103171. PMID: 33007916; PMCID.

APPENDIX II: Review article

Reviews in Endocrine and Metabolic Disorders
https://doi.org/10.1007/s11154-021-09671-z

Inborn errors of metabolism: Lessons from iPSC models

Rubén Escribá[1,2,3] · **Raquel Ferrer-Lorente**[1,2,3] · **Ángel Raya**[1,2,3,4]

Accepted: 30 June 2021

Abstract
The possibility of reprogramming human somatic cells to pluripotency has opened unprecedented opportunities for creating genuinely human experimental models of disease. Inborn errors of metabolism (IEMs) constitute a greatly heterogeneous class of diseases that appear, in principle, especially suited to be modeled by iPSC-based technology. Indeed, dozens of IEMs have already been modeled to some extent using patient-specific iPSCs. Here, we review the advantages and disadvantages of iPSC-based disease modeling in the context of IEMs, as well as particular challenges associated to this approach, together with solutions researchers have proposed to tackle them. We have structured this review around six lessons that we have learnt from those previous modeling efforts, and that we believe should be carefully considered by researchers wishing to embark in future iPSC-based models of IEMs.

Keywords Disease modeling · Human induced pluripotent stem cells · Reprogramming · Lysosomal storage disorders · CRISPR/Cas9 · Targeted genome edition

Abbreviations

2D	Two-dimensional
3D	Three-dimensional
CRISPR	Clustered regularly interspaced short palindromic repeats
dAMP	Deoxyadenosine monophosphate
dGMP	Deoxyguanosine monophosphate
DGUOK	Deoxyguanosine kinase
ESCs	Embryonic stem cells
FD	Fabry disease
GAA	Alpha-glucosidase
GAG	Glycosaminoglycan
GBA	Glucocerebrosidase
HipSci	Human Induced Pluripotent Stem Cells Initiative
IEMs	Inborn errors of metabolism
iPSCs	Induced pluripotent stem cells
LDL-C	Low-density lipoprotein-cholesterol
LSDs	Lysosomal storage disorders
MELAS	Mitochondrial encephalomyopathy, lactic acidosis and stroke episodes
MPSIIIB	Mucopolysaccharidosis type IIIB
NPC	Niemman-Pick disease type C
OAT	Ornithine-δ-aminotransferase
OMIM	Online mendelian inheritance in man
PD	Parkinson's disease
SphK	Sphingosine kinase
SSIEM	Society for the Study of Inborn Errors of Metabolism
TALENs	Transcription activator-like effector nuclease
VEGF	Vascular endothelial growth factor
ZFN	Zinc-finger nucleases

Rubén Escribá and Raquel Ferrer-Lorente contributed equally to this work.

✉ Ángel Raya
araya@idibell.cat

[1] Regenerative Medicine Program, Institut d'Investigació Biomèdica de Bellvitge - IDIBELL, L'Hospitalet de Llobregat, Spain

[2] Program for Clinical Translation of Regenerative Medicine in Catalonia – P-[CMRC], L'Hospitalet de Llobregat, Spain

[3] Center for Networked Biomedical Research On Bioengineering, Biomaterials and Nanomedicine (CIBER-BBN), Barcelona, Spain

[4] Institució Catalana de Recerca I Estudis Avançats (ICREA), Barcelona, Spain

1 Introduction

Inborn errors of metabolism (IEMs) are heritable monogenic disorders that often present congenitally with multi-system manifestations affecting various organs. Commonly, gene

Published online: 09 July 2021

mutations in IEMs lead to inadequate enzyme or transporter activity and result in the accumulation of toxic substrates or a deficiency of essential metabolites. Although individually rare, IEMs are collectively quite common, with an estimated incidence of 1 in 4000 newborns [1, 2]. Even though various therapeutic approaches, including replacement therapy and small molecule drugs, have proven effective to treat several IEMs, there is still no cure for most of them, emphasizing the critical need for developing disease-modifying strategies that can ameliorate or halt disease progression.

Gaining a better understanding of the pathophysiological bases underlying IEMs is absolutely critical in order to develop new therapeutic agents. Animal models have provided invaluable insights into the pathophysiology of IEMs, but there remain questions of translatability to humans due to interspecies differences in physiology [3–6]. Additionally, recapitulating key phenotypes of IEMs *in vivo* has been challenging because transgenic animal models of these disorders are often nonviable or show early mortality [7]. Because of the limited availability of disease-relevant patients' samples (especially for rare monogenic diseases with limited number of patients available worldwide and limited access to the affected tissues), there is an urgent need for the development of human cellular models that recapitulate the most salient features of IEMs in order to investigate disease progression and to develop new therapeutic approaches. In this sense, the advent of induced pluripotent stem cell (iPSC) technology [8] has opened new perspectives for modeling human diseases. The possibility to reprogram human somatic cells to pluripotency offers an unprecedented opportunity to generate disease-specific iPSCs [9–12], for the development of cell-based experimental models.

In this review, we focus on the use of iPSC technology to model IEMs and how these models provide a valuable tool to set up innovative treatment approaches for particular IEMs. We discuss published iPSC models of inherited metabolic diseases and summarize the main lessons learnt from these efforts.

2 Induced pluripotent stem cells as a powerful tool for disease modeling

In 2006, Takahashi and Yamanaka published a major technological breakthrough in the field of disease modeling, describing a method for reprogramming terminally differentiated adult dermal fibroblasts into cells with a gene expression profile and developmental potential similar to those of embryonic stem cells (ESCs) [8, 13, 14].

iPSC technology offers the possibility to generate patient-specific cells for modeling human diseases. While animal-based models have provided valuable insights into the pathogenic mechanisms of numerous human diseases [15–17], substantial species-specific differences prevent the recapitulation of key features characteristic of many human conditions [18–20]. Indeed, several rodent models have been described to not be adequate in the context of metabolic disorders: Lesch-Nyhan syndrome models do not recapitulate the common neurobehavioral aspects [21], vascular endothelial dysfunction is not recapitulated in Fabry disease models [22, 23], Niemman-Pick disease type C (NPC) models do not cover all aspects of the disease pathology [24], and the pathological phenotypes observed in sialidosis models appear to be shared across multiple lysosomal storage disorders (LSDs) and Alzheimer's disease [25]. Similarly, the use of primary cultures of patient-derived cells, while helpful for studying disease etiology, is limited by the lack of expandable sources of patients' cells, particularly for hard-to-access cells such as neurons and cardiomyocytes. Therefore, iPSC-based disease modeling appears as an attractive alternative to animal- and primary cell-based methods.

Identification of novel therapeutic approaches requires recapitulating key features of IEMs and relevant pathogenic mechanisms, a frequent limitation of conventional *in vitro* models. iPSC-based models can provide disease-related phenotypes in cell types relevant for the specific disease, thus representing a clear advantage over the use of fibroblasts or immortalized cell lines. For example, hiPSC-derived cells are more vulnerable to the toxic effects of substrate accumulation that are characteristic of several IEMs [26–28] and display a metabolic rate more similar to disease-relevant cells [29]. For inherited metabolic disorders affecting hepatocytes, immortalized cells lines are widely used. However, they do not resemble primary hepatocytes, have dysfunctional apoptotic pathways due to their carcinogenic nature and present restricted genotypic variability [30]. Similarly, primary hepatocytes, considered the gold standard for *in vitro* drug testing, gradually lose their hepatic functions during culture and are unable to proliferate [31]. Therefore, iPSC derivatives could provide an excellent alternative platform to overcome an important limitation associated with the identification of novel pharmacological treatments for IEMs.

Only fifteen years after the original description of induced reprogramming to pluripotency, enormous progress has been made in stem cell biology and regenerative medicine using iPSC technology [9, 24, 32–34]. Furthermore, iPSCs derived from healthy individuals and patients have accelerated advances in developing genuinely human experimental models of disease, novel pathogenic mechanisms or associated phenotypes have been elucidated [25, 26, 28, 35–37], new drugs initiated from iPSC-based screenings are in the pipeline [38–40] and the first clinical trials using human iPSC-derived products have been initiated [24, 41–43].

3 Modeling inborn errors of metabolism *in vitro*

IEMs are a class of heterogeneous and rare diseases commonly caused by a defect in metabolic proteins, usually an enzyme or a transporter, that result in accumulation of harmful metabolites or deficiency of particular metabolites needed for cellular homeostasis [44]. Their classification can be difficult because of the multitude and variety of metabolic pathways involved. According to the hierarchical classification set forth by the Society for the Study of Inborn Errors of Metabolism (SSIEM), IEMs comprise 612 diseases with OMIM numbers, categorized into 15 main groups (www.ssiem.org/resources/resources/inborn-errors-classification). Although disease modeling remains a challenge in the context of IEMs, to date, dozens of these disorders have been modeled to some extent using patient-specific iPSC. We have identified from scientific literature a total of 107 IEMs for which iPSC lines have been generated, referenced with a total of 291 publications (Supplemental Table 1), among which lysosomal disorders have attracted special attention (Fig. 1A). In combination with specific protocols for differentiating patient-specific iPSC into disease-relevant cell types, these models are able to recapitulate key phenotypic features of IEMs and provide insight into disease mechanisms, as well as aiding in the identification of novel drug targets (Fig. 1B). Some of the most successful efforts at IEM modeling, together with the main lessons learnt from them, are discussed below.

3.1 First lesson: iPSCs vs fibroblasts, highlighting the importance of the disease-relevant cell type

For most IEMs, disease-relevant phenotypes cannot be investigated in fibroblasts, highlighting the importance of developing iPSC-derived models (Fig. 2). Nonetheless, in some cases, fibroblasts display disease-related phenotypes and thus, engaging into somatic cell reprogramming and subsequent iPSC differentiation might appear unnecessary. Several studies carried out with patients' fibroblasts have contributed to our understanding of the pathogenic mechanisms of diseases [45], and provided valuable readouts for screening novel compounds [46–48]. Using this approach, Lee et al. reported on the key role of vascular endothelial growth factor (VEGF) and sphingosine kinase (SphK) in NPC pathogenesis [45]. The activity of SphK, a crucial enzyme in modulating the levels of sphingosine, was significantly decreased in fibroblasts from NPC patients, leading to abnormal sphingosine storage and autophagic defects. This dysfunction of SphK activity was linked to decreased VEGF expression. Thus, VEGF treatment ameliorated the NPC phenotype in patients' fibroblasts and increased SphK activity. Several studies carried out with NPC fibroblasts, which showed an accumulation of unesterified cholesterol and lipids in lysosomal storage organelles, reported the evaluation of compound efficacy [46–48]. The benefit of compounds such as β-cyclodextrins, histone deacetylase inhibitors or rapamycin has been confirmed using NPC patient-derived fibroblasts. However, later studies found

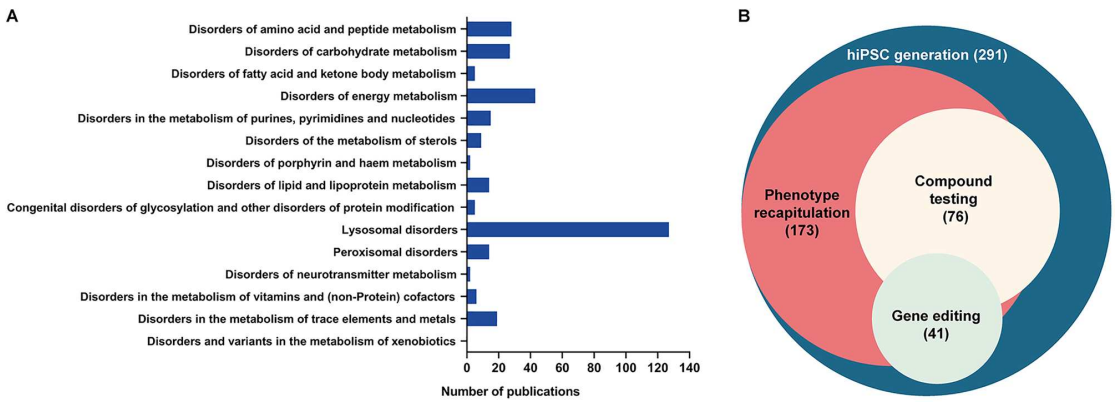

Fig. 1 Analysis of published studies using iPSC technology for modeling of IEMs **A** Number of publications related to each of the fifteen main IEM groups as classified by the Society for the Study of Inborn Errors of Metabolism (SSIEM; classification available at www.ssiem.org/images/centralstore/resources/SSIEMClassificationIEM2011.pdf). **B** Distribution of the 291 publications reviewed for the current study, indicating those that reported recapitulation of phenotypic features of IEMs, screening of novel compounds, and the combination of iPSC technology with gene editing techniques

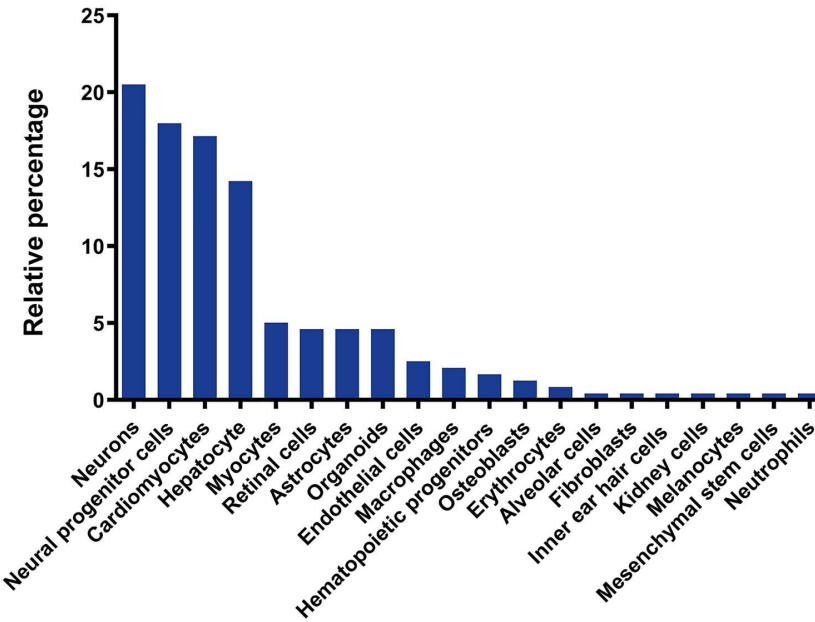

Fig. 2 Main cell types differentiated from hiPSC for modeling of IEMs. Pie chart indicating the main cell types differentiated from hiPSC and used for disease modeling of IEMs in the reviewed literature, displayed following alphabetical order in clockwise direction. Out of the 20 different cell types identified in the relevant literature, neural derivatives and cardiomyocytes were used in over 50% of the published studies

differences in drug responses between NPC neuronal cells and dermal fibroblasts even though they were derived from the same NPC patient. The application of human NPC neural stem cells as a cell-based disease model established that six out of the nine compounds reported as efficacious in NPC, fibroblasts, and mouse models, did not have significant effects in these cells [29]. Using the appropriate molecular and biochemical context is also fundamental for deciphering new cell type-specific pathogenic mechanisms: Seol et al. provided the first evidence that lysosomal sialidase gene (NEU1) deficiency alters, not only lysosomal dynamics, but also autophagic activity [25]; Odaka et al. revealed defective presynaptic exocytosis and excessive enhancement of AMPA-evoked Ca^{2+} influx in sialidosis [26]; and Liedtke et al. uncovered possible differences between NPC1 and NPC2 that showed indistinguishable biochemical phenotypes [28], among others.

IEMs comprise metabolic defects that can either affect almost all tissues, such as disorders of glycosylation, or specific cell types in which the mutated enzyme plays a critical role. In this sense, patient's fibroblast can provide valuable information for diseases in which the associated biochemical defects are ubiquitously altered in nearly all cell types or the underlying phenotypes of the disease can be observed systemically.

3.2 Second lesson: Important metabolic defects underlie IEMs -but iPSCs do not seem to care

For most IEMs modeled through iPSC-based technology to date, the metabolic defects that characterize these diseases do not seem to affect iPSC generation or maintenance, thereby enabling successful modeling of those diseases. Nevertheless, in some particular cases, iPSC generation from diseased somatic cells can be challenging, and reprogramming efficiency may be compromised by their severe pathophysiological defects. As examples, the generation of iPSC colonies for Gaucher disease, Pearson syndrome, Mucopolysaccharidosis type IIIB (MPSIIIB), Pompe disease, or NPC was found to be reduced when compared with that of healthy somatic cells [29, 49–53]. In a study by Huang et al. reprogramming fibroblasts from Pompe disease patients was not possible unless they conditionally rescued the expression of alpha-glucosidase (GAA) [51]. Nevertheless, later studies [54–57] successfully generated iPSC from infantile-onset and late-onset Pompe disease patients without the need of using rescue-based strategies. Similarly, iPSC generation from MPSIIIB patients by Lemonnier et al. required the exogenous complementation of the enzymatic defect [52]. In this case, reprogramming of MPSIIIB cells was efficient, but patient iPSC

proliferated poorly and were inefficiently cloned unless the missing enzyme (α-N-acetyl-glucosaminidase) was exogenously supplied [52]. Lastly, iPSC generation was also hampered in NPC [29]. The authors initially found that only a few iPSC-like colonies appeared during the reprogramming process, disappearing after 5–7 passages. The difficulty in NPC-iPSC generation was due to cholesterol accumulation in fibroblasts. Thus, after the treatment of NPC fibroblasts with tocopherol, a compound that reduces cholesterol accumulation, NPC-iPSC stable in culture for over 20 passages could be successfully established [29].

IEMs encompass a plethora of highly diverse disorders. The presence and severity of the disease can also vary within individuals carrying the same pathogenic mutation. In any case, the known IEM mutations observed in patients are not developmentally lethal, and the early stages during the embryonic development are not severely compromised. In this regard, although the reprogramming efficiency might occasionally be reduced, the metabolic defects underlying IEMs do not seem to affect the generation and maintenance of iPSCs, which has been accomplished for dozens of these disorders. This finding reinforces iPSC technology as an important experimental tool to provide valuable insights into the pathophysiology of these diseases, further encouraging researchers to apply this powerful approach for IEM modeling.

3.3 Third lesson: Variability needs to be accounted for when using iPSC to model IEMs

A defining characteristic of pluripotent stem cells is their potential to differentiate into cells of all three germ layers. However, a limiting factor regarding the use of iPSCs is, precisely, the variability in their differentiation potential. Not only the inter-individual differences among iPSC may have a strong impact in the differentiation capacity toward a specific cell type, but also between hiPSC clones from the same individual [58, 59]. There have been several attempts to characterize the sources of such variability. Prolonged culture and maintenance of pluripotent stem cells has been shown to promote genomic alterations, most frequently on chromosomes 12 and 17, likely reflecting the selective pressure processes taking place in culture [60]. Frequent amplifications of the WNT3/WNT9B cluster in the 17q21 chromosomal region have also been found to have important functional consequences affecting neural differentiation [61]. More recently, a comprehensive examination of the major sources of genetic and phenotypic variations in iPSC lines was undertaken by genome-wide characterization of 711 iPSC lines derived from 301 healthy individuals, established by the Human Induced Pluripotent Stem Cells Initiative (HipSci). The authors were able to identify consistent inter-individual effects that explained more than 46% of the phenotypic variation among iPSC lines [62].

Irrespective of the origin, phenotypic interline variability of iPSCs complicates assigning specific genotypes to disease-related cellular phenotypes. In this sense, the use of targeted nucleases as gene-editing tools is increasingly being used to counteract such variability, enabling the generation of isogenic controls that only differ in the presence/absence of the genetic variants under study. The versatility of targeting almost any locus in the genome to generate the desired targeted genetic modification becomes essential for the interpretation of the results and to strengthen the relationship between the genotype and phenotype.

The earliest attempts at generating sequence-specific changes in IEMs-derived iPSC were established with BAC- or AAV-based vectors targeting the ornithine-δ-aminotransferase (*OAT*) and *HPRT1* gene [63, 64]. Engineered nucleases, such as TALENs and zinc-finger nucleases (ZFN) have also been used to introduce specific mutations in iPSCs to model several diseases, such as ubiquinone deficiency, pyruvate kinase deficiency, NPC or LDLR deficiency [65–68]. More recently, CRISPR/Cas9 has emerged as the leading genome-editing technique in the context of iPSC-based disease modeling. The advent of CRISPR/Cas9 technology has opened unprecedented opportunities for this purpose due to its simplicity [69]. Successful efforts have been made in modeling inherited hypercholesterolemia with iPSC-corrected isogenic controls. Omer et al. and Okada et al. used CRISPR/Cas9 to correct a 3-base pair homozygous deletion and a homozygous point mutation in the *LDLR* gene, respectively, restoring low-density lipoprotein-cholesterol (LDL-C) uptake [70–72]. Recent studies generated corrected-isogenic controls of Fabry- iPSC lines carrying heterozygous mutations in the *GLA* gene. Differentiated cardiomyocytes and vascular endothelial cells from gene-corrected iPSC lines displayed restored levels of α-gal A protein [73, 74]. CRISPR/Cas9-based modeling of Sandhoff disease has also been achieved using isogenic controls in which one of the mutant alleles in the *HEXB* gene was corrected. In this way, cerebral organoids from mutant and gene-corrected iPSC were developed, demonstrating that accumulation of GM2 ganglioside was diminished and the neuronal differentiation was not impaired in isogenic controls when compared with the mutant *HEXB* line [75].

The use of genetic engineering and iPSC technology is a powerful combination especially for ultra-rare diseases where patients' samples for iPSC generation are particularly limited. In order to overcome this limitation, specific mutations can be introduced in healthy control iPSC. Although the complex genomic background of real patients is not recapitulated when using control iPSC, these efforts provide valuable insights into the pathogenesis of specific gene mutations [76, 77].

The generation of iPSCs from healthy and diseased individuals allows capturing the complex genomic background from each individual. Genomic variability may impact in the differentiation capacity towards the cell of interest or even in the observed phenotypes. Thus, formally ascribing the appearance of disease-related phenotypes to the presence of particular gene mutations often requires the analysis of isogenic control cells that only differ in the specific mutation of interest. Although the studies combining iPSCs and gene-editing techniques for the modeling of IEMs are still only a small fraction (Fig. 1B), there is an increasing trend towards the use of such techniques in recent years, highlighting the importance of genome edition to address causality between gene mutations/variants and disease phenotypes.

3.4 Fourth lesson: High-content/throughput screens may be feasible, but still a long way to go

For decades, the identification of novel compounds for treating human conditions has relied on high-throughput screening systems primarily based on cellular assays. Most cell-based screening assays have used either immortalized tumor-derived cell lines, in which the desired molecular target is heterologously expressed, or primary cells that better resemble the functions and phenotypes found *in vivo* [78]. Although more physiologically and preclinically relevant than immortalized cells, disadvantages of primary cell cultures such as their limited expansion and thus availability, have precluded their widespread adoption in high-throughput screening of small compounds. Major efforts are now aimed toward the use of iPSCs in drug discovery as they provide theoretically unlimited, homogeneous cell populations for cell type-specific compound screening, profiling and optimization [40, 79].

Although iPSC technology has facilitated the understanding of disease pathogenesis and the impact of compound modulators, drug development for monogenic diseases, including those related to IEMs, is still challenging [34, 80, 81]. In the field of lysosomal storage disorders much attention has been directed to target-based drug testing. Lysosomal accumulation of sphingolipids or cholesterol esters has been observed in iPSC-based models of Tay-Sachs, Niemann-Pick disease type A, B and C, Neural Ceroid Lipofuscinoses, and Wolman disease. In these studies, treatment with tocopherols and hydroxypropyl-cyclodextrins ameliorate lysosomal cholesterol and lipid accumulation, indicating their potential therapeutic use for these diseases [29, 67, 82–86]. Gaucher disease is arguably the most characterized iPSC model of lysosomal disorders, probably owing to the fact that mutations in the glucocerebrosidase gene (GBA1) constitute an important genetic risk factor for Parkinson's disease (PD) [87]. In recent years, several target-based compound screens have been performed to identify molecules capable of decreasing the accumulation of glucosylsphingosine. In a study by Kim et al. inhibition of acid ceramidase by carmofur resulted, not only in the reduction of glucosylsphingosine levels, but also in a decrease in oxidized α-synuclein levels in GBA1-PD patient-derived dopaminergic neurons [88]. More recently, a small molecule inhibitor of mTOR (Torin 1) was able to upregulate lysosomal biogenesis and to enhance the autophagic clearance of Gaucher neurons [89].

However, the use of iPSC-based models of IEMs for medium- and high-throughput screening approaches is scarce to date. This most likely reflects the inherent challenges in generating disease affected cell types at high scale and purity [40]. In a study from Cayo et al. iPSC-derived hepatocytes from familial hypercholesterolemia patients were used to perform a large screening of existing drugs that could potentially increase exogenous LDL trafficking to endosomes and reduce exogenous LDL-C levels, including apoB. A total of 2,320 existing small molecules were tested for their ability to reduce apoB levels. The authors found that cardiac glycosides, such as digoxin, proscillaridin or ouabain, could lower the levels of apoB in culture medium by promoting its proteolytic turnover [90]. In a second high-content drug screening, the same laboratory generated a deoxyguanosine kinase (DGUOK) loss-of-function iPSC using CRISPR/Cas9 and differentiated them into hepatocyte-like cells [91]. DGUOK deficiency is the most common cause of mitochondrial DNA depletion syndrome, in which the production of deoxyadenosine monophosphate (dAMP) and deoxyguanosine monophosphate (dGMP) is diminished mainly in the liver. Using the same drug collection library, the authors interrogated the compounds for their ability to restore ATP levels in DGUOK-deficient hepatocytes. They identified NAD^+ as a potential drug candidate that could increase not only ATP levels, but also the expression of all mitochondrial-encoded electron transport chain genes examined *in vitro* and *in vivo* [91]. Recently, iPSC-derived neurons have been used in two high-content drug screenings. In one study, neuronal progenitor cells from GM1 gangliosidosis were tested with 2.217 already approved drugs. Two compounds, amodiaquine and thiethylperazine were capable of activating autophagy both *in vitro* and *in vivo* [92]. In a second study, Lesch-Nyhan-derived neural progenitor cells were screened with 3.838 pharmacological compounds for their ability to increase cell viability. The authors identified 6 adenosine-like compounds that ameliorated cell survival and neurogenesis in HGPRT-deficient cells [93].

Over the past few years, compound-screening assays using iPSC-derived cells has emerged as a new powerful strategy for the pharmaceutical industry, facilitating target and lead identification, and lead optimization. However,

there is still a long way to go in the context of IEMs. iPSCs are particularly important given that they can be reproducibly cultured in high abundance and give rise to different cell types from the same individual, which facilitates optimization for compound safety, selectivity and efficacy. In addition, the importance of stringent quality controls and well defined and established workflows at every stage of the process will be indispensable for the identification of novel compounds, and thus for the successful use of iPSC-based platforms for drug discovery and preclinical studies.

3.5 Fifth lesson: iPSC-based technology opens the door to modeling pre-clinical stages of disease

Theoretically at least, almost any genetic disease lends itself to be modeled employing iPSC-based technology. However, this strategy has proved so far to be more amenable for tackling monogenic diseases associated to highly penetrant disease-causing mutations, as opposed to environmentally modulated, sporadic or diseases of unknown cause [94]. Congenital or early-onset diseases also appear to be more readily modeled *in vitro* using iPSC-based strategies than late-onset diseases. This could be linked to the fact that current iPSC differentiation protocols yield cells with immature or fetal-like characteristics, but it may reflect the difficulty of recapitulating aging, a major risk factor in many late-onset diseases, in standard laboratory conditions. These limitations notwithstanding, several studies have decribed the appearance of disease-related phenotypes in iPSC-based models of PD, Huntington disease, and Alzheimer's disease [95, 96]. Although these disorders may appear late in life, aberrant molecular and cellular phenotypes are detectable in culture, illustrating the possibility to study early stages of disease progression.

Canals et al. generated an iPSC-based experimental model of Sanfilippo type C syndrome, a lysosomal storage disorder with progressive neurodegeneration [97]. Differentiated mature neurons were able to recapitulate the main known phenotypes of the disease, such as the accumulation of glycosaminoglycan (GAG) over time and abnormal vacuoles morphology. The authors found that neuronal GAG accumulation was not statistically significant until cells had been in culture for 9 weeks, in concordance with the progressive nature of the disease. However, the authors found that neuronal network activity and connectivity were already altered at 3 weeks of differentiation, suggesting that similar approaches could be used to detect early functional signs that predate the clinical onset of other diseases as well. If realized, this would facilitate the identification of potential therapeutic strategies that would prevent, rather than revert, the appearance of clinical signs of the disease in patients.

3.6 Sixth lesson: Advanced culture systems, new tools to overcome the limitations of 2D cultures

One of the main challenges associated with iPSC-based experimental approaches is the relative immaturity of iPSC derivatives obtained with current differentiation protocols, which are typically carried out under standard two dimensional (2D) culture conditions [98, 99]. It is commonly thought that 2D cell culture systems lack critical information cues for cell differentiation/maturation, including tissue-specific architecture and biomechanical and biochemical signals originating from cell–cell and cell–matrix interactions [100]. Many of those information cues are present in organoid-type 3D culture systems, which offer levels of cell differentiation, tissue organization and response to drugs more closely resembling the *in vivo* situation [101, 102].

For example, Akbari et al. reported on the generation of functional hepatic organoids for Citrullinemia type I that recapitulated important disease-related phenotypes such as the decrease in ammonia detoxification capacity [103]. Similarly, a robust spinal cord organoid system derived from iPSCs of a MELAS (Mitochondrial encephalomyopathy, lactic acidosis and stroke episodes) patient was developed to further investigate the neurogenesis defects in this disease. Motor neurons, which could not be reproducibly obtained using conventional 2D differentiation protocols, were reproducibly generated in the organoid model [104]. More recently, a brain organoid model of Leigh syndrome, the most severe pediatric manifestation of mitochondrial diseases, revealed compromised neural morphogenesis due to defective metabolic state. This model offers hope for solving a major obstacle for developing effective therapies for this syndrome: the lack of suitable model systems recapitulating the human disease course. Thanks to this model, Inak et al. provided novel mechanistic insights and suggested potential interventional strategies for this incurable disease [105].

Organoids are valuable tools for precision medicine and, in combination with genetic-engineering approaches, can be used to directly test the role of pathogenic mutations in a controlled environment. Despite the numerous advantages of organoids over conventional 2D cell culture systems, some limitations remain, such as the relative lack of standardized protocols to generate organoids and the absence of vascularization and of complex inter-organ communication. To address current technical challenges in organoid research, the integration of organoids with microfluidic on-a-chip devices is emerging as an advanced, yet complementary, bioengineering approach. Organ-on-a-chip devices are able to control the biochemical and biophysical microenvironment, resulting in increased tissue maturation and vascularization, and offering a more *in vivo*-like phenotype with multi-organ capabilities for IEM disease modelling [106–108]. A pioneering adoption of on-a-chip approaches in the field of IEM modeling investigated the

pediatric cardiomyopathy Barth syndrome. Combining gene editing and heart-on-a-chip technology, the authors were able to provide new insights into the disease mechanisms [108]. However, organ-on-a-chip devices are typically of very low throughput, limiting its applicability in the early stages of drug discovery [109].

4 Concluding remarks

The ability to reprogram somatic cells to iPSCs is gradually changing the way we develop experimental disease models, especially for rare monogenic diseases, offsetting the limited number of patients available worldwide, the difficulty in gaining access to the mostly affected tissues, and the lack of bona fide experimental animal models. The combination of human iPSC-based technology and site-directed genome edition constitutes an exciting and powerful platform for complex disease modeling and drug screening. However, despite the promising advantages offered by combining these two technologies, important limitations and challenges need to be taken into account if disease models are to be exploited to their fullest (Fig. 3). Efforts at modeling human diseases in general, and IEMs in particular, have taught us already some lessons that we believe ought to be considered when devising future experimental models (Fig. 4): 1) iPSC technology emphasizes the importance of the disease-relevant cell types. Fibroblasts can provide valuable readouts for primary screening of novel compounds, but the differential response between fibroblasts and the specific cell type(s) affected in the disease highlights that, in many cases, iPSC-based cell models could be the preferred option for this purpose; 2) the characteristic metabolic defects that underlie IEMs do not seem to affect iPSC generation and maintenance, reinforcing iPSC technology as an important experimental tool to provide insights into the pathophysiology of IEMs; 3) the inter-line and inter-clone variability in differentiation potential of iPSCs needs to be accounted for when modeling IEM. A straightforward manner to address this limitation consists on the parallel interrogation of isogenic controls, which are currently easily generated thanks to CRISPR/Cas9-based genomic edition technology; 4) although still a long way to go in the context of IEMs, iPSCs-based models emerge as serious candidates to be used as medium- and high-throughput screening platforms since they can provide theoretically unlimited amounts of homogeneous, patient-specific, and disease-relevant cell types; 5) iPSC-based technology offers the possibility to model pre-clinical stages of late-onset diseases and to identify early functional signs that predate the clinical phenotypes. This pre-clinical time window could facilitate the development of potential therapeutic strategies that would prevent the appearance of clinical disease; and 6) Advanced culture systems hold remarkable potential for increasing the maturation state of iPSC derivatives, thus extending the validity of such disease models to phenotypes not easily attainable in conventional 2D culture systems.

In conclusion, carefully designed and properly controlled iPSC-based models of IEMs recapitulate key features of the disease phenotype and respond to pharmacologic manipulation predictably. As such, iPSC-based models of IEMs have enabled uncovering the role of novel pathogenic mechanisms in sialidosis and NPC, identifying new drug compounds potentially effective for DGUOK deficiency

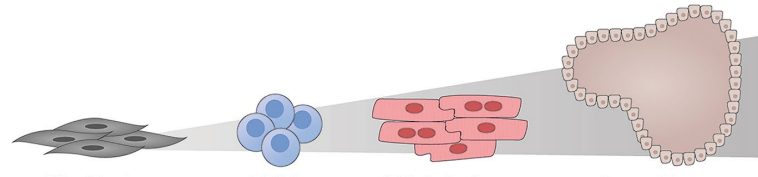

	Fibroblasts	hiPSCs	iPS-derivatives	Organoids
Physiological complexity	+	+	+ + / + + +	+ + +
Recapitulation of human disease	+	+	+ + / + + +	+ + +
Genetic manipulation	+	+ + +	+ + +	+ + +
High-throughput drug screening	+ +	+ + +	+ +	+
Affordability	+ + +	+ +	+	+

Fig. 3 Comparison of different cell culture systems for modeling of IEMs. Patient-specific fibroblasts, along with their reprogrammed hiPSC and hiPSC-derivatives (in form of 2D cell cultures or organoid systems), are compared for their relative limitations and benefits. Score marks are represented as follows: '+': not suitable; '++': good and '+++': optimal

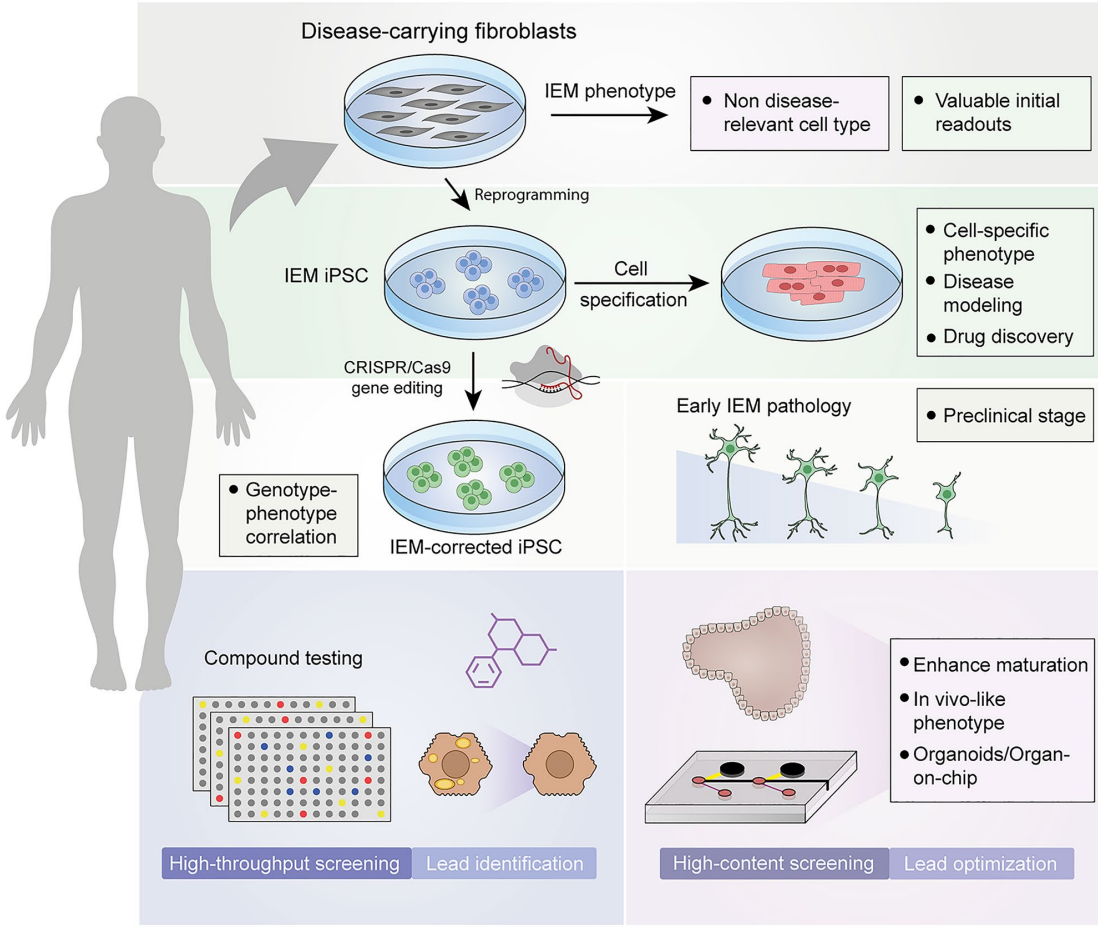

Fig. 4 Schematic representation of the lessons learnt from iPSC models of IEMs. Somatic cells such as fibroblasts can be obtained from patients with IEMs to study pathogenic mechanisms, but in a cellular and metabolic context that may differ from that of disease-affected cells. Somatic cells can be reprogrammed into iPSC carrying the IEM-specific genetic alteration. iPSC can be differentiated into the disease-relevant cell type (such as cardiomyocytes to study disorders of energy metabolism or glycogen storage disorders). CRISPR/Cas9-based gene-editing technology allows the generation of isogenic sets of iPSC that can be used to properly associate genetic alterations to specific phenotypes. The combination of gene editing and iPSC technology is a remarkable tool to study preclinical stages (such as the neural defects in Sanfilippo C) and to perform high-throughput drug screenings (for example to reduce the hypercholesterolemia in iPSC-derived hepatocytes). The immature phenotype of iPSC derivatives is a current limitation in the field, which can be overcome by using advanced culture systems such as organoids and organ-on-a-chip devices, which generate cells more similar to their *in vivo* counterpart, making them suitable for high-content screenings and lead optimization

and hypercholesterolemia, and developing novel drug candidates and target pathways for GM1 gangliosidosis, among many other examples of success. Whereas remarkable progress has been made over the past decade, iPSC technology is still in its infancy and important challenges will need to be addressed. Of note, the functional immaturity of iPSC-derived cells is an important consideration when studying IEM and age-related diseases. As developments in iPSC technology itself progress towards better reproducibility and scalability, we believe that iPSC-based approaches will become a powerful tool for precision medicine, capable of predicting disease trajectories and potential effective treatments at the individual level, not only for IEMs but also applicable to many other diseases.

Supplementary Information The online version contains supplementary material available at https://doi.org/10.1007/s11154-021-09671-z.

Acknowledgements Authors would like to thank all members of the laboratory for fruitful discussions and Daniel Grinberg (Universitat de Barcelona) for valuable comments on the manuscript.

Funding Funding in AR laboratory to work on this topic comes from the Spanish Ministry of Economy and Competitiveness-MINECO (RTI2018-095377-B-100), Instituto de Salud Carlos III-ISCIII/FEDER (Red de Terapia Celular—TerCel RD16/0011/0024), Departament de Salut/Generalitat de Catalunya (PERIS SLT002/16/00234). Generalitat de Catalunya-AGAUR (2017-SGR-899), Fundació La Marató de TV3 (201534–30), and CERCA Programme / Generalitat de Catalunya.

Declarations

Ethical approval This article is a review of published literature, for which no ethical approval is required.

Conflict of interest The authors have no conflicts of interest to declare that are relevant to the content of this article.

References

1. Chace DH, Kalas TA, Naylor EW. The application of tandem mass spectrometry to neonatal screening for inherited disorders of intermediary metabolism. Annu Rev Genomics Hum Genet. 2002;3:17–45.
2. Matalonga L, Gort L, Ribes A. Small molecules as therapeutic agents for inborn errors of metabolism. J Inherit Metab Dis. 2017;40(2):177–93.
3. Haskins M. Gene therapy for lysosomal storage diseases (LSDs) in large animal models. ILAR J. 2009;50(2):112–21.
4. Hemsley KM, Hopwood JJ. Lessons learnt from animal models: pathophysiology of neuropathic lysosomal storage disorders. J Inherit Metab Dis. 2010;33(4):363–71.
5. Pastores GM, Torres PA, Zeng BJ. Animal models for lysosomal storage disorders. Biochemistry (Mosc). 2013;78(7):721–5.
6. Wager K, Mahmood F, Russell C. Modelling inborn errors of metabolism in zebrafish. J Inherit Metab Dis. 2014;37(4):483–95.
7. Demaret T, et al. Longitudinal study of Pex1-G844D NMRI mouse model: A robust pre-clinical model for mild Zellweger spectrum disorder. Biochim Biophys Acta Mol Basis Dis. 2020;1866(11):165900.
8. Takahashi K, Yamanaka S. Induction of pluripotent stem cells from mouse embryonic and adult fibroblast cultures by defined factors. Cell. 2006;126(4):663–76.
9. Lee G, Studer L. Induced pluripotent stem cell technology for the study of human disease. Nat Methods. 2010;7(1):25–7.
10. Dolmetsch R, Geschwind DH. The human brain in a dish: the promise of iPSC-derived neurons. Cell. 2011;145(6):831–4.
11. Sanchez-Danes A, et al. Disease-specific phenotypes in dopamine neurons from human iPS-based models of genetic and sporadic Parkinson's disease. EMBO Mol Med. 2012;4(5):380–95.
12. Matamoros-Angles A, et al. iPS Cell Cultures from a Gerstmann-Straussler-Scheinker Patient with the Y218N PRNP Mutation Recapitulate tau Pathology. Mol Neurobiol. 2018;55(4):3033–48.
13. Takahashi K, et al. Induction of pluripotent stem cells from adult human fibroblasts by defined factors. Cell. 2007;131(5):861–72.
14. Yu J, et al. Induced pluripotent stem cell lines derived from human somatic cells. Science. 2007;318(5858):1917–20.
15. Bonten EJ, et al. Chaperone-mediated gene therapy with recombinant AAV-PPCA in a new mouse model of type I sialidosis. Biochim Biophys Acta. 2013;1832(10):1784–92.
16. Fog CK, Kirkegaard T. Animal models for Niemann-Pick type C: implications for drug discovery & development. Expert Opin Drug Discov. 2019;14(5):499–509.
17. Reed E, Lutsenko S, Bandmann O. Animal models of Wilson disease. J Neurochem. 2018;146(4):356–73.
18. Dawson TM, Ko HS, Dawson VL. Genetic animal models of Parkinson's disease. Neuron. 2010;66(5):646–61.
19. Puzzo D, et al. Rodent models for Alzheimer's disease drug discovery. Expert Opin Drug Discov. 2015;10(7):703–11.
20. Onos KD, et al. Toward more predictive genetic mouse models of Alzheimer's disease. Brain Res Bull. 2016;122:1–11.
21. Moro CA, Hanna-Rose W. Animal Model Contributions to Congenital Metabolic Disease. Adv Exp Med Biol. 2020;1236:225–44.
22. Ohshima T, et al. alpha-Galactosidase A deficient mice: a model of Fabry disease. Proc Natl Acad Sci U S A. 1997;94(6):2540–4.
23. Tseng WL, et al. Imbalanced Production of Reactive Oxygen Species and Mitochondrial Antioxidant SOD2 in Fabry Disease-Specific Human Induced Pluripotent Stem Cell-Differentiated Vascular Endothelial Cells. Cell Transplant. 2017;26(3):513–27.
24. Volkner C, et al. Pluripotent Stem Cells for Disease Modeling and Drug Discovery in Niemann-Pick Type C1. Int J Mol Sci. 2021;22(2).
25. Seol B, Kim YD, Cho YS. Modeling Sialidosis with Neural Precursor Cells Derived from Patient-Derived Induced Pluripotent Stem Cells. Int J Mol Sci. 2021;22(9).
26. Odaka H, et al. An iPSC-based neural model of sialidosis uncovers glycolytic impairment-causing presynaptic dysfunction and deregulation of Ca(2+) dynamics. Neurobiol Dis. 2021;152:105279.
27. Song HY, et al. Reversal of the Inflammatory Responses in Fabry Patient iPSC-Derived Cardiovascular Endothelial Cells by CRISPR/Cas9-Corrected Mutation. Int J Mol Sci. 2021;22(5).
28. Liedtke M, et al. Pathophysiological *In Vitro* Profile of Neuronal Differentiated Cells Derived from Niemann-Pick Disease Type C2 Patient-Specific iPSCs Carrying the NPC2 Mutations c.58G>T/c.140G>T. Int J Mol Sci. 2021;22(8).
29. Yu D, et al. Niemann-Pick Disease Type C: Induced Pluripotent Stem Cell-Derived Neuronal Cells for Modeling Neural Disease and Evaluating Drug Efficacy. J Biomol Screen. 2014;19(8):1164–73.
30. Corbett JL, Duncan SA. iPSC-Derived Hepatocytes as a Platform for Disease Modeling and Drug Discovery. Front Med (Lausanne). 2019;6:265.
31. Zabulica M, et al. Gene Editing Correction of a Urea Cycle Defect in Organoid Stem Cell Derived Hepatocyte-like Cells. Int J Mol Sci. 2021;22(3).

32. Shi Y, et al. Induced pluripotent stem cell technology: a decade of progress. Nat Rev Drug Discov. 2017;16(2):115–30.
33. Omole AE, Fakoya AOJ. Ten years of progress and promise of induced pluripotent stem cells: historical origins, characteristics, mechanisms, limitations, and potential applications. PeerJ. 2018;6:e4370.
34. Yamashita T, et al. Pharmaceutical Research for Inherited Metabolic Disorders of the Liver Using Human Induced Pluripotent Stem Cell and Genome Editing Technologies. Biol Pharm Bull. 2019;42(3):312–8.
35. Burkhardt MF, et al. A cellular model for sporadic ALS using patient-derived induced pluripotent stem cells. Mol Cell Neurosci. 2013;56:355–64.
36. Wen Z, et al. Synaptic dysregulation in a human iPS cell model of mental disorders. Nature. 2014;515(7527):414–8.
37. di Domenico A, et al. Patient-Specific iPSC-Derived Astrocytes Contribute to Non-Cell-Autonomous Neurodegeneration in Parkinson's Disease. Stem Cell Rep. 2019;12(2):213–29.
38. Lee G, et al. Large-scale screening using familial dysautonomia induced pluripotent stem cells identifies compounds that rescue IKBKAP expression. Nat Biotechnol. 2012;30(12):1244–8.
39. Shcheglovitov A, et al. SHANK3 and IGF1 restore synaptic deficits in neurons from 22q13 deletion syndrome patients. Nature. 2013;503(7475):267–71.
40. Elitt MS, Barbar L, Tesar PJ. Drug screening for human genetic diseases using iPSC models. Hum Mol Genet. 2018;27(R2):R89–98.
41. Naryshkin NA, et al. Motor neuron disease. SMN2 splicing modifiers improve motor function and longevity in mice with spinal muscular atrophy. Science. 2014;345(6197):688–93.
42. Mullard A. Stem-cell discovery platforms yield first clinical candidates. Nat Rev Drug Discov. 2015;14(9):589–91.
43. Kletzl H, et al. The oral splicing modifier RG7800 increases full length survival of motor neuron 2 mRNA and survival of motor neuron protein: Results from trials in healthy adults and patients with spinal muscular atrophy. Neuromuscul Disord. 2019;29(1):21–9.
44. Campeau PM, Scriver CR, Mitchell JJ. A 25-year longitudinal analysis of treatment efficacy in inborn errors of metabolism. Mol Genet Metab. 2008;95(1–2):11–6.
45. Lee H, et al. Pathological roles of the VEGF/SphK pathway in Niemann-Pick type C neurons. Nat Commun. 2014;5:5514.
46. Rosenbaum AI, et al. Endocytosis of beta-cyclodextrins is responsible for cholesterol reduction in Niemann-Pick type C mutant cells. Proc Natl Acad Sci U S A. 2010;107(12):5477–82.
47. Pipalia NH, et al. Histone deacetylase inhibitor treatment dramatically reduces cholesterol accumulation in Niemann-Pick type C1 mutant human fibroblasts. Proc Natl Acad Sci U S A. 2011;108(14):5620–5.
48. Wehrmann ZT, et al. Quantitative comparison of the efficacy of various compounds in lowering intracellular cholesterol levels in Niemann-Pick type C fibroblasts. PLoS One. 2012;7(10):e48561.
49. Tiscornia G, et al. Neuronopathic Gaucher's disease: induced pluripotent stem cells for disease modelling and testing chaperone activity of small compounds. Hum Mol Genet. 2013;22(4):633–45.
50. Cherry AB, et al. Induced pluripotent stem cells with a mitochondrial DNA deletion. Stem Cells. 2013;31(7):1287–97.
51. Huang HP, et al. Human Pompe disease-induced pluripotent stem cells for pathogenesis modeling, drug testing and disease marker identification. Hum Mol Genet. 2011;20(24):4851–64.
52. Lemonnier T, et al. Modeling neuronal defects associated with a lysosomal disorder using patient-derived induced pluripotent stem cells. Hum Mol Genet. 2011;20(18):3653–66.
53. Higuchi T, et al. The generation of induced pluripotent stem cells (iPSCs) from patients with infantile and late-onset types of Pompe disease and the effects of treatment with acid-alpha-glucosidase in Pompe's iPSCs. Mol Genet Metab. 2014;112(1):44–8.
54. Raval KK, et al. Pompe disease results in a Golgi-based glycosylation deficit in human induced pluripotent stem cell-derived cardiomyocytes. J Biol Chem. 2015;290(5):3121–36.
55. Sato Y, et al. Disease modeling and lentiviral gene transfer in patient-specific induced pluripotent stem cells from late-onset Pompe disease patient. Mol Ther Methods Clin Dev. 2015;2:15023.
56. Zhang Y, et al. Generation of induced pluripotent stem cells (iPSCs) from an infant with Pompe disease carrying with compound mutations of R608X and E888X in GAA gene. Stem Cell Res. 2019;41:101621.
57. Cheng YS, et al. A human induced pluripotent stem cell line (TRNDi007-B) from an infantile onset Pompe patient carrying p.R854X mutation in the GAA gene. Stem Cell Res. 2019;37:101435.
58. Kajiwara M, et al. Donor-dependent variations in hepatic differentiation from human-induced pluripotent stem cells. Proc Natl Acad Sci U S A. 2012;109(31):12538–43.
59. Hu BY, et al. Neural differentiation of human induced pluripotent stem cells follows developmental principles but with variable potency. Proc Natl Acad Sci U S A. 2010;107(9):4335–40.
60. Baker DE, et al. Adaptation to culture of human embryonic stem cells and oncogenesis *in vivo*. Nat Biotechnol. 2007;25(2):207–15.
61. Lee CT, et al. Functional consequences of 17q213.1/WNT3-WNT9B amplification in hPSCs with respect to neural differentiation. Cell Rep. 2015;10(4):616–32.
62. Kilpinen H, et al. Common genetic variation drives molecular heterogeneity in human iPSCs. Nature. 2017;546(7658):370–5.
63. Howden SE, et al. Genetic correction and analysis of induced pluripotent stem cells from a patient with gyrate atrophy. Proc Natl Acad Sci U S A. 2011;108(16):6537–42.
64. Khan IF, et al. Engineering of human pluripotent stem cells by AAV-mediated gene targeting. Mol Ther. 2010;18(6):1192–9.
65. Frank S, Skryabin BV, Greber B. A modified TALEN-based system for robust generation of knock-out human pluripotent stem cell lines and disease models. BMC Genomics. 2013;14:773.
66. Garate Z, et al. Generation of a High Number of Healthy Erythroid Cells from Gene-Edited Pyruvate Kinase Deficiency Patient-Specific Induced Pluripotent Stem Cells. Stem Cell Rep. 2015;5(6):1053–66.
67. Maetzel D, et al. Genetic and chemical correction of cholesterol accumulation and impaired autophagy in hepatic and neural cells derived from Niemann-Pick Type C patient-specific iPS cells. Stem Cell Rep. 2014;2(6):866–80.
68. Yang J, et al. Generation of Human Liver Chimeric Mice with Hepatocytes from Familial Hypercholesterolemia Induced Pluripotent Stem Cells. Stem Cell Rep. 2017;8(3):605–18.
69. Jinek M, et al. A programmable dual-RNA-guided DNA endonuclease in adaptive bacterial immunity. Science. 2012;337(6096):816–21.
70. Omer L, et al. CRISPR Correction of a Homozygous Low-Density Lipoprotein Receptor Mutation in Familial Hypercholesterolemia Induced Pluripotent Stem Cells. Hepatol Commun. 2017;1(9):886–98.
71. Okada H, et al. Function and Immunogenicity of Gene-corrected iPSC-derived Hepatocyte-Like Cells in Restoring Low Density Lipoprotein Uptake in Homozygous Familial Hypercholesterolemia. Sci Rep. 2019;9(1):4695.
72. Omer L, et al. Familial hypercholesterolemia class II low-density lipoprotein receptor response to statin treatment. Dis Model Mech. 2020;13(4).

73. Birket MJ, et al. A Human Stem Cell Model of Fabry Disease Implicates LIMP-2 Accumulation in Cardiomyocyte Pathology. Stem Cell Rep. 2019;13(2):380–93.
74. Do HS, et al. Enhanced thrombospondin-1 causes dysfunction of vascular endothelial cells derived from Fabry disease-induced pluripotent stem cells. EBioMedicine. 2020;52:102633.
75. Allende ML, et al. Cerebral organoids derived from Sandhoff disease-induced pluripotent stem cells exhibit impaired neurodifferentiation. J Lipid Res. 2018;59(3):550–63.
76. Beneto N, et al. Neuronal and Astrocytic Differentiation from Sanfilippo C Syndrome iPSCs for Disease Modeling and Drug Development. J Clin Med. 2020;9(3).
77. Hayashi H, et al. Modeling Human Bile Acid Transport and Synthesis in Stem Cell-Derived Hepatocytes with a Patient-Specific Mutation. Stem Cell Rep. 2021;16(2):309–23.
78. Eglen R, Reisine T. Primary cells and stem cells in drug discovery: emerging tools for high-throughput screening. Assay Drug Dev Technol. 2011;9(2):108–24.
79. Zuba-Surma EK, et al. Stem cells as a novel tool for drug screening and treatment of degenerative diseases. Curr Pharm Des. 2012;18(18):2644–56.
80. Matsa E, Burridge PW, Wu JC. Human stem cells for modeling heart disease and for drug discovery. Sci Transl Med. 2014;6(239):239ps6.
81. Chanana AM, Rhee JW, Wu JC. Human-induced pluripotent stem cell approaches to model inborn and acquired metabolic heart diseases. Curr Opin Cardiol. 2016;31(3):266–74.
82. Vu M, et al. Neural stem cells for disease modeling and evaluation of therapeutics for Tay-Sachs disease. Orphanet J Rare Dis. 2018;13(1):152.
83. Long Y, et al. Induced Pluripotent Stem Cells for Disease Modeling and Evaluation of Therapeutics for Niemann-Pick Disease Type A. Stem Cells Transl Med. 2016;5(12):1644–55.
84. Soga M, et al. HPGCD outperforms HPBCD as a potential treatment for Niemann-Pick disease type C during disease modeling with iPS cells. Stem Cells. 2015;33(4):1075–88.
85. Sima N, et al. Neural stem cells for disease modeling and evaluation of therapeutics for infantile (CLN1/PPT1) and late infantile (CLN2/TPP1) neuronal ceroid lipofuscinoses. Orphanet J Rare Dis. 2018;13(1):54.
86. Aguisanda F, et al. Neural stem cells for disease modeling of Wolman disease and evaluation of therapeutics. Orphanet J Rare Dis. 2017;12(1):120.
87. Sidransky E, et al. Multicenter analysis of glucocerebrosidase mutations in Parkinson's disease. N Engl J Med. 2009;361(17):1651–61.
88. Kim MJ, et al. Acid ceramidase inhibition ameliorates alpha-synuclein accumulation upon loss of GBA1 function. Hum Mol Genet. 2018;27(11):1972–88.
89. Brown RA, et al. mTOR hyperactivity mediates lysosomal dysfunction in Gaucher's disease iPSC-neuronal cells. Dis Model Mech. 2019;12(10).
90. Cayo MA, et al. A Drug Screen using Human iPSC-Derived Hepatocyte-like Cells Reveals Cardiac Glycosides as a Potential Treatment for Hypercholesterolemia. Cell Stem Cell. 2017;20(4):478-489e5.
91. Jing R, et al. A Screen Using iPSC-Derived Hepatocytes Reveals NAD(+) as a Potential Treatment for mtDNA Depletion Syndrome. Cell Rep. 2018;25(6):1469-1484e5.
92. Kajihara R, et al. Novel Drug Candidates Improve Ganglioside Accumulation and Neural Dysfunction in GM1 Gangliosidosis Models with Autophagy Activation. Stem Cell Rep. 2020;14(5):909–23.
93. Ruillier V, et al. Rescuing compounds for Lesch-Nyhan disease identified using stem cell-based phenotypic screening. JCI Insight. 2020;5(4).
94. Zeltner N, Studer L. Pluripotent stem cell-based disease modeling: current hurdles and future promise. Curr Opin Cell Biol. 2015;37:102–10.
95. Calatayud C, et al. Modeling the genetic complexity of Parkinson's disease by targeted genome edition in iPS cells. Curr Opin Genet Dev. 2017;46:123–31.
96. Avior Y, Sagi I, Benvenisty N. Pluripotent stem cells in disease modelling and drug discovery. Nat Rev Mol Cell Biol. 2016;17(3):170–82.
97. Canals I, et al. Activity and High-Order Effective Connectivity Alterations in Sanfilippo C Patient-Specific Neuronal Networks. Stem Cell Rep. 2015;5(4):546–57.
98. Chen YF, et al. Rapid generation of mature hepatocyte-like cells from human induced pluripotent stem cells by an efficient three-step protocol. Hepatology. 2012;55(4):1193–203.
99. Feric NT, Radisic M. Maturing human pluripotent stem cell-derived cardiomyocytes in human engineered cardiac tissues. Adv Drug Deliv Rev. 2016;96:110–34.
100. Pampaloni F, Reynaud EG, Stelzer EH. The third dimension bridges the gap between cell culture and live tissue. Nat Rev Mol Cell Biol. 2007;8(10):839–45.
101. Lancaster MA, Knoblich JA. Organogenesis in a dish: modeling development and disease using organoid technologies. Science. 2014;345(6194):1247125.
102. Duval K, et al. Modeling Physiological Events in 2D vs. 3D Cell Culture. Physiology (Bethesda). 2017;32(4):266–77.
103. Akbari S, et al. Robust, Long-Term Culture of Endoderm-Derived Hepatic Organoids for Disease Modeling. Stem Cell Rep. 2019;13(4):627–41.
104. Winanto, et al. Organoid cultures of MELAS neural cells reveal hyperactive Notch signaling that impacts neurodevelopment. Cell Death Dis. 2020;11(3):182.
105. Inak G, et al. Defective metabolic programming impairs early neuronal morphogenesis in neural cultures and an organoid model of Leigh syndrome. Nat Commun. 2021;12(1):1929.
106. Sances S, et al. Human iPSC-Derived Endothelial Cells and Microengineered Organ-Chip Enhance Neuronal Development. Stem Cell Rep. 2018;10(4):1222–36.
107. Novak R, et al. Robotic fluidic coupling and interrogation of multiple vascularized organ chips. Nat Biomed Eng. 2020;4(4):407–20.
108. Wang G, et al. Modeling the mitochondrial cardiomyopathy of Barth syndrome with induced pluripotent stem cell and heart-on-chip technologies. Nat Med. 2014;20(6):616–23.
109. Low LA, et al. Organs-on-chips: into the next decade. Nat Rev Drug Discov. 2021;20(5):345–61.

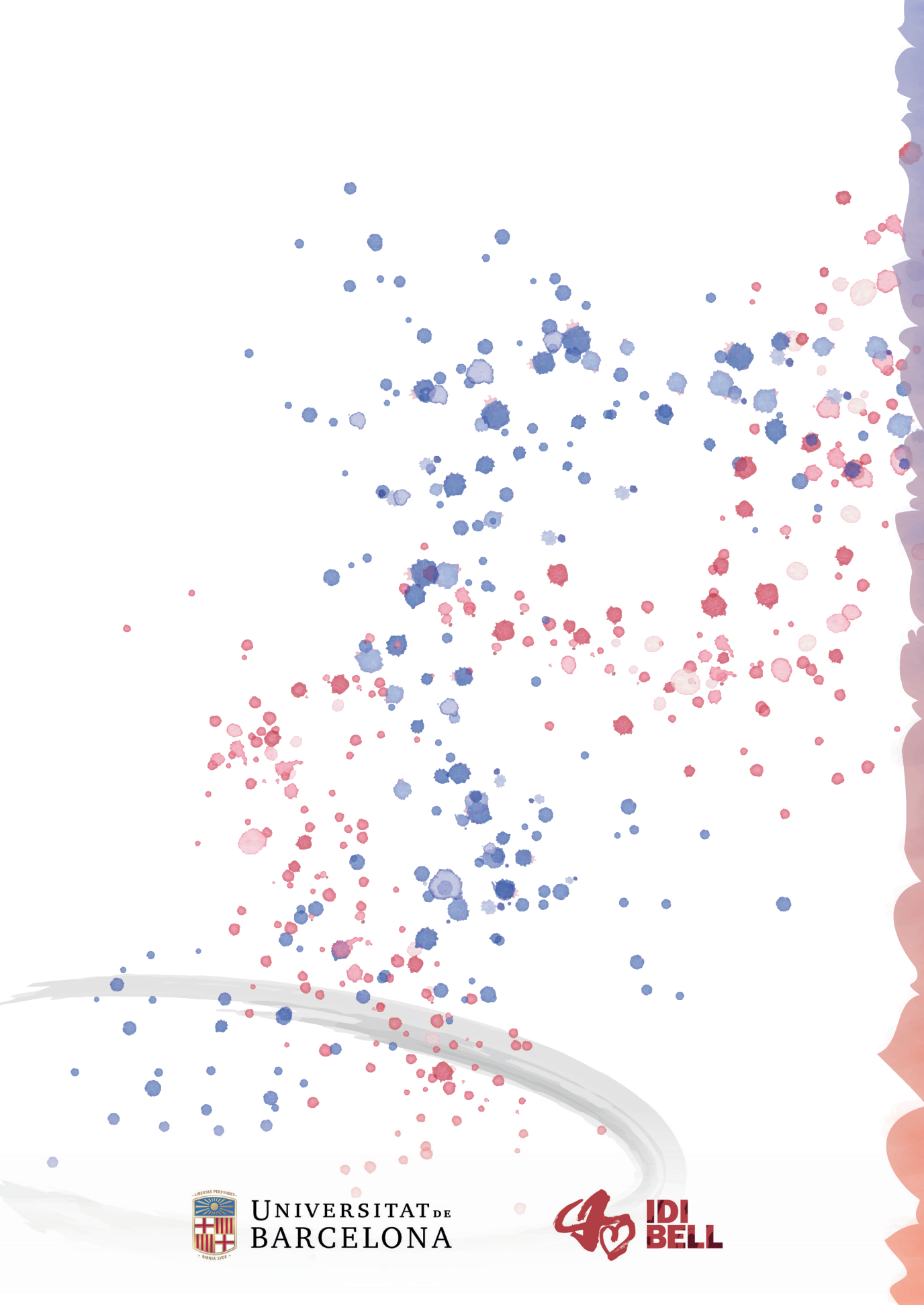
UNIVERSITAT DE BARCELONA
IDIBELL